Doctoral Dissertation

博士論文

# Searching for an emergent SU(4) symmetry in real materials

# (現実の物質における創発SU(4)対称性の探求)

A Dissertation Submitted for the Degree of Doctor of Philosophy

December 2019

令和元年１２月博士（理学）申請

Department of Physics, Graduate School of Science,

The University of Tokyo

東京大学大学院理学系研究科物理学専攻

Masahiko Yamada

山田　昌彦

# Abstract

Beauty of mathematics appears everywhere in modern condensed matter physics, but the importance of the theory of higher-rank Lie groups has been ignored for a long time. The enhancement of the spin-space symmetry from the usual SU(2) to SU($N$) with $N > 2$ is promising for finding nontrivial quantum spin liquids, but the realization of SU($N$) spin systems in real materials is still challenging. Although there is a proposal in cold atomic systems, in magnetic materials with a spin-orbital degree of freedom it is difficult to achieve the SU($N$) symmetry by fine tuning. Here we propose a new mechanism by which the SU(4) symmetry emerges in the strong spin-orbit coupling limit. In $d^1$ transition metal compounds with edge-sharing anion octahedra, the spin-orbit coupling gives rise to strongly bond-dependent and apparently SU(4)-breaking hopping between the $J_{\text{eff}} = 3/2$ quartets. However, in the honeycomb structure, a gauge transformation maps the system to an SU(4)-symmetric Hubbard model, which means that the system has a hidden symmetry in spite of its large spin-orbit coupling. In the strong repulsion limit at quarter filling, as expected in $\alpha$-$ZrCl_3$, the low-energy effective model is the SU(4) Heisenberg model on the honeycomb lattice, which cannot have a trivial gapped ground state and is expected to host a gapless spin-orbital liquid. In such quantum spin-orbital liquids, both the spin and orbital degrees of freedom become fractionalized and correlated together at low temperature due to the strong frustrated interactions between them. Similarly to spinons in pure quantum spin liquids, quantum spin-orbital liquids can host not only spinon excitations, but also fermionic "orbitalon" excitations at low temperature, which we have named here in distinction from orbitons in the symmetry-broken Jahn-Teller phases. In fact, the SU(4) Heisenberg model on the honeycomb lattice is known to host such gapless exotic excitations (spinons and orbitalons) by numerical calculations. By generalizing this model to other three-dimensional lattices, we also propose crystalline spin-orbital liquids protected by the combination of an emergent SU(4) symmetry and space group symmetries.

# List of published papers

## Papers

1. Masahiko G. Yamada, Tomohiro Soejima, Naoto Tsuji, Daisuke Hirai, Mircea Dincă, and Hideo Aoki, "First-principles design of a half-filled flat band of the kagome lattice in two-dimensional metal-organic frameworks", Phys. Rev. B **94**, 081102(R) (2016), as a Rapid Communication. (arXiv:1510.00164)

2. Masahiko G. Yamada, Hiroyuki Fujita, and Masaki Oshikawa, "Designing Kitaev Spin Liquids in Metal-Organic Frameworks", Phys. Rev. Lett. **119**, 057202 (2017). (arXiv:1605.04471) [1]

3. Masahiko G. Yamada, Vatsal Dwivedi, and Maria Hermanns, "Crystalline Kitaev spin liquids", Phys. Rev. B **96**, 155107 (2017), as Editors' Suggestion. (arXiv:1707.00898) [2]

4. Masahiko G. Yamada, Masaki Oshikawa, and George Jackeli, "Emergent SU(4) Symmetry in $\alpha$-$ZrCl_3$ and Crystalline Spin-Orbital Liquids", Phys. Rev. Lett. **121**, 097201 (2018). (arXiv:1709.05252) [3]

This PhD thesis is mostly based on Paper 4, and the texts in Paper 4 were partially used in this thesis with permission of American Physical Society. The appendix also includes a result from Paper 3.

## Preprints

1. Masahiko G. Yamada, and George Jackeli, "Magnetic and Electronic Properties of Spin-Orbit Coupled Dirac Electrons on a (001) Thin Film of Double Perovskite $Sr_2FeMoO_6$", arXiv:1711.08674.

2. Masahiko G. Yamada, and Yasuhiro Tada, "Quantum valence bond ice theory for proton-driven quantum spin-dipole liquids", arXiv:1903.03567.

## Thesis

1. Masahiko Yamada, "Designing various quantum spin liquids in metal-organic frameworks (金属有機構造体における様々な量子スピン液体の物質設計)", Master's thesis, the Department of Physics, the University of Tokyo (2017).

Il s'agit de ce fait, que dans mon approche de la mathématique, et plus généralement, dans ma démarche spontanée à la découverte du monde, la tonalité de base de mon être est **yin, "féminin"**... Ce qui est exceptionnel par contre dans mon cas (me semble-t-il), c'est que dans ma démarche de découverte et notamment, dans mon travail mathématique, j'aie été toute ma vie pleinement fidèle à cette nature originelle, sans aucune velléité d'y apporter des retouches ou rectificatifs, que ce soit en vertu des desiderata d'un Censeur intérieur (lequel de toutes façons n'y a jamais vu que du feu, tellement on serait loin de soupçonner une sensibilité et une approche créatrice "féminine" dans une affaire "entre hommes" comme la mathématique!), ou par souci de me conformer aux canons de bon goût en vigueur dans le monde extérieur, et plus particulièrement, dans le monde scientifique. Il n'y a aucun doute pour moi que c'est grâce surtout à cette fidélité à ma propre nature, dans ce domaine limité de ma vie tout au moins, que ma créativité mathématique a pu se déployer pleinement et sans entrave, comme un arbre vigoureux, solidement planté en pleine terre, se déployé librement au rythme des nuits et des jours, des vents et des saisons. Il en a été ainsi, alors pourtant que mes "dons" sont plutôt modestes, et que les débuts ne s'annonçaient nullement sous les meilleurs auspices.

— Alexander Grothendieck, *Récoltes et Semailles*, 1985–1987.

# Contents

# Chapter 1

# Introduction

Nontrivial quantum spin liquids (QSLs) are expected to exhibit many exotic properties such as fractionalized excitations [4, 5], in addition to the absence of a long-range order. Despite the vigorous studies in the last several decades, however, material candidates for such QSLs are still rather limited.

An intriguing scenario to realize a nontrivial QSL is by generalizing the spin system, which usually consists of spins representing the SU(2) symmetry, to SU($N$) "spin" systems with $N > 2$. We expect stronger quantum fluctuations in SU($N$) spin systems with a moderate $N$, which could lead the system to an SU($N$) QSL even on unfrustrated, bipartite lattices, including the honeycomb lattice [6–9].

The SU($N$) spin systems with $N > 2$ can be realized in ultracold atomic systems, using the nuclear spin degrees of freedom [10]. In electron spin systems, however, realization of this SU($N$) symmetry is more challenging. It would be possible to combine the spin and orbital degrees of freedom, so that local electronic states are identified with a representation of SU($N$). QSL realized in this context may be called quantum spin-orbital liquids (QSOLs) because it involves spin and orbital degrees of freedom. Despite the appeal of such a possibility, the actual Hamiltonian is usually not SU($N$)-symmetric, reflecting the different physical origins of the spin and orbital degrees of freedom. For example, the relevance of an SU(4) QSOL has been discussed for $Ba_3CuSb_2O_9$ (BCSO) with a decorated honeycomb lattice structure [8, 11, 12]. It turned out, however, that the estimated parameters for BCSO are rather far from the model with an exact SU(4) symmetry [13]. Moreover, the spin-orbit coupling (SOC) and the directional dependence of the orbital hopping usually break both the spin-space and orbital-space SU(2) symmetries, as exemplified in iridates [14]. Thus, it would seem even more difficult to realize an SU($N$)-symmetric system in real magnets with SOC. (See Refs. 15–18 for proposed realization of SU($N$) symmetry. However, they do not lead to QSOL because of their crystal structures.)

In this thesis, we demonstrate a novel mechanism for realizing an SU(4) spin system in a solid-state system with an onsite SOC. Paradoxically, the symmetry of the spin-orbital space can be *enhanced* to SU(4) when the SOC is strong. In particular, we propose $\alpha$-$ZrCl_3$ [19–21] as the first candidate for an SU(4)-symmetric QSOL on the honeycomb lattice. Its $d^1$ electronic configuration in the octahedral ligand field, combined with the strong SOC, implies that the ground state of the electron is described by a $J_{\text{eff}} =$

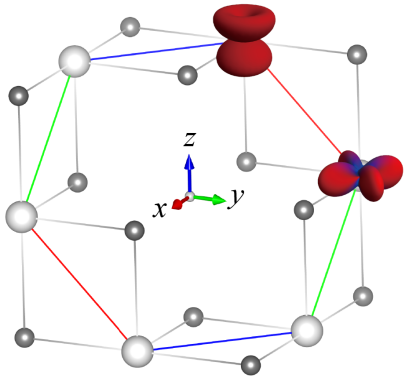


Figure 1.1: Schematic structure of honeycomb $\alpha$-$ZrCl_3$. White and grey spheres represent Zr and Cl atoms, respectively.

3/2 quartet [22]. In fact, the resulting effective Hamiltonian appears to be anisotropic in the quartet space. Nevertheless, we show that the model is gauge-equivalent to an SU(4)-symmetric Hubbard model. In the strong repulsion limit, its low-energy effective Hamiltonian is the Kugel-Khomskii model [23] on the honeycomb lattice, exactly at the SU(4) symmetric point:

$$H_{\text{eff}} = J \sum_{\langle jk \rangle} \left( \boldsymbol{S}_j \cdot \boldsymbol{S}_k + \frac{1}{4} \right) \left( \boldsymbol{T}_j \cdot \boldsymbol{T}_k + \frac{1}{4} \right), \tag{1.1}$$

where $J > 0$, and $\boldsymbol{S}_j$ and $\boldsymbol{T}_j$ are pseudospin-1/2 operators defined for each site $j$. The SU(4) symmetry can be made manifest by rewriting the Hamiltonian, up to a constant shift, as $H_{\text{eff}} = \frac{J}{4} \sum_{\langle jk \rangle} P_{jk}$, where the spin state at each site forms the fundamental representation of SU(4), and $P_{jk}$ is the operator which swaps the states at sites $j$ and $k$. This is a natural generalization of the antiferromagnetic SU(2) Heisenberg model to SU(4).

The ground state of the SU(2) spin-1/2 antiferromagnet on the honeycomb lattice is simply Néel-ordered [24, 25], reflecting the unfrustrated nature of the lattice. On the other hand, the SU($N$) generalization of the Néel state by putting different flavors on neighboring sites gives a macroscopic number of classical ground states when $N > 2$ [26–28], implying its instability. In fact, it was argued that the SU(4) antiferromagnet on the honeycomb lattice has a QSOL ground state without any long-range order [8, 9].

In this Introduction, we first review three types of magnetic frustrations, geometric frustration, exchange frustration, and SU($N$) frustration with introduction to the Lieb-Schultz-Mattis-type theorems [29]. Next, we discuss previous methods to realize SU($N$) spin systems and known results for QSOLs with an SU($N$) symmetry, which is the central topic of this thesis.

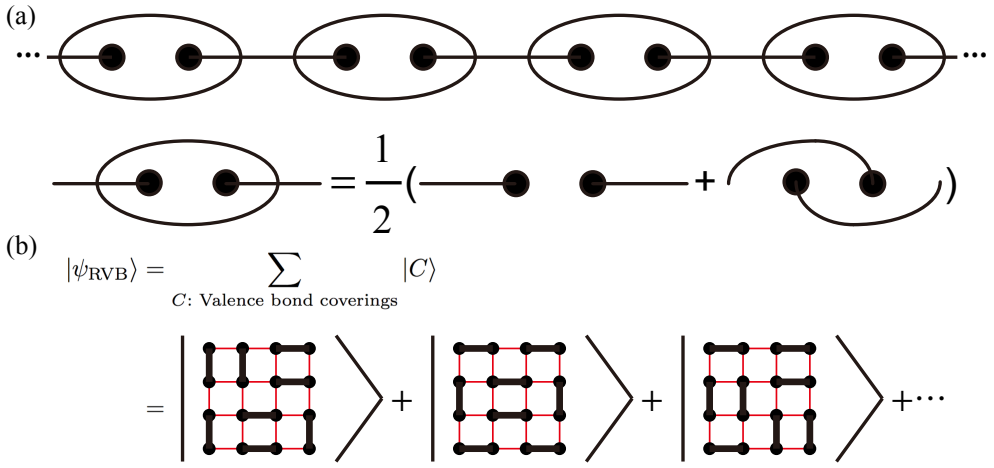


Figure 1.2: VBS and RVB states. (a) VBS ground state of the AKLT model. (b) RVB ansatz state, where $C$ is every possible valence bond covering on the square lattice.

## 1.1 SU(2) spin systems and quantum spin liquids

Among two-dimensional (2D) SU(2) spin systems, a QSL state was first proposed on the triangular lattice by P. W. Anderson [30–32]. He proposed a symmetric ground state called resonating valence bond (RVB) as a candidate ground state for the SU(2) Heisenberg model (Eq. (1.2)) on the triangular lattice.

$$H_{\mathrm{Heisenberg}} = J \sum_{\langle jk \rangle} \boldsymbol{S}_j \cdot \boldsymbol{S}_k, \tag{1.2}$$

where a coupling $J = 4t^2/U$ is determined from a hopping $t$ and an interaction strength $U > 0$ of the underlying Hubbard model. Though the true ground state for this model (spin-1/2) was found to have long-range ordering with a 120-degree antiferromagnetic configuration later [33, 34], some triangular organic/inorganic materials are found to be QSLs in experiments [35, 36]. Although we can still hope to explain such a spin liquid state in the weak-coupling regime of the Hubbard model [37], we focus on the SU(2) Heisenberg model in this section.

Before going on to the RVB state, we quickly discuss a valence bond solid (VBS) state to show what a valence bond is. A valence bond is a singlet pair of spins and the periodic alignment of valence bonds on the lattice is called VBS. This state is known to be a ground state of the Majumdar-Ghosh model [38], or more famously of the Affleck-Kennedy-Lieb-Tasaki (AKLT) model [39–41] after the projection onto the spin-1 Hilbert space [see Fig. 1.2(a)]. In these VBS states, spin-1/2 excitations are confined and are not included in QSLs. We can regard an RVB state as an disordered version of the VBS configuration.

Though the RVB state is a bad guess for the square lattice (even for the triangular lattice), it is instructive to investigate its property first. In fact, it is known that the RVB ground state is an exact ground state for a dimer model on the square lattice at a

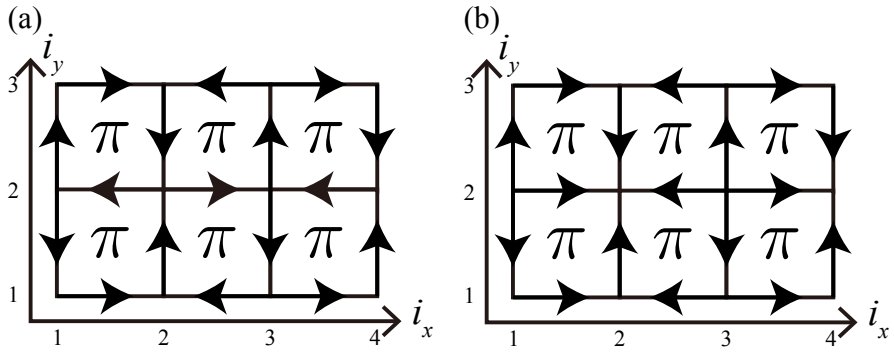


Figure 1.3: Affleck-Marston's $\pi$-flux mean-field ansatz. (a) Symmetric gauge. (b) Real (or pure imaginary) gauge. Arrows determine the direction of $\langle j \to k \rangle$ in the Hamiltonian and $(i_x, i_y)$ labels each site of the square lattice.

fine-tuned point called Rokhsar-Kivelson point [42],[1] though it is supposed to be unstable on the square lattice. Just to catch a feeling, it is a good starting point to show a form of its wavefunction.

$$|\psi_{\mathrm{RVB}}\rangle = \sum_{C\text{: Valence bond coverings}} |C\rangle\,, \tag{1.3}$$

where $C$ is every possible valence bond covering, *i.e.* the way in which the lattice is completely covered by valence bonds (singlet pairs), and the square lattice case is illustrated in Fig. 1.2(b).

This RVB ground state shows the following important properties and we adopt these three features as the definition of a QSL [43]:

1. Absence of magnetic long-range order.
2. Absence of spontaneous symmetry breaking.
3. Existence of fractionalized excitations.

We note that the second one is necessary to exclude the case where the ground states are degenerate because of spontaneous symmetry breaking. Actually, the RVB state does not break any space group symmetries of the square lattice, and all the correlations are apparently short-ranged, though the state itself shows a *long-range entanglement*, which is a critical feature of QSLs. The existence of fractionalized excitations called spinons is intuitively understood as follows. First, we can locally excite a valence bond by changing a singlet into a triplet. Then, due to the superposition of all the possible coverings on the spin-1/2 lattice model, the separation of the excited triplet pair (of spinons!) does not cost energy. This is contrary to VBS where the separation of the excited pair costs energy proportional to the distance. In this sense, we can think that almost free spin-1/2 spinons are fractionalized excitations in the RVB state. They are called "fractionalized" in the sense that they carry a spin-1/2 degree of freedom instead of spin-1 for magnons, and are fermionic despite the fact that the system was originally bosonic.

[1] In the Rokhsar-Kivelson state, $|C\rangle$ are orthogonal with each other.

Similarly to the above mentioned RVB state, Affleck and Marston [44, 45] proposed the so-called $\pi$-flux ansatz state for the square lattice QSL. We can also regard this $\pi$-flux state as one variation of generalized RVB states, and it obeys three definitions of QSL. The derivation requires a large-$N$ limit, which will be discussed in Sec. 1.3, so we here only present a mean-field parton model to describe this state.

$$H_{\mathrm{MF}} = -\chi_0 \sum_{\langle j\to k\rangle,\,\sigma} (e^{\frac{i\pi}{4}} f^\dagger_{j\sigma} f_{k\sigma} + h.c.), \tag{1.4}$$

where $f^\dagger_{j\sigma}$ and $f_{j\sigma}$ are creation and annihilation operators for spinons with a spin $\sigma = \uparrow, \downarrow$ at the $j$th site. The condition $\sum_\sigma f^\dagger_{j\sigma} f_{j\sigma} = 1$ for each $j$ maps the spinon representation to the original spin model, as will be discussed in Sec. 1.3. The direction of $\langle j \to k\rangle$ is always determined by Fig. 1.3(a). This is called $\pi$-flux state because a magnetic flux inside each plaquette is always $\pi$ and spinons feel $-1$ phase factor from the Aharonov-Bohm effect.

Here we used one of the most symmetric gauges on the square lattice, and this is why an imaginary part appears in the hopping. Such a gauge does not necessarily exist for other lattices, so we always use a real gauge with only $\pm 1$ in the latter part. In such a gauge, the Hamiltonian is transformed into

$$H'_{\mathrm{MF}} = -\chi_0 \sum_{\langle j\to k\rangle,\,\sigma} (i f^\dagger_{j\sigma} f_{k\sigma} + h.c.), \tag{1.5}$$

where a factor $i$ is actually unnecessary, and we will omit it from now on to make it real [43]. The direction of $\langle j \to k\rangle$ is always determined by Fig. 1.3(b). The sign has been changed to meet the $\pi$-flux condition. It seems that assigning mean-field variables to meet the $\pi$-flux condition (the product of the phase factors around each plaquette must be $-1$) always breaks translation and other lattice symmetries, but all the lattice symmetries are correctly implemented *projectively* in this model and gauge degrees of freedom ignored in this mean-field form always compensate the symmetry transformation. Thus, there is no spontaneous symmetry breaking or long-range ordering.

One traditional way to understand this kind of phenomena in QSLs is the projective symmetry group (PSG) theory [46].[2] We will not review the entire theory of this framework because usually counting all PSGs is not efficient, but we will check how it works in some specific models. In the case of Affleck-Marston's $\pi$-flux ansatz, the gauge structure is known to be SU(2) and it is a mother of many other spin liquid states. Actually, the spectrum includes two Dirac cones [43] and the translation symmetry is implemented projectively. As shown in Fig. 1.3(b), the translation along the $x$-axis (or $y$-axis) changes the sign of hopping matrix $U^0_{jk}$. However, this sign can be absorbed by a gauge transformation defined by $W_i = (-1)^{i_y}$, where the coordinate of the $i$th site is defined as $(i_x, i_y)$ shown in Fig. 1.3, because $W_j = -W_k$ for any nearest-neighbor bond $\langle jk\rangle$ along the $y$-axis. Thus, as soon as the translation changes $U^0_{jk}$ into $\tilde{U}^0_{jk} = -U^0_{jk}$, we can do a gauge transformation $W_i \tilde{U}^0_{jk} W^\dagger_j = U^0_{jk}$ to recover the translation symmetry. In spin liquids, the symmetry is usually supplemented by an additional gauge transformation explained by PSG. We also

[2] The naming of PSG is confusing because the group itself is extended, not projective. What is projective in this theory is its representation.

review PSGs of Kitaev models [47] in Appendix B.[3]

Even though the SU(2) Heisenberg models on the square and triangular lattices have a long-range order at zero temperature, there is still a hope to find a 2D lattice whose Heisenberg model hosts a QSL. In order to kill any classical magnetic ordering, the lattice has to have a strong geometric frustration. One of the most important possibilities is a kagome lattice, and most studies support the claim that the SU(2) Heisenberg model on the kagome lattice has no magnetic ordering [48, 49]. Although the nature (*e.g.* PSG) of the observed QSL is still under debate, many numerical studies suggest the existence of a gapped $Z_2$ spin liquid or a gapless $U(1)$ spin liquid in this model [48, 50].

As for three-dimensional (3D) SU(2) spin systems, a quantum spin ice state is expected on nearly SU(2)-symmetric pyrochlore antiferromagnets, for example. The Heisenberg model (or more correctly an XXZ-type model) on the pyrochlore lattice is actually related to a dimer model on the diamond lattice (more correctly it can be mapped to a 6-vertex model on the diamond lattice), and perturbatively realize the physics of RVB states [5, 51]. Numerically, the 6-vertex model on the diamond lattice is shown to host a gapless U(1) spin liquid in the wide range of parameters by sign-free quantum Monte Carlo (QMC) simulations [52]. This asymptotically shows the existence of a U(1) spin liquid in the Heisenberg model on the pyrochlore lattice.

## 1.2 Spin-orbit coupling and Kitaev spin liquids

So far we discussed a quantum spin liquid in completely SU(2)-symmetric systems with geometric frustration, but another type of frustration, called exchange frustration, can be introduced by destroying the SU(2) symmetry. Usually this can be realized in heavier elements with a strong SOC because in $4d$ or $5d$ transition metals spin interactions become highly anisotropic and bond-dependent. This results in bond-dependent interactions with noncommuting operators, and leads to frustrations between "exchange" Hamiltonians for each bond. This new type of frustration can be found especially in iridates or Ru-compounds, which would potentially realize the Kitaev model [47]. This model is interesting because it is exactly solvable *e.g.* on the honeycomb lattice. See Appendix B for more details. The discussion here follows Ref. 53. We use a first-quantization picture for simplicity, though we use a second-quantization picture in the rest of the thesis.

The Kitaev model on the honeycomb lattice is defined as follows.

$$H_{\text{Kitaev}} = K_x \sum_{\langle jk\rangle\in a} S_j^x S_k^x + K_y \sum_{\langle jk\rangle\in b} S_j^y S_k^y + K_z \sum_{\langle jk\rangle\in c} S_j^z S_k^z \tag{1.6}$$

where $\langle jk\rangle \in \alpha$ means that a nearest neighbor bond $\langle jk\rangle$ belongs to the $\alpha$-bond, and $K_x$, $K_y$, and $K_z$ are real parameters. $a$-, $b$-, and $c$-bonds are defined as bonds on the $yz$-, $zx$-, and $xy$-planes, respectively, as shown in Fig. 1.4(c). This $abc$-notation will be used in the main text.[4] This model actually has a gapless or gapped spin liquid ground state

[3] The meaning of PSG in exactly solvable Kitaev models is slightly different from that of mean-field solutions because it describes a "direct" action of the symmetry on quasiparticles. See *e.g.* Appendix F of Ref. 47 for the gapped case.

[4] Some may think that it is better to use $K_a$, $K_b$, and $K_c$ for Kitaev parameters, but here we followed the standard notation.

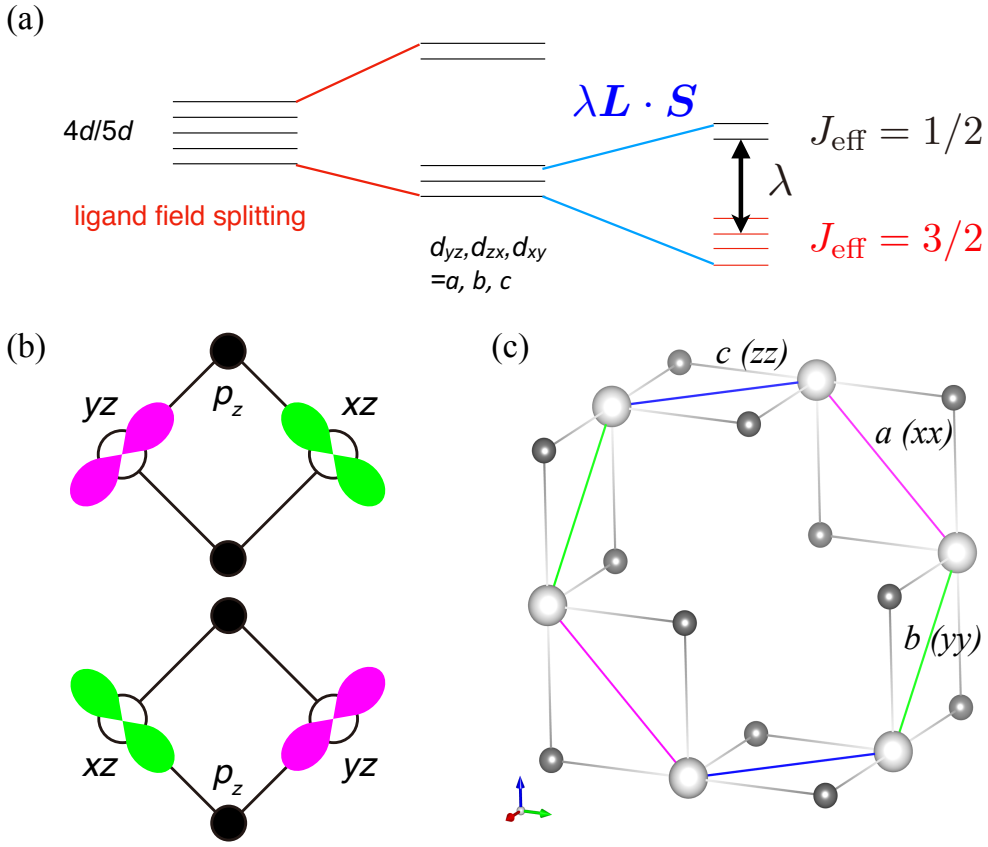


Figure 1.4: Jackeli-Khaliullin mechanism. (a) Energy splitting of the $d$-orbitals in the octahedral ligand field. (b) Superexchange pathways for $c$-bonds between the two adjacent $Ru^{3+}$ or $Ir^{4+}$ ions. There are two possible pathways between $yz$ and $xz$, and between $xz$ and $yz$. (c) Structure of $\alpha$-$RuCl_3$ or $\alpha$-$A_2IrO_3$-type iridates ($A$ = Li, Na). If it is seen from the (111) direction, the structure is basically the layered honeycomb lattice, and the bond direction becomes ideal to realize the Kitaev interaction. Magenta, light green, and blue bonds represent $a$-, $b$-, and $c$-bonds on the $yz$-, $zx$-, and $xy$-planes, respectively. We note that we used magenta instead of red used in the following part for $a$-bonds to show them more clearly.

depending on its parameter, as discussed in Appendix B. Here we would only discuss how such a bond-dependent exchange frustration arises in real materials. In fact, Jackeli and Khaliullin [14] discovered that the onsite spin-orbit coupling of the $Ir^{4+}$ (or $Ru^{3+}$) ion in the octahedral coordination can indeed produce this type of models in the Mott insulator limit with a strong Hubbard $U$, while there is also a proposal for a topological insulator in the itinerant limit [54].

We will consider the low-spin (*i.e.* spin-1/2) $d^5$ system of the transition metal. Following Jackeli and Khaliullin, we assume iridates (*i.e.* Ir-oxides) with the $Ir^{4+}$ ions in the strong (infinite) octahedral ligand field, but the same thing will apply to other $d^5$ metal ions like $Ru^{3+}$ as long as they show the low-spin configuration. The strong octahedral ligand field breaks 5-fold degenerate $5d$-orbitals into 2-fold degenerate $e_g$-orbitals and 3-fold degenerate $t_{2g}$-orbitals.[5] The $d^5$ electronic configuration can be regarded as a situation where one hole is put on the closed $t_{2g}$-shell. Moving on to the hole picture, the local ground state for this hole has 6-fold degeneracy, 3 coming from the orbital degrees of freedom and 2 coming from the spin degrees of freedom.

In this hole picture, the onsite SOC can be treated as follows. The effective orbital angular momentum operator $\boldsymbol{l}_{\mathrm{eff},j}$ can be defined for each $t_{2g}$-manifold of $Ir^{4+}$ because which orbital the hole belongs to among the $yz$-, $xz$- and $xy$-orbitals (we use a basis set ${}^t(|yz\rangle, |xz\rangle, |xy\rangle)$ for these orbitals, respectively, and represent the transformation/rotation of this triplet by a $3 \times 3$ matrix) can be regarded as the vector representation of the (cubic) rotational symmetry. Clearly, it is a triplet with $l_{\mathrm{eff}} = 1$ with $|l^z = 0\rangle = |xy\rangle$, $|l^z = \pm 1\rangle = -(i|xz\rangle \pm |yz\rangle)/\sqrt{2}$, and onsite SOC conserves the local total angular momentum $\boldsymbol{J}_{\mathrm{eff},j} = \boldsymbol{l}_{\mathrm{eff},j} + \boldsymbol{S}_j$ for each $j$. The onsite SOC has the form of antiferromagnetic interaction between the effective orbital angular momentum and the spin angular momentum for each $j$ in the hole picture, as follows.

$$H_{\mathrm{SOC}} = \sum_j [\lambda \boldsymbol{l}_{\mathrm{eff},j} \cdot \boldsymbol{S}_j + \Delta_z (l^z_{\mathrm{eff},j})^2], \tag{1.7}$$

where $\lambda > 0$ is the strength of the onsite effective SOC and $\Delta_z$ is the tetragonal distortion of the $IrO_6$ octahedra along the $z$-direction. When $\Delta_z = 0$ the ground state Kramers doublet is clearly a $J_{\mathrm{eff}} = 1/2$ doublet, and in the general case, the ground state doublet (pseudospin) can be written as

$$|\tilde{\uparrow}\rangle = \sin\theta\,|0\rangle \otimes |\uparrow\rangle - \cos\theta\,|+1\rangle \otimes |\downarrow\rangle\,, \tag{1.8}$$

$$|\tilde{\downarrow}\rangle = \sin\theta\,|0\rangle \otimes |\downarrow\rangle - \cos\theta\,|-1\rangle \otimes |\uparrow\rangle\,, \tag{1.9}$$

where the left-hand side of $\otimes$ means the value of $l^z_{\mathrm{eff}}$, and the right-hand side means $S^z$, while $\theta$ parametrizes the tetragonal distortion as $\tan(2\theta) = 2\sqrt{2}\lambda/(\lambda - 2\Delta_z)$. In the following, we assume $\Delta_z = 0$, $\sin\theta = 1/\sqrt{3}$, *i.e.* the completely cubic case, for simplicity.

As shown in Fig. 1.4(b), the superexchange hopping pathways between the two adjacent $Ir^{4+}$ ions $j$ and $k$ in the case of $c$-bonds via the oxygen $p$-orbitals with 90-degree

[5] These $t_{2g}$-orbitals split into a famous $J_{\mathrm{eff}} = 1/2$ doublet and a $J_{\mathrm{eff}} = 3/2$ quartet by SOC, as shown in Fig. 1.4(a), and here we will use the former.

configuration can be written as the following matrix.

$$H_{\rm hop}^{k\leftarrow j} = \begin{pmatrix} 0 & -t & 0 \\ -t & 0 & 0 \\ 0 & 0 & 0 \end{pmatrix} \otimes I_2, \tag{1.10}$$

where $I_m$ is the $m \times m$ identity matrix, acting on the spin space in this case, and $t$ is the real hopping parameter between $xz$ and $yz$-orbitals via the oxygen $p$-orbitals as shown in Fig. 1.4(b). The most important observation is that this matrix has no matrix elements between the adjacent $J_{\rm eff} = 1/2$ doublets and, therefore, there is no contribution to the antiferromagnetic exchange interaction due to the Pauli principle if we project this superexchange interaction onto the $J_{\rm eff} = 1/2$ pseudospin model. Thus, if we make the $J_{\rm eff} = 1/2$ pseudospin model from this hopping, the strongest interaction we have to consider is the contribution from the second-order perturbation involving the onsite ferromagnetic Hund interaction between the $J_{\rm eff} = 3/2$ and $J_{\rm eff} = 1/2$ orbitals on the $k$th site. The second-order contribution is just a hole going from $J_{\rm eff} = 1/2$ on $j$ to $J_{\rm eff} = 3/2$ on $k$ and then coming back from $J_{\rm eff} = 3/2$ on $k$ to $J_{\rm eff} = 1/2$ on $j$, while, on the other side, the other hole remains sitting in the $J_{\rm eff} = 1/2$ manifold on $k$. This perturbative contribution can roughly be estimated as the following effective Hamiltonian.

$$\begin{aligned} H_{\rm eff}^{t_{2g}} &= \frac{H_{\rm hop}^{j\leftarrow k} H_{\rm hop}^{k\leftarrow j}}{-(\Lambda - J_H \boldsymbol{S}_j \cdot \boldsymbol{S}_k)} && (1.11) \\ &\sim \frac{1}{\Lambda^2} H_{\rm hop}^{j\leftarrow k} H_{\rm hop}^{k\leftarrow j} \cdot (-J_H \boldsymbol{S}_j \cdot \boldsymbol{S}_k) \\ &= -\frac{J_H t^2}{\Lambda^2} P_{l^z=\pm 1}(\boldsymbol{l}_{{\rm eff},\, j}) \boldsymbol{S}_j \cdot \boldsymbol{S}_k, && (1.12) \end{aligned}$$

where $J_H > 0$ is the ferromagnetic Hund interaction inside the same ion, $\Lambda$ is the potential energy for the excited $J_{\rm eff} = 3/2$ state which is almost proportional to $\lambda$, and $P_{l^z=\pm 1}$ is a projection operator onto the manifold with a condition $l^z = \pm 1$. By projecting this effective Hamiltonian onto the pseudospin system with only $J_{\rm eff} = 1/2$ degrees of freedom, we finally get the ferromagnetic Ising interaction with anisotropy along the $z$-direction because the operator $P_{l^z=\pm 1}(\boldsymbol{l}_{{\rm eff},\, j})$ and the projection onto $J_{\rm eff} = 1/2$ will completely kill the terms $S_j^+ S_k^-$ and $S_j^- S_k^+$. The final form of the interaction between two adjacent spins becomes

$$H_{\rm eff}^{J_{\rm eff}=1/2} \sim -\frac{J_H t^2}{\lambda^2} \cos\theta(\sin\theta + \cos\theta) J_{{\rm eff},\, j}^z J_{{\rm eff},\, k}^z, \tag{1.13}$$

assuming $\Lambda \propto \lambda$. This $z$-directional anisotropy comes from the oxygen configuration in the $xy$-plane. Thus, in the honeycomb geometry of a (111) thin film of iridates as shown in Fig. 1.4(c), the whole interactions between $J_{\rm eff} = 1/2$ pseudospins become the Kitaev model assuming the perfect cubic coordination and the 90-degree oxygen configuration.

Because the superexchange Kitaev interaction coming from this mechanism is ferromagnetic, it is advantageous to realize the Kitaev spin liquid phase in the Kitaev-Heisenberg model (*i.e.* the sum of the Kitaev model and the nearest-neighbor Heisenberg model) on the honeycomb lattice, which is known to be more stable in the ferromagnetic case than in the antiferromagnetic case [55, 56].

Additionally, Kitaev [47] discussed the classification of symmetry-enriched topological (SET) phases of the Kitaev model and the toric code [57] based on a modern theory of weak symmetry breaking, but we will follow the PSG theory [46] in this thesis for simplicity. Thermodynamic properties of the Kitaev model were also examined by QMC due to the accidental absence of a sign problem on this model [58]. The sign problem of QMC is a major theoretical difficulty to study spin liquids, but we will not discuss this point in this thesis.[6]

## 1.3 SU($N$) spin systems and large-$N$ limits

Here we review the physics of one-dimensional (1D) and 2D SU($N$) systems. Increasing the number of flavors to a large $N$ actually leads to the third type of quantum frustration. Even in the 1D case there is macroscopic degeneracy of classical ground states in 1D SU($N$) antiferromagnets when $N > 2$, suggesting a possibility that increasing $N$ results in a large quantum (zero-point) oscillation in any dimensions. When $N = 2$, the corresponding classical model is the Ising model with two states $\sigma = \uparrow, \downarrow$ per site. Thus, antiferromagnetic ground states are just twofold degenerate in the 1D Ising model. When $N > 2$, (even with $N = 3$) if we label an onsite degree of freedom by A, B, and C, then the ground states of this classical model are already macroscopically degenerate even in one dimension, including *e.g.* ABABABABABAB, ABCABCABCABC, ACBCACBCACBC, etc. This degenerate classical ground state manifold allows us to construct a highly-entangled quantum ground state by a macroscopic superposition of such states, leading to a possibility of realizing a *long-range entangled* state in higher dimensions. Although a real $N \to \infty$ limit is classical, for an intermediate $N$ quantum fluctuation gets stronger than either $N = 2$ or $N \to \infty$ and it possibly leads to a new QSL state.

First, let us discuss how to generalize the SU(2) Heisenberg interaction to general cases. As we already discussed, the SU(2) Heisenberg interaction can be rewritten in terms of a swapping operator $P_{jk}$ between the $j$th and $k$th sites. Thus, a natural generalization of the SU($N$) Heisenberg interaction with $N > 2$ is also written by this swapping operator for SU($N$) fundamental representations.

$$H_{\mathrm{SU}(N)} = \frac{J}{N} \sum_{\langle jk \rangle} P_{jk}, \tag{1.14}$$

where $J$ is the Heisenberg term. The Hilbert space is defined by putting a fundamental representation spin on each site of the lattice. We note that any representations can be used to define a similar model, but we only consider a fundamental representation in this thesis. Let us simply check that this is a natural generalization for the $N = 2$ and spin-1/2 case by looking at a two-body model. The energy splitting according to the representation can be described by the following Young tableaux. Each box represents fundamental representation of SU($N$), and change in the dimension of the representation is shown below.

[6] The origin of the sign problem of the SU(4) Heisenberg models on 2D bipartite lattices is quite complicated.

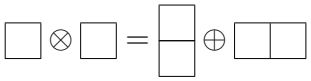

$$N \times N = \frac{N(N-1)}{2} + \frac{N(N+1)}{2}. \tag{1.16}$$

As easily seen from the above diagrams, a two-body model $P_{jk}$ simply separates the anti-symmetrized state from the symmetrized state and $N(N-1)/2$ states have a lower energy out of the original $N^2$ states. We note that in the $N = 2$ case only a singlet state has the lower energy, but in the $N > 2$ case the two-body solution still has (macroscopic) degeneracy and finding a quantum ground state out of degenerate "valence bond" coverings is already a nontrivial problem when the system is constructed over some periodic lattice.

Next, let us discuss the 1D chain of the SU($N$) Heisenberg model [59]. An accurate description requires non-Abelian bosonization [60], but we will qualitatively explain it using a naïve Tomonaga-Luttinger liquid theory [61–64]. The SU($N$) Heisenberg model can always be derived from the SU($N$) Hubbard model at $1/N$ filling:

$$H_{\text{Hubbard}} = -t \sum_{\langle jk \rangle} (c^\dagger_{j\alpha} c_{k\alpha} + h.c.) + \frac{U}{2} \sum_j n_j (n_j - 1), \tag{1.17}$$

where a fermion $c_{j\alpha}$ has a flavor (index) $\alpha = 1, 2, \ldots, N$, and a number operator $n_j = \sum_\alpha c^\dagger_{j\alpha} c_{j\alpha}$. At $1/N$ filling with a large $U/|t|$ a metal-insulator transition to a Mott insulator always happens. In the $U/|t| \to \infty$ limit, the Hilbert space is spanned by states with exactly one fermion per site, and the (degenerate) second-order perturbation inside this Hilbert space is always reduced to Eq. (1.14).

A metal-insulator transition into a Mott insulator usually accompanies some magnetic order, but in one dimension the enhanced quantum fluctuation is known to suppress any long-range ordering, leading to a gapless liquid state with spinon excitations, as is well-known in the case $N = 2$. Every correlation decays algebraically, resulting in a "solvable" liquid state. This is the famous Tomonaga-Luttinger liquid theory, where the charge and "spin" degrees of freedom are separated, and only the charge sector is gapped in the Mott-insulating phase. Thus, the only thing left in the $U/|t| \to \infty$ limit, *i.e.* Eq. (1.14), is a gapless "spin" liquid with $N - 1$ fermionic spinon excitations. They are described by the theory of bosonization. We note that a 1D SU(4) Heisenberg chain is also free of a sign problem and its thermodynamic property has been investigated very well [65]. The results almost agree with the previous studies based on bosonization [60], so we have unbiased reproduction of the effective theory in the $N = 4$ case. If we separate $N = 4$ degrees of freedom into the spin sector and the orbital sector, we can name fractionalized orbital excitations orbitalons.

From now on we would like to discuss an SU($N$) Heisenberg on the 2D square lattice. In this case a large $N$ limit is actually useful for an intermediate $N$ region, though for $N \leq 4$ the ground state is known to be ordered in most numerical simulations. In a real $N \to \infty$ limit, the mean-field theory suggests the ground state to be a chiral spin liquid (CSL) state. CSL is not a QSL in a strict sense because it spontaneously breaks the time-reversal symmetry with an effective magnetic field acting on quasiparticles. However, apart from

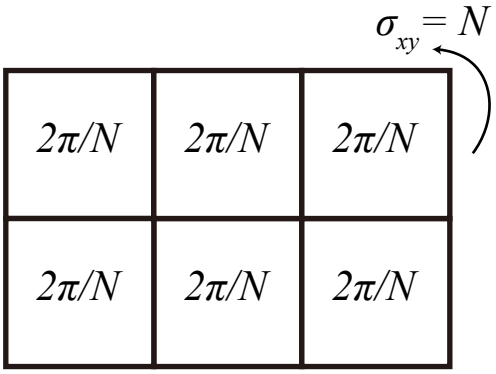


Figure 1.5: Chiral spin liquid state proposed in Ref. 26. The fractional flux inside each plaquette breaks the time-reversal symmetry giving a quantum Hall conductance of $\sigma_{xy} = N$ in a dimensionless form.

that, CSL states are usually regarded as a variant of QSLs without an explicit long-range correlation (in two-body operators) and with fractionalized topological excitations assuming the existence of a gap.

In the same spirit as we used the Hubbard model to describe spinons, we can represent spin operators by fermions in the fundamental representation of SU($N$). Since swapping operators can be decomposed into a product of two hopping terms $f^\dagger_\alpha f_\beta$ and $f^\dagger_\beta f_\alpha$, assuming SU($N$) spin operators are represented as $S^\beta_\alpha = f^\dagger_\alpha f_\beta$ for each site,[7] so

$$H_{\mathrm{SU}(N)} \propto \sum_{\langle jk\rangle,\alpha,\beta} f^\dagger_{j\alpha} f_{j\beta} f^\dagger_{k\beta} f_{k\alpha}, \tag{1.18}$$

where $f_{j\alpha}$ is a spinon annihilation operator with $\alpha = 1, \ldots, N$ on the $j$th site. By imposing a constraint $\sum_\alpha f^\dagger_{j\alpha} f_{j\alpha} = 1$ for each $j$, which is the same as the $U \to \infty$ limit of the Hubbard model, the model is exactly mapped to the original SU($N$) Heisenberg model. The four-fermion terms can be decomposed by a mean-field approximation [44,45].

After introducing this (Schwinger-Wigner) fermionic representation, taking an $N \to \infty$ limit is the same as considering a classical solution at a saddle point,[8] and the problem results in finding a solution of the following self-consistent equations.

$$H_f = -\sum_{\langle jk\rangle,\alpha} \left( \chi_{jk} f^\dagger_{j\alpha} f_{k\alpha} + h.c. \right), \tag{1.19}$$

$$\chi_{jk} = \left\langle \sum_\beta f^\dagger_{k\beta} f_{j\beta} \right\rangle, \tag{1.20}$$

where the expectation value is taken for a free-fermionic model $H_f$.

Though it is still approximate to find out a solution in the sense that there is no way to impose a local number constraint in classical calculations, for $5 \leq N \leq 10$ (or even

[7] $S^\beta_\alpha$ operators are redundant because only $N^2 - 1$ components are independent

[8] There is a subtlety when taking this limit [26].

$5 \leq N$), the following CSL solution is known to be a large-$N$ solution [26]: $|\chi_{jk}| = \chi_0$ is a constant and the phase of $\chi_{jk}$ is determined for each square plaquette to carry a $2\pi/N$ flux, *i.e.* $\prod_{\langle jk\rangle \in C} \chi_{jk} = \chi_0^4 e^{\frac{2\pi i}{N}}$ for each plaquette $C$. We will omit a fluxoid quantum to make it dimensionless.

This solution is very similar to the lattice quantum Hall state with a fractional flux quantum $2\pi/N$ per plaquette and it is expected to host anyonic excitations, useful for universal quantum computation, after the Gutzwiller projection. This ansatz is the same as Affleck-Marston's when $N = 2$, and only in this case it does not break the time-reversal symmetry.[9] When $N > 2$, it is a CSL with a fractional magnetic flux, and only if $N > 4$ it can possibly be a ground state of the SU($N$) Heisenberg model on the square lattice. Though a large-$N$ limit is always a classical saddle-point solution, it is a good starting point even for an intermediate $N$, and it is expected that the $1/N$ correction includes a quantum fluctuation which is neglected in the mean-field model without a gauge degree of freedom. A real QSL/CSL must have a gauge fluctuation, which is exemplified in the Kitaev model for example [see Appendix B], so we should always confirm that the quantum fluctuation does not destroy the classical state, as is the case with a small $N$.

## 1.4 Lieb-Schultz-Mattis theorem and its extension

In order to clarify the relation between the absence of spontaneous symmetry breaking or long-range ordering and the existence of fractionalized excitations, we would like to discuss an important theorem called Lieb-Schultz-Mattis (LSM) theorem [29] and its extension by Oshikawa [67, 68] and Hastings [69]. The discussion here follows Ref. 53 and some proofs are included in Appendix A.

Let us begin with the 1D case, where the quantum fluctuation is strong enough to destroy any kinds of magnetic ordering. For a 1D SU(2) Heisenberg (or more generally XXZ) chain, the Bethe ansatz solution indicates the existence of gapless spinon excitations above the ground state. Such spinon excitations are sometimes regarded as fractionalized because they are spin-1/2 instead of spin-1 for magnons. The gapless nature of the $S = 1/2$ Heisenberg chain is protected by the LSM theorem [29] and there cannot exist a gapped ground state with no ground state degeneracy (GSD) for the spin-1/2 (or half-odd-integer spin) chain [70]. We assume the lattice translation symmetry, the $S^z_{\mathrm{tot}}$ conservation, and the bond-centered space-inversion (or time-reversal) symmetry of the Hamiltonian, all of which are natural for quantum spin liquids, and also assume that the ground state is unique in a finite system. Then, it is straightforward to prove the LSM theorem by introducing the following twist operator $U$.

$$U := \exp\Big[i \sum_{j=1}^{L} \frac{2\pi j}{L} S^z_j\Big], \tag{1.21}$$

where $\boldsymbol{S}_j$ is a spin operator in the usual definition (assuming $\hbar = 1$) and $\boldsymbol{S}_j = \boldsymbol{\sigma}_j/2$ for the spin-1/2 case. This $U$ can be regarded as a creation operator for the lowest-energy "spin

[9] This is because $\pi = -\pi \pmod{2\pi}$. Such a magnetic field is only available on neutron stars [66] and exists only *emergently* on earth.

wave" excitation, so $|\Psi_t\rangle := U|\Psi_0\rangle$ would be the first excited state. This is orthogonal to the ground state, *i.e.* $\langle\Psi_0|\Psi_t\rangle = 0$ as follows.

$$\begin{aligned}\langle\Psi_0|\Psi_t\rangle &= \langle\Psi_0|U|\Psi_0\rangle = \langle\Psi_0|T^{-1}UT|\Psi_0\rangle \\ &= \langle\Psi_0|U\exp\left[-i\frac{2\pi}{L}S^z_{\rm tot}\right]\exp(2\pi iS^z_1)|\Psi_0\rangle = -\langle\Psi_0|U|\Psi_0\rangle\,, \end{aligned} \tag{1.22}$$

using $S^z_{\rm tot} = 0$ for the ground state, and an operator identity $\exp(2\pi iS^z_1) = -1$ for half-odd spins, where $T$ is a translation operator. With a 1D local Hamiltonian $H$, the energy difference $\langle\Psi_t|H|\Psi_t\rangle - \langle\Psi_0|H|\Psi_0\rangle = \mathcal{O}(L^{-1})$ becomes zero due to the inversion (or time-reversal) symmetry of the ground state. Here we illustrate the proof in the specific case of the XXZ model. The XXZ model is defined as,

$$H = \sum_j H_j, \tag{1.23}$$

$$H_j = S^x_jS^x_{j+1} + S^y_jS^y_{j+1} + \Delta S^z_jS^z_{j+1}. \tag{1.24}$$

Therefore, $\langle\Psi_t|H_j|\Psi_t\rangle - \langle\Psi_0|H_j|\Psi_0\rangle \propto \langle\Psi_0|\frac{i}{L}[S^+_jS^-_{j+1} - S^-_jS^+_{j+1}] + \mathcal{O}(L^{-2})|\Psi_0\rangle$ and the order $1/L$ term vanishes due to the inversion (or time-reversal) symmetry. Thus, $|\Psi_t\rangle$ becomes the degenerate ground state in the thermodynamic limit. This proves that either the system is gapless or the ground state is not unique (*i.e.* spontaneous symmetry breaking in 1D) in the thermodynamic limit of half-odd spin chains. This is consistent with the gapless nature of the spin-1/2 (and half-odd spin) Heisenberg chain(s). Nevertheless, as for the spin chain with an integer spin quantum number, the situation is different because $\exp(2\pi iS^z_1) = 1$.

LSM-type theorems are more important in higher dimensions because GSD suggests the existence of a so-called topological order. The generalization of the LSM theorem was done by Oshikawa [67, 68] and more rigorously by Hastings and others [69, 71]. The assertion for SU(2)-symmetric quantum spin models on the lattice from the Hastings-Oshikawa-Lieb-Schultz-Mattis (HOLSM) theorem [29, 67, 69] is the following.

**Theorem 1.** *For the spin system in 2D or higher dimensions, assuming the translation symmetry for the Hamiltonian and there are an odd number of total spin quantum numbers in the unit cell, the ground state of the lattice spin system must either be gapless, break the spin-space or translation symmetry, or have multiple GSD.*

This theorem is intuitively understandable by the following arguments [72]. For simplicity, we here only consider the case with a spin-1/2 degree of freedom per unit cell. If we map a spin-1/2 lattice model into hard-core bosons, where spin up is an empty site and spin down is a site occupied by a boson. Then, a ground state with no GSD must have a half-odd filling of bosons. To get a featureless insulator[10] [73] from this bosonic system with a translation symmetry, the bosons must be fractionalized into half-charged entities, which is distributed uniformly in the lattice. Translated back to the spin language, this implies that to obtain a symmetric ground state, we need a spin-1/2 excitation in the bulk, but there is no local excitation carrying a spin-1/2 degree of freedom, and therefore it must be nonlocal (*i.e.* topological).

[10] A featureless insulator is usually defined as a symmetric gapped phase with a unique ground state.

In two or higher dimensions, GSD always implies the existence of topological order in gapped systems. We do not discuss the direct relationship between GSD and the nature of the topological order, but we quickly review an easy example of topological order. A 2D $Z_2$ topological order is the simplest Abelian topological order in closed gapped systems. This topological order is realized in the ground state of Kitaev's toric code [57] or the Kitaev model [47] in the gapped phase [see Appendix B]. These models have physically proven that the ground states with a topological order always carry fractionalized excitations above the energy gap. The $Z_2$ topological order is known to possess GSD depending on the genus if it is defined on the closed surface. If the genus of the surface is $g$, then GSD is $4^g$. The dependence of the ground states property on the global topology suggests the existence of a *long-range entanglement* in the system.

Many numerical results of a spin-1/2 antiferromagnetic Heisenberg model on the kagome lattice actually suggests the absence of magnetic ordering at very low temperature [48, 49]. We can simply conclude from the HOLSM theorem that, assuming the absence of spontaneous symmetry breaking, this model has either a gapless ground state or a gapped ground state with multiple GSD because it has odd number of spin-1/2 degrees of freedom in the unit cell. In either case, we can conclude that the ground state of the spin-1/2 antiferromagnetic Heisenberg model on the kagome lattice should be exotic with a fractionalized excitation beyond the Ginzburg-Landau theory,[11] and we will refer to this ground state as kagome spin liquid [53, 74]. Whether this kagome spin liquid is gapped or gapless is still under debate among both theorists and experimentalists. A gapped spin liquid with a $Z_2$ topological order is sometimes called $Z_2$ spin liquid, which is one of the most important candidates of the kagome spin liquids [48]. Another candidate is a Dirac spin liquid [74], which is similar to the Affleck-Marston state.

Though the meaning of a long-range entanglement in gapped systems is clear based on this topological order/GSD, it is subtle in gapless systems. There are many measures for it, such as entanglement entropy and entanglement spectrum, but we will not seek this direction deeply. We note that in the case of Ref. 8 the bond dimension $D$ for iPEPS calculations is used as a measure for quantum entanglement. More generally, in tensor network calculations including density matrix renormalization group (DMRG) this bond dimension is known to be a good measure to detect quantum entanglement of the ground state.

In relation to the main focus of this thesis, the extension of the theorem by Affleck and Lieb for SU($N$) spin systems [70] is more important. This is called Lieb-Schultz-Mattis-Affleck (LSMA) theorem and will be discussed in detail in Appendix A.

## 1.5 Dirac spin liquids in the SU(4) Heisenberg model

So far we explained previous candidates for QSLs with geometric/exchange frustrations. A fairly new approach was the SU($N$) magnetism and it has many advantages. Gapless excitations can be guaranteed by the LSMA theorem [see Appendix A], and QSLs with an SU($N$) symmetry without a symmetry breaking (not CSL) would be a great playground

[11] In the gapless case, this point is subtle but we can say that the excitations are exotic in the sense that it is still fractionalized even if we gap out these excitations without breaking the symmetry.

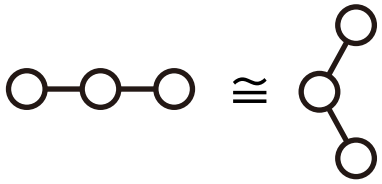

Figure 1.6: Accidental isomorphism between $\mathfrak{su}(4)$ and $\mathfrak{so}(6)$.

to study fractionalization of excitations. We already presented a theoretical background, but here we would like to introduce one concrete example of SU($N$) spin liquids, which is a main target of this thesis. We introduce parton mean-field theories for the SU(4) Heisenberg model. There are mainly two types of representations, a Schwinger-Wigner fermionic representation [46] and a Wang-Vishwanath Majorana representation [17]. The former is the same as Affleck-Marston's theory or the one used in Sec. 1.3, so let us first review an SO(6) Majorana representation for SU(4) spins. Though we will not use this representation in the main text, we quickly review it because it is beautiful and useful for $N = 4$.

There is a mathematical accidental isomorphism between Lie algebras $\mathfrak{so}(6)$ and $\mathfrak{su}(4)$, which is clearly reflected in their Dynkin diagrams [see Fig. 1.6]. An accidental isomorphism is always for Lie algebras, but we abuse terminology like SO(6) $\cong$ SU(4), for simplicity, to mention this fact.[12] Since SU(4) $\cong$ SO(6), there is also an isomorphism between an antisymmetric tensor representation of SU(4) and a vector representation of SO(6). Though we will not explicitly show this isomorphism, it is the reason behind the fact that we can construct an SO(6) Majorana representation.

The representation is similar to the one used by Kitaev for the SU(2) spin [47] except for the number of physical subspaces. First, similarly to the previous section, we divide the SU(4) fundamental representation into spin and orbital degrees of freedom. Then, a spin $\boldsymbol{S}_j$ and an orbital $\boldsymbol{T}_j$ can be decomposed into a cross product of two SO(3) Majorana fermions.

$$S_j^\gamma = -\frac{i}{4}\varepsilon^{\alpha\beta\gamma}\eta_j^\alpha\eta_j^\beta, \tag{1.25}$$

$$T_j^\gamma = -\frac{i}{4}\varepsilon^{\alpha\beta\gamma}\theta_j^\alpha\theta_j^\beta, \tag{1.26}$$

where $\varepsilon^{\alpha\beta\gamma}$ is a Levi-Civita symbol, and $\boldsymbol{\eta}$ and $\boldsymbol{\theta}$ are SO(3) Majorana fermions with $\{\eta_j^\alpha, \eta_k^\beta\} = \{\theta_j^\alpha, \theta_k^\beta\} = 2\delta_{jk}\delta^{\alpha\beta}$, and $\{\eta_j^\alpha, \theta_k^\beta\} = 0$. These 6 Majorana fermions per site have an SU(4) $\cong$ SO(6) symmetry. This representation is redundant and for each site an extended Hilbert space for Majorana fermions has a dimension $(\sqrt{2})^6 = 8$. Thus, we have to halve the dimension and project them onto the physical subspace in an SO(6)-symmetric way.

The simplest and most useful constraint for the projection is

$$i\eta_j^x\eta_j^y\eta_j^z\theta_j^x\theta_j^y\theta_j^z = 1 \quad \text{for } \forall j, \tag{1.27}$$

[12] Here, $\cong$ means local isomorphism.

or

$$i\eta_j^x\eta_j^y\eta_j^z\theta_j^x\theta_j^y\theta_j^z = -1 \quad \text{for}\,\forall j. \tag{1.28}$$

Differently from Kitaev's representation, both Eq. (1.27) and Eq. (1.28) can simplify the original Hamiltonian and result in the same Majorana Hamiltonian. In either case, all higher order terms in the original SU(4) Heisenberg model are reduced to quartic terms:

$$H_{\text{Majorana}} \propto -\frac{1}{8}\sum_{\langle jk\rangle}\left(i\boldsymbol{\eta}_j\cdot\boldsymbol{\eta}_k + i\boldsymbol{\theta}_j\cdot\boldsymbol{\theta}_k\right)^2. \tag{1.29}$$

Thus, at a saddle point we can simply define a real mean field to solve a self-consistent equation by $\chi_{jk}^R = \langle i\boldsymbol{\eta}_j\cdot\boldsymbol{\eta}_k + i\boldsymbol{\theta}_j\cdot\boldsymbol{\theta}_k\rangle$, and

$$H_{\text{MF}}^R = \sum_{\langle jk\rangle}\left[-\frac{\chi_{jk}^R}{4}\left(i\boldsymbol{\eta}_j\cdot\boldsymbol{\eta}_k + i\boldsymbol{\theta}_j\cdot\boldsymbol{\theta}_k\right) + \frac{(\chi_{jk}^R)^2}{8}\right]. \tag{1.30}$$

We note that the mean field $\chi_{jk}^R = -\chi_{kj}^R$ is always real, and Majorana fermions cannot feel a complex magnetic field like in a quantum Hall state. This is one important difference between a Majorana $\chi_{jk}^R$ mean field and a complex $\chi_{jk}$ mean field.

We note that there is no conservation of the fermion number except for the $Z_2$ parity, so usually we make a mean-field ansatz wavefunction by filling a Fermi sea until half filling, and do a Gutzwiller projection to the physical subspace, which is an approach similar to the Kitaev model [see Appendix B]. Two different fermionic approaches are *a priori* describing symmetric SU(4) spin liquids equally well with a symmetric flux ansatz which does not break any symmetry of the Hamiltonian. Since Lieb's theorem [66] is not applicable to the quarter-filling case, there is no *a priori* guess for the lowest-energy mean field.[13] In order to systematically compare energies for different mean-field assumptions, a variational Monte Carlo (VMC) method [75] is the most powerful numerical tool. Although we will not review the technical details for this method, as well as tensor network methods, we trust the results of VMC and infinite projected entangled-pair state (iPEPS) calculations [76, 77], and will not argue about the appropriateness of their methods.

From combined VMC and iPEPS calculations, the SU(4) Heisenberg model on the honeycomb lattice is expected to host a QSOL [8]. The state is roughly described by a $\pi$-flux Schwinger-Wigner ansatz with an algebraic decay in correlation. They compared 0-flux and $\pi$-flux states for both Schwinger-Wigner and Wang-Vishwanath representations, and found the $\pi$-flux Schwinger-Wigner state has the lowest energy, very close to the ground state energy. Since the spectrum of this $\pi$-flux state is described by a Dirac fermion (spinon) in the mean-field theory, the ground state must be a Dirac spin liquid with doubly degenerate Dirac cones. The gauge structure is unknown in the previous study. The Dirac cone spectrum is discussed in detail in Appendix B. If we use the language of spin-orbital systems, the unbroken SU(4) symmetry makes two types of fractionalized excitations, spinons and orbitalons, equivalent. This point would be discussed again in Chapter 3.

[13] Lieb's theorem may be applicable to the Majorana representation, but it works only within this representation.

We note that this $\pi$-flux ansatz is consistent with the famous Affleck-Marston argument [44], though there is no reason to assume such guiding principles to find out the correct flux sector. Indeed, a similar numerical analysis has been done for the hyperhoneycomb lattice [78], but it does not obey the Affleck-Marston rule.

## 1.6 Cold atomic realization

Motivated by theoretical interests, experiments to realize the SU($N$) magnetism in reality are also ongoing. Usual spin systems only have the SU(2) symmetry at most, so we have to seek for unusual experimental tools to increase the symmetry. Approaching SU(3) quantum chromodynamics (QCD) requires a very high energy, so we would need a low-energy effective SU($N$) symmetry in table-top systems. First, we would like to review the realization of SU($N$) systems in ultracold atoms. Although the main topic of this thesis is magnetic materials, atomic systems can also be regarded as some quantum simulator of spin models. Especially, the breakthrough in optical technology enables us to make an optical lattice, and inside this optical lattice we can simulate a periodic model Hamiltonian where atoms are hopping between modulated effective potentials induced by light. In order to realize "a Mott insulator" of atoms, we mainly focus on fermionic atom gases to realize spin models, where correlated electrons are replaced by interacting atoms themselves. This section follows a review paper [10].

Fermionic condensate can be realized in alkaline-earth atoms. We also include atoms like Yb into alkaline-earth atoms, though Yb is rare-earth. Those atoms (Sr, Yb, etc.) are often used as Fermi gases, and we here focus on alkaline-earth-atomic Fermi gases. For an alkaline-earth atom in the symmetric ground state ($^1S_0$), there are no degree of freedom with spin or orbital angular momentum, so nuclear spin ($F > 0$) is decoupled from the electronic state due to the absence of hyperfine interactions. Because of the electronic-nuclear spin decoupling in the fermionic isotopes, the scattering parameters involving the $^1S_0$ and $^3P_0$ states have to be independent of its nuclear spin. Thus, in the so-called clock states, all of the scattering lengths become equal. Under these conditions, the interaction and kinetic parts of the Hamiltonian are *emergently* SU($N$)-symmetric, where $N = 2F + 1$. Especially, $^{173}$Yb gases have the SU(6) symmetry and $N$ up to 10 is likely to be feasible [27, 79].

In addition to isolated gases, condensed matter systems like the SU($N$) Hubbard (or Heisenberg) model can be implemented in optical lattices. In order to simulate the periodic (Bloch) potential experienced by electrons in crystalline systems, we can use ultracold atomic gases by confining them in periodic arrays of light potentials [80]. Thus, SU($N$) physics discussed in previous sections can be realized in cold atoms.

Though most Fermi gases on the optical lattice are treated by the SU($N$) Hubbard model, in reality there exists a symmetry-breaking term, even in an ideal setup. In the case of $F = 3/2$ and $N = 4$, the symmetry is reduced to SO(5) $\subset$ SU(4) by additional interactions [81]. This is because the coupling of spin-3/2 and spin-3/2 results in two independent interaction terms with a total spin-0 and spin-2. We note that spin-1 is impossible because of the statistics. These terms in the form of a 4-component spinor no longer have an SU(4) symmetry, while they still have a (hidden) SO(5) symmetry. This mathematical structure will be discussed again in Sec. 2.7. It was proposed that $^{135}$Ba

and $^{137}$Ba are close to an ideal SU(4)-symmetric line [81]. Thus, these atoms are the most important candidates for SU(4) magnetism in ultracold systems.

Though SU($N$) Heisenberg models with an even $N$ may essentially be realized in the optical lattice,[14] the realization in magnetic materials also has many advantages because every technology accumulated for many decades in condensed matter physics is directly applicable. Magnetic materials can be investigated in moderate environment and requires no extreme technology of cooling or a laser control. From a theoretical perspective, a question "what is a realistic spin-(orbital) model feasible in real magnetic materials" is an important unresolved problem, though such problems are reduced to a technological one in cold atomic systems. This perspective in condensed matter theory has long been neglected, and, until Jackeli and Khaliullin [14] discovered iridates as candidate Kitaev spin liquids, the importance of discussing the material realization of some "designer" Hamiltonian [82] was underestimated. From now on, we will concentrate on such open questions especially for SU($N$) spin models.

## 1.7 Spin-orbital systems and quantum spin-orbital liquids

A spin-orbital system is another important candidate for SU($N$) magnetism, especially in the case of $N = 4$, as will be discussed in Chapter 2. Both spin and orbital degrees of freedom are angular momenta, so it is a "magnetic material" in a usual sense. Before going on to the realization of the SU($N$) symmetry, we will review the previous studies on orbital physics.

A quantum orbital liquid (QOL) itself has been discussed in some literature [83, 84]. This notion is defined for a system where orbital degeneracy survives on some metal ion. $LaTiO_3$ is an original candidate for this orbital liquid, an extension of the RVB theory to the orbital sector active in the $d^1$ electronic configuration [84]. In the same spirit as QSL is a state without a magnetic transition, if the Jahn-Teller (JT) transition does not break an effective symmetry between multiple degenerate orbitals even at low temperature, the state is usually called orbital liquid, especially QOL if this is due to the quantum fluctuation/entanglement of orbital degrees of freedom.[15] There is a nice review paper for orbital physics in general [85].

A possibility that the orbital fluctuation enhances the spin fluctuation, leading to a QSOL (quantum spin-orbital liquid), has been discussed for a long time in the Kugel-Khomskii-type models [86], but finding a real material candidate is not an easy task. Though the coupling between spin and orbital sectors is strong especially in the $d^9$ system, we need to confine a $d^9$ ion in a rigid octahedral cage to protect the orbital degeneracy. As already discussed, BCSO ($Ba_3CuSb_2O_9$) is a prominent candidate for a QSOL [8, 11, 12], where both spin and orbital degrees of freedom are fluctuating at the lowest temperature. Based on the crystallographic structure presented in Ref. 87, both Cu and Sb ions are in a good octahedral coordination. Especially, Cu is in the 2+ state with an orbital

[14] The realization of SU($N$) with an odd $N$ might still be difficult.

[15] We are not sure whether a "pure" QOL is a well-defined notion because SOC in real materials always mixes two degrees of freedom.

degeneracy between the $d_{x^2-y^2}$ and $d_{z^2}$ orbitals which is as active as a spin degeneracy, forming a decorated honeycomb lattice. Thus, in this structure both spin and orbital degrees of freedom can be unfrozen. A QSOL realized in BCSO is a combination of a QSL and a QOL. Though there is a possibility that disorder plays an important role in this material [88], experiments clearly show surviving quantum fluctuations for both spin and orbital degrees of freedom. In the case of BCSO, finite-frequency electron spin resonance (ESR) [89] and extended X-ray absorption fine structure (EXAFS) [12] are used to observe quantum orbital fluctuations dynamically. They should still be important tools, so we will discuss this experimental approach later again.

Previously, such orbital liquid states are thought to be impossible because the fluctuation between two wavefunctions of different orbitals always couples to the lattice motion (Jahn-Teller coupling). Especially, an orbital liquid without a cooperative JT order may abandon an energy gain $O(1000)$ times larger than that of QSLs. This is because of the energy discrepancy between electronic and phononic (lattice) degrees of freedom. However, as we shall see, in the case that a QOL stabilizes a symmetric coordination of ligands (*e.g.* octahedral coordination) and the lattice (phonon) energy is still minimized at this symmetric coordination even with an electronic fluctuation, the energy scale difference does not matter.

Though BCSO was a good candidate for QSOLs, the estimated parameters for BCSO are rather far from the model with an exact SU(4) symmetry [13]. Moreover, SOC and the directional dependence of the orbital hopping usually break both the spin-space and orbital-space SU(2) symmetries. It would seem even more difficult to realize an SU($N$)-symmetric system in real magnets with SOC, and thus it is very challenging to find an SU($N$) symmetry in materials with a strong SOC.

The organization of this thesis is as follows. In Chapter 2, we first propose a honeycomb magnetic material with an emergent SU(4) symmetry, derive its effective Hamiltonian, extend the discussion to 3D systems, and give a new perspective on the protection of topological properties by crystalline symmetries. This part follows the organization of Ref. 3. In the latter half of Chapter 2, we discuss the triangular lattice case, boundary condition effects, a Hund coupling effect, and flux variables determination for 3D tricoordinated lattices. In Chapter 3, we first summarize the main contents, and then discuss another candidate system for an SU(4) symmetry, called twisted bilayer graphene/dichalcogenide. Finally, Appendix A is discussing one extension of the LSM theorem, and Appendix B supplements the definition of a crystalline (Kitaev) spin liquid with a concrete example.

# Chapter 2

# Emergent SU(4) symmetry and its realization

As we saw in the Introduction, SU($N$) systems are new important candidates for QSLs, but are restricted to some artificial systems like cold atoms. Thus, we would like to discuss a possible realization in magnetic materials. In this chapter, we mostly focus on $\alpha$-$ZrCl_3$ and its low-energy effective model. We also discuss how to generalize the result to other materials or lattices. In addition to what were discussed in the Introduction, metal-organic frameworks (MOFs) are another playground for SU(4) magnetism, and a variety of candidate materials will enable us to seek many unknown spin-orbital liquids beyond a honeycomb Dirac spin liquid.

## 2.1 Honeycomb materials

As we mentioned in Chapter 1, we propose $\alpha$-$ZrCl_3$ with a honeycomb geometry as the first candidate for the $d^1$ honeycomb system, as shown in Fig. 2.1. More generally, we consider the class of materials $\alpha$-$MX_3$, with $M$ = Ti, Zr, Hf, etc., $X$ = F, Cl, Br, etc. Their crystal structure is almost the same as that of $\alpha$-$RuCl_3$ shown in Fig. 1.4(c), which is known to be an approximate realization of the Kitaev honeycomb model [47, 90]. However, the electronic structure of $\alpha$-$MX_3$ is different from $\alpha$-$RuCl_3$: here, $M$ is in the 3+ state with a $d^1$ electronic configuration in the octahedral ligand field. While in the $d^5$ configuration of $Ru^{3+}$ the $J_{\rm eff} = 1/2$ doublet is the ground state, a $d^1$ electronic configuration which is a particle-hole inversion counterpart will potentially realize the $J_{\rm eff} = 3/2$ ground state, as shown in Fig. 1.4(a). Our strategy for realizing SU(4) spin models starts with a low-energy quartet of electronic states with the effective angular momentum $J_{\rm eff} = 3/2$ on each $M$.

For this description to be valid, the SOC has to be strong enough. As the atomic number increases from Ti to Hf, SOC gets stronger and the description by the effective angular momentum becomes more accurate. The compounds $\alpha$-$MCl_3$ with $M$ = Ti, Zr and related $Na_2VO_3$ have been already reported experimentally. For $\alpha$-$TiCl_3$, a structural transition and opening of the spin gap at $T = 217$ K have been reported [91]. This implies a small SOC, as it is consistent with a massively degenerate manifold of spin-singlets expected in the limit of a vanishing SOC [92]. In compounds with heavier elements, the

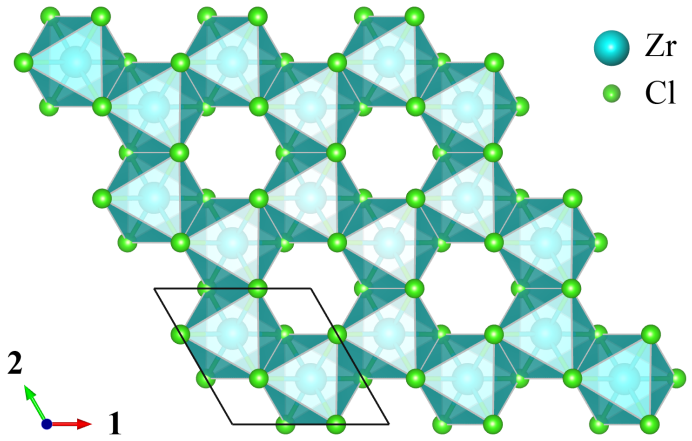


Figure 2.1: Geometric structure of honeycomb $\alpha$-$ZrCl_3$. Cyan and light green spheres represent Zr and Cl, respectively. The crystallographic axes are shown and labelled as the 1- and 2-directions. Reprinted figure with permission from [3] Copyright 2017 by the American Physical Society.

strong SOC can convert this extensively degenerate manifold of product states into a resonating quantum state. Thus, we expect realization of the SU(4) QSOL due to strong SOC with metal ions heavier than Ti. In the following, we pick up $\alpha$-$ZrCl_3$ as an example, although the same analysis should apply to $\alpha$-$HfCl_3$, and $A_2M'O_3$ ($A$ = Na, Li, etc., $M'$ = Nb, Ta, etc.) as well.

## 2.2 Effective Hamiltonian

In the strong-ligand-field limit, the description with one electron in the threefold degenerate $t_{2g}$-shell for $\alpha$-$ZrCl_3$ becomes accurate. We denote these $d_{yz}$, $d_{zx}$, and $d_{xy}$-orbitals by $a$, $b$, $c$, respectively. Let $a_{j\sigma}$, $b_{j\sigma}$ and $c_{j\sigma}$ represent annihilation operators on these orbitals on the $j$th site of $Zr^{3+}$ with spin-$\sigma$, and $n_{\xi\sigma j}$ with $\xi \in \{a, b, c\}$ be the corresponding number operators. We also use this ($a$, $b$, $c$) = ($yz$, $zx$, $xy$) notation to label bonds: each Zr — Zr bond is called $\xi$-bond ($\xi = a$, $b$, $c$) when the superexchange pathway is on the $\xi$-plane,[1] as illustrated in Fig. 2.2.

We define a $J_{\text{eff}} = 3/2$ spinor as $\psi = (\psi_{\uparrow\uparrow}, \psi_{\uparrow\downarrow}, \psi_{\downarrow\uparrow}, \psi_{\downarrow\downarrow})^t = (\psi_{3/2}, \psi_{-3/2}, \psi_{1/2}, \psi_{-1/2})^t$, where $\psi_{J^z}$ is the annihilation operator for the $|J = 3/2, J^z\rangle$ state. Assuming the SOC is the largest electronic energy scale, except for the ligand field splitting, fermionic operators

[1] The Cartesian $xyz$ axes are defined as in Fig. 2.2(b).

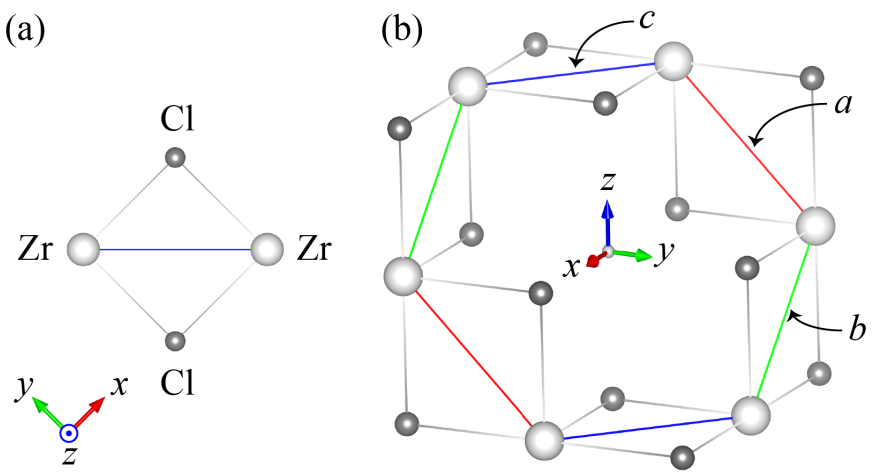


Figure 2.2: (a) Superexchange pathways between two Zr ions connected by a $c$-bond (blue) in $\alpha$-$ZrCl_3$. White and grey spheres represent Zr and Cl atoms, respectively. (b) Three different types of bonds in $\alpha$-$ZrCl_3$. Red, light green, and blue bonds represent $a$-, $b$-, and $c$-bonds on the $yz$-, $zx$-, and $xy$-planes, respectively. Reprinted figure with permission from [3] Copyright 2017 by the American Physical Society.

can be rewritten by the quartet $\psi_{j\tau\sigma}$ as follows.

$$a^\dagger_{j\sigma} \to \frac{\sigma}{\sqrt{6}}(\psi^\dagger_{j\uparrow\bar{\sigma}} - \sqrt{3}\psi^\dagger_{j\downarrow\sigma}), \tag{2.1}$$

$$b^\dagger_{j\sigma} \to \frac{i}{\sqrt{6}}(\psi^\dagger_{j\uparrow\bar{\sigma}} + \sqrt{3}\psi^\dagger_{j\downarrow\sigma}), \tag{2.2}$$

$$c^\dagger_{j\sigma} \to \sqrt{\frac{2}{3}}\psi^\dagger_{j\uparrow\sigma}, \tag{2.3}$$

where the indices $\tau$ and $\sigma$ of $\psi_{j\tau\sigma}$ label the pseudoorbital and pseudospin indices, respectively. Here $\bar{\sigma}$ is an opposite spin to $\sigma$. We begin from the following Hubbard Hamiltonian for $\alpha$-$ZrCl_3$.

$$H = -t \sum_{\sigma,\langle ij\rangle\in\alpha} (\beta^\dagger_{i\sigma}\gamma_{j\sigma} + \gamma^\dagger_{i\sigma}\beta_{j\sigma}) + h.c. + \frac{U}{2} \sum_{j,(\delta,\sigma)\neq(\delta',\sigma')} n_{\delta\sigma j} n_{\delta'\sigma' j}, \tag{2.4}$$

where $t$ is a real-valued hopping parameter through the hopping shown in Fig. 2.2(a), $U > 0$ is the Hubbard interaction, $\langle ij\rangle \in \alpha$ means that the bond $\langle ij\rangle$ is an $\alpha$-bond, $\langle \alpha, \beta, \gamma\rangle$ runs over every cyclic permutation of $\langle a, b, c\rangle$, and $\delta, \delta' \in \{a, b, c\}$. By inserting Eqs. (2.1)-(2.3), we get

$$H = -\frac{t}{\sqrt{3}} \sum_{\langle ij\rangle} \psi^\dagger_i U_{ij} \psi_j + h.c. + \frac{U}{2} \sum_j \psi^\dagger_j \psi_j (\psi^\dagger_j \psi_j - 1), \tag{2.5}$$

where $\psi_j$ is the $J_{\text{eff}} = 3/2$ spinor on the $j$th site, and $U_{ij} = U_{ji}$ is a $4 \times 4$ matrix

$$U_{ij} = \begin{cases} U^a = \tau^y \otimes I_2 & (\langle ij \rangle \in a) \\ U^b = -\tau^x \otimes \sigma^z & (\langle ij \rangle \in b) \\ U^c = -\tau^x \otimes \sigma^y & (\langle ij \rangle \in c) \end{cases}, \tag{2.6}$$

where $\boldsymbol{\tau}$ and $\boldsymbol{\sigma}$ are Pauli matrices acting on the $\tau$ and $\sigma$ indices of $\psi_{j\tau\sigma}$, respectively. We note that $U^{a,b,c}$ are unitary and Hermitian, and thus $U_{ji} = {U_{ij}}^\dagger = U_{ij}$.

Now we consider a (local) SU(4) gauge transformation,

$$\psi_j \to g_j \cdot \psi_j, \qquad U_{ij} \to g_i U_{ij} g_j^\dagger, \tag{2.7}$$

where $g_j$ is an element of SU(4) defined for each site $j$. For every loop $C$ on the lattice, the SU(4) flux defined by the product $\prod_{\langle ij \rangle \in C} U_{ij}$ is invariant under the gauge transformation.

Remarkably, for each elementary hexagonal loop (which we call plaquette) $p$ in the honeycomb lattice with the coloring illustrated in Fig. 2.2(b),

$$\prod_{\langle ij \rangle \in \hexagon_p} U_{ij} = U^a U^b U^c U^a U^b U^c = (U^a U^b U^c)^2 = -I_4, \tag{2.8}$$

which corresponds to just an Abelian phase $\pi$. Since all the flux matrices on the honeycomb lattice can be made of some product of these plaquettes, there is an SU(4) gauge transformation to reduce the model (2.5) to the $\pi$-flux Hubbard model $H$ with a global SU(4) symmetry, as proven in Sec. 2.6.

$$H = -\frac{t}{\sqrt{3}} \sum_{\langle ij \rangle} \eta_{ij} \psi_i^\dagger \psi_j + h.c. + \frac{U}{2} \sum_j \psi_j^\dagger \psi_j (\psi_j^\dagger \psi_j - 1), \tag{2.9}$$

where the definition of $\eta_{ij} = \pm 1$, arranged to insert a $\pi$ flux inside each plaquette, is included in Sec. 2.6. At quarter filling, *i.e.* one electron per site, which is the case in $\alpha$-$ZrCl_3$, the system becomes a Mott insulator for a sufficiently large $U/|t|$. We note that in this Mott regime other contributions, such as a Hund coupling, can be ignored as discussed in Sec. 2.7. The low-energy effective Hamiltonian for the spin and orbital degrees of freedom, obtained by the second-order perturbation theory in $t/U$, is the Kugel-Khomskii model exactly at the SU(4) point (1.1), with $\boldsymbol{S} = \boldsymbol{\sigma}/2$, $\boldsymbol{T} = \boldsymbol{\tau}/2$, and $J = 8t^2/(3U)$ in the transformed basis set. We note that the effective Hamiltonian does not depend on the phase factor $\eta_{ij}$, as it cancels out in the second-order perturbation in $t/U$. Corboz *et al.* argued that this SU(4) Heisenberg model on the honeycomb lattice hosts a gapless QSOL [8]. Therefore, we have found a possible realization of gapless QSOL in $\alpha$-$ZrCl_3$ with an *emergent* SU(4) symmetry.

The nontrivial nature of this model may be understood in terms of the LSMA theorem for the SU($N$) spin systems [28, 29, 70, 93], generalized to higher dimensions [29, 67, 69, 94, 95]. As a result, under the SU($N$) symmetry and the translation symmetry, the ground state of the SU($N$) spin system with $n$ spins of the fundamental representation per unit cell cannot be unique, if there is a non-vanishing excitation gap and $n/N$ is not an integer [see Appendix A]. This rules out a featureless Mott insulator phase, which is defined as

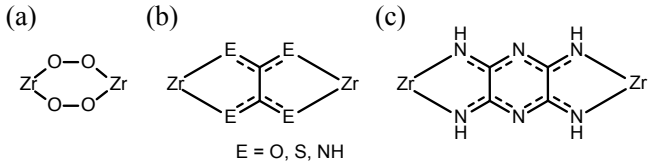


Figure 2.3: Other possible superexchange pathways between two metal ions. (a) Zr — O — O — Zr. (b) Oxalate-based metal-organic motif. ($E$ = O, S, NH.) (c) Tetraaminopyrazine-bridged metal-organic motif. Reprinted figure with permission from [3] Copyright 2017 by the American Physical Society.

a gapped phase with a unique ground state, namely without any spontaneous symmetry breaking or topological order.

For the honeycomb lattice ($n = 2$) there is no LSMA constraint for an SU(2) spin system [96]. Nevertheless, for the SU(4) spin system we discuss in this thesis, a two-fold ground-state degeneracy is required to open a gap. This suggests the stability of a gapless QSOL phase of the SU(4) Heisenberg model on the honeycomb lattice. Especially, assuming the $\pi$-flux Dirac spin-orbital liquid ansatz proposed in Ref. 8 is correct, a trivial mass gap for the Dirac spectrum is forbidden unless the SU(4) or translation symmetry is broken.

## 2.3 Other possible structures

In addition to 3D inorganic polymorphs, MOFs with motifs listed in Fig. 2.3 are an interesting playground to explore a variety of SU(4) QSOLs. Actually, Kitaev spin liquids can be realized in MOFs by a mechanism similar to the one in iridates [1, 14]. Since the present derivation of an emergent SU(4) symmetry shares the same $t_{2g}$ hopping model as in Ref. 14, it is also expected to apply to Zr- or Hf-based MOFs. While Fig. 2.3(a) is a longer superexchange pathway expected in oxides similar to triangular iridates [97], Fig. 2.3(b) and (c) show the superexchange pathways possible in Zr- or Hf-based MOFs. With these oxalate- or tetraaminopyrazine-based ligands, we can expect the two independent superexchange pathways similar to $\alpha$-$ZrCl_3$ as discussed in Ref. 1.

Following the case of the honeycomb lattice, we can repeat the same analysis to derive the effective spin-orbital model for each 3D tricoordinated lattice. Recently, the classification of spin liquids on various tricoordinated lattices attracts much attention, so it is worth investigating [98–100]. All the tricoordinated lattices considered in this thesis are listed in Table 2.1. This table is based on the classification of tricoordinated nets by Wells [101]. We use a Schläfli symbol $(p, c)$ to label a lattice, where $p$ is the shortest elementary loop length of the lattice, and $c = 3$ means the tricoordination of the vertices. For example, (6,3) is the 2D honeycomb lattice, and all the other lattices are 3D tricoordinated lattices, distinguished by additional letters following Wells [101]. $8^2.10$-$a$ is a nonuniform lattice and, thus, the notation is different from the other lattices.

Generalizing the discussion on the honeycomb lattice, if the SU(4) flux for any loop $C$ is reduced to an Abelian phase $\zeta_C = \pm 1$ as $\prod_{\langle ij\rangle \in C} U_{ij} = \zeta_C I_4 \quad (\text{for}\ ^\forall C)$, the Hubbard model acquires the SU(4) symmetry. We have examined this for each lattice in Table 2.1, where

a checkmark is put on the SU(4) column if the above condition holds. Details are included in Sec. 2.8. Moreover, in order to form a stable structure with the present mechanism, the bonds from each site must form 120 degrees and an octahedral coordination. This condition is again checked for each lattice, and indicated in the 120° bond column [100] of Table 2.1. We also put a checkmark on the LSMA column, when the LSMA theorem implies a ground state degeneracy or gapless excitations for the SU(4)-symmetric Hubbard model. For example, the LSMA constraint applies to the (8,3)-$b$ lattice, since $n/N = 6/4$ is fractional.

Table 2.1: Tricoordinated lattices discussed in this thesis. Space groups are shown in number indices. Nonsymmorphic ones are underlined. $n$ is the number of sites per unit cell.

| Wells' notation | Lattice name | SU(4) | 120° bond | $n$ | Space group | LSMA |
|---|---|---|---|---|---|---|
| (10,3)-$a$ | hyperoctagon | ✓[2] | ✓ | 4 | **214** | ✓[3] |
| (10,3)-$b$ | hyperhoneycomb | ✓[2] | ✓ | 4 | **70** | ✓[3] |
| (10,3)-$c$ | | – | – | 6 | **151** | ✓ |
| (10,3)-$d$ | – | ✓[2] | – | 8 | **52** | ✓[3] |
| (9,3)-$a$ | hypernonagon | – | – | 12 | **166** | – |
| $8^2$.10-$a$ | – | ✓ | ✓ | 8 | **141** | – |
| (8,3)-$b$ | hyperhexagon | ✓ | ✓ | 6 | **166** | ✓[4] |
| – | stripyhoneycomb | ✓ | ✓ | 8 | **66** | – |
| (6,3) | 2D honeycomb | ✓ | ✓ | 2 | | ✓[5] |

## 2.4 Crystalline spin liquids and crystalline spin-orbital liquids

Crystalline spin liquids (XSL) [2] are defined originally for Kitaev models and the discussion is in Ref. 2. We would quickly review the definition and generalize this notion to SU(4)-symmetric models based on the LSMA theorem.

In the context of gapless Kitaev spin liquids as originally proposed in Ref. 2, a crystalline spin liquid is defined as a spin liquid state where a gapless point (or a gapped topological phase) is protected not just by the unbroken time-reversal or translation symmetry, but by the space group symmetry of the lattice. This is a simple analogy with a topological crystalline insulator, where a symmetry-protected topological order is protected by some space group symmetry.

[2]The product of hopping matrices along every elementary loop is unity, resulting in the SU(4) Hubbard model with zero flux.

[3]Nonsymmorphic symmetries of the lattice are enough to protect a QSOL state, hosting an XSOL state.

[4]Although the model has a $\pi$ flux, with an appropriate gauge choice the unit cell is not enlarged. Therefore, the LSMA theorem straightforwardly applies to the $\pi$-flux SU(4) Hubbard model.

[5]While the standard LSMA theorem is not effective for the $\pi$-flux SU(4) Hubbard model here, the magnetic translation symmetry works to protect a QSOL state [102].

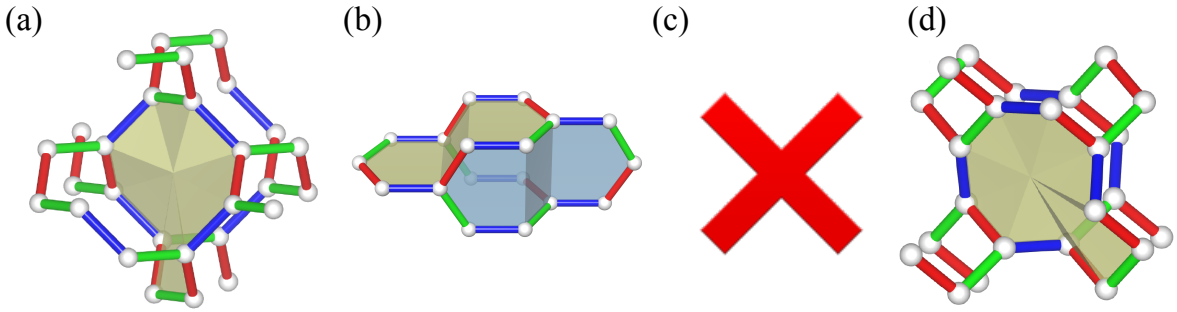


Figure 2.4: (10,3) lattices. (a) (10,3)-$a$ hyperoctagon lattice. (b) (10,3)-$b$ hyperhoneycomb lattice. (c) (10,3)-$c$ does not support the SU(4) symmetry. (d) (10,3)-$d$ lattice.

Differently from topological crystalline insulators, the classification or identification of crystalline spin liquids is not easy. This is because a symmetry could be implemented *projectively* in spin liquids and the representation of the symmetry (action) becomes a projective (fractionalized) one. The classification depends not only on its original symmetry of the lattice but also on its PSG, so there are a macroscopic number of possible crystalline spin liquids. The only thing we can do is to identify the mechanism of the symmetry protection for each specific case. In Ref. 2, two Kitaev spin liquids are identified, one with 3D Dirac cones, and the other with a nodal line protected by the lattice symmetry, not by the time-reversal symmetry. The former is discussed in Appendix B, and the latter is a nodal-line spin liquid robust under the time-reversal breaking, both of which are beyond the classification of Kitaev spin liquids based on the internal symmetries [100].

Sometimes, however, extended LSM-type theorems can prove the existence of a gapless point or a topological state in the gapped case. Thus, the LSM theorem can potentially prove that some spin liquid is XSL without a microscopic investigation, if we ignore whether it is gapped or gapless [103]. This is a subtle point, but LSM-type theorems extended to include a nonsymmorphic symmetry is very powerful to discuss the property of spin liquids abstractly [see also Appendix A]. We note that this type of spin liquids are called filling-enforced QSLs in Ref. 53

Next, we would like to discuss the generalization of the concept of XSL to SU(4)-symmetric models. In the (10,3) lattices [see Fig. 2.4] listed in Table 2.1, the unit cell consists of a multiple of 4 sites, and thus the generalized LSMA theorem seems to allow a featureless insulator if we only consider the translation. Following Refs. 103–105, however, we can effectively reduce the size of the unit cell by dividing the unit cell by the nonsymmorphic symmetry, and thus the filling constraint becomes tighter with a nonsymmorphic space group. Even in the (10,3) lattices, the gapless QSOL state can be protected by the further extension of the LSMA theorem. We call them crystalline spin-orbital liquids (XSOLs) in the sense that these exotic phases are protected in the presence of both the SU(4) symmetry and (nonsymmorphic) space group symmetries. We put a checkmark on the LSMA column of Table 2.1 if either the standard or extended LSMA theorem applies.

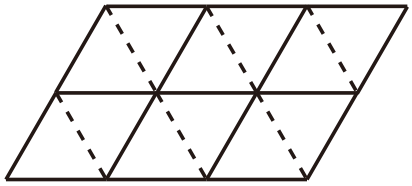

Figure 2.5: Triangluar $d^1$ model. Solid bonds have the SU(4) Heisenberg interaction, but dashed bonds have an exotic interaction Eq. (2.12). If we ignore dashed bonds, it becomes the SU(4) Heisenberg model on the square lattice [76].

## 2.5 Triangular $d^1$ system

It would be interesting to investigate SU(4) Heisenberg models on nontricoordinated lattices. Especially, on the lattice with 1 or 3 sites per unit cell, the LSMA theorem can exclude the possibility of a simply gapped $\mathbb{Z}_2$ spin liquid and suggests a $\mathbb{Z}_4$ QSOL or new SET phases instead. This can be understood by applying the proof of the LSMA theorem to a cylinder boundary condition because the fourfold GSD on a cylinder suggests the existence of a gapless edge mode, or a topological order beyond $\mathbb{Z}_2$ topological order, for example. The case of the triangular lattice is also mentioned in Ref. 78.

From now on, we only consider a triangular lattice case for simplicity because it may be relevant to some accumulated graphene/transition metal dichalcogenide (TMDC) systems [106]. We can easily expect the existence of an unknown spin liquid state even for the SU(4) Heisenberg model on the triangular lattice. However, unfortunately real triangluar $d^1$ systems cannot host an exact SU(4) Heisenberg model. Instead, we found a new "$\Gamma^5$" flux inside each triangluar plaquette and the resulting spin-orbital model becomes exotic, reflecting this additional (non-Abelian) flux.

Similarly to $Ba_3IrTi_2O_9$ [97], we can imagine a triangular $d^1$ system as a starting point. In this case, each triangular plaquette binds the following flux:

$$\prod_{\langle ij\rangle\in\triangle} U_{ij} = U^a U^b U^c =: i\Gamma^5. \tag{2.10}$$

We note that the representation of $\Gamma^5$ here is different from Sec. 2.7. For simplicity, we use a chiral representation as follows:

$$\Gamma^5 = -\tau^z \otimes I_2 = \begin{pmatrix} -I_2 & 0 \\ 0 & I_2 \end{pmatrix}. \tag{2.11}$$

A gauge transformation can always concentrate a flux matrix to only one bond for each triangular plaquette, so it is enough to focus on one bond $\langle ij\rangle$ with $U_{ij} = i\Gamma^5$ in order to derive an effective spin-orbital model by the second-order perturbation in $t/U$. The rest of the bonds are all SU(4)-symmetric, in which case the discussion is completely parallel to the honeycomb case. As for a bond with $U_{ij} = i\Gamma^5$, the second-order perturbation leads to the following spin-orbital model:

$$H_{ij} = J\Big(\boldsymbol{S}_i \cdot \boldsymbol{S}_j + \frac{1}{4}\Big)\Big(T_i^z T_j^z - T_i^x T_j^x - T_i^y T_j^y + \frac{1}{4}\Big), \tag{2.12}$$

if $\langle ij \rangle$ is a dashed bond shown in Fig 2.5. This term breaks the SU(4) symmetry, but still has a high symmetry, SU(2) × SU(2). We can expect an exotic frustration, which is absent even in the SU($N$) Heisenberg model. This is a new Hamiltonian which we first derived, and there is no previous study for this model, so it is worthwhile to study it in the future.

Discussions here are essentially relevant to 1T-$TaS_2$ [107–109] in a symmetric phase without a structural distortion. However, it is usually regarded as a spin-1/2 system after the charge density wave transition. If the symmetric phase survives at very low temperature, 1T-$TaS_2$ should also be an important playground for the quasi-SU(4) magnetism.

$NaZrO_2$ is also a candidate for the same triangular $d^1$ state, though the density functional theory (DFT) claims that it is a nonmagnetic metallic state [110]. It could possibly lead to the above model after the Mott transition. A DFT study for $LiZrO_2$ was also found [111].

## 2.6 Boundary condition effects on the SU($N$) gauge transformation

Until here we concentrate on the physical realization and implication, but from now on we will discuss more about the mathematical structure of our theory. In this section, we would like to discuss the mathematical construction of the gauge transformation. First, we begin from the 1D Hubbard model with an open boundary condition (OBC).

$$H_{\text{1DOBC}} = -t \sum_{j=1}^{L-1} \psi_j^\dagger U_{j,j+1} \psi_{j+1} + h.c. + \frac{U}{2} \sum_{j=1}^{L} \psi_j^\dagger \psi_j (\psi_j^\dagger \psi_j - 1), \tag{2.13}$$

where $L$ is a system size, $\psi_j$ is a $N$-component spinor, $U_{j,j+1}$ is an $N \times N$ unitary matrix defined on the $j$th site, and $t$ and $U$ are real-valued hopping and Hubbard terms, respectively. The (local) gauge transformation is simply given by the following string operator $g_j$.

$$g_j = \prod_{k=1}^{j-1} U_{k,k+1}, \tag{2.14}$$

$$\psi'_j = g_j \cdot \psi_j, \tag{2.15}$$

$$U'_{j,j+1} = g_j U_{j,j+1} g_{j+1}^\dagger = I_N. \tag{2.16}$$

Thus, 1D Hubbard model with OBC is a trivial case where we can always make it SU($N$)-symmetric.

$$H_{\text{1DOBC}} = -t \sum_{j=1}^{L-1} \psi_j'^\dagger \psi'_{j+1} + h.c. + \frac{U}{2} \sum_{j=1}^{L} \psi_j'^\dagger \psi'_j (\psi_j'^\dagger \psi'_j - 1), \tag{2.17}$$

Therefore, in 1D electronic systems on a linear chain with nearest-neighbor hoppings only, if the $N \times N$ hopping matrices are all unitary, the tight-binding Hubbard model is trivially gauge-equivalent to the 1D SU($N$) Hubbard model [18,112–114]. Such emergence of the SU($N$) symmetry by the gauge transformation becomes more nontrivial in higher

dimensions because there is a topological obstruction coming from the lattice geometry and also a possibility to realize topological ground state degeneracy, which is impossible in 1D systems [115].

Before going to higher dimensions, it is instructive to consider the 1D Hubbard model with a periodic boundary condition (PBC).

$$H_{\text{1DPBC}} = -t\sum_{j=1}^{L}\psi_j^\dagger U_{j,j+1}\psi_{j+1} + h.c. + \frac{U}{2}\sum_{j=1}^{L}\psi_j^\dagger\psi_j(\psi_j^\dagger\psi_j - 1), \tag{2.18}$$

where $\psi_{L+1}$ is identified as $\psi_1$. Clearly the gauge transformation does not change the flux inside the loop, so there is a necessary condition to have a gauge transformation which makes the Hamiltonian SU($N$)-symmetric,

$$\prod_{j=1}^{L} U_{j,j+1} = \zeta I_N, \tag{2.19}$$

with some $|\zeta| = 1$. This is also a sufficient condition. If we apply the same gauge transformation $g_j = \prod_{k=1}^{j-1} U_{k,k+1}$ as the OBC case for $j = 1, \ldots, L$, the transformed matrices become

$$U'_{j,j+1} = \begin{cases} \prod_{k=1}^{L} U_{k,k+1} = \zeta I_N & (j = L) \\ I_N & (\text{otherwise}) \end{cases}. \tag{2.20}$$

Thus, the resulting Hamiltonian is completely SU($N$)-symmetric with a factor $\zeta$,

$$H_{\text{1DPBC}} = -t\Big(\sum_{j=1}^{L-1}\psi_j'^\dagger\psi'_{j+1} + \zeta\psi_L'^\dagger\psi'_1\Big) + h.c. + \frac{U}{2}\sum_{j=1}^{L}\psi_j'^\dagger\psi'_j(\psi_j'^\dagger\psi'_j - 1). \tag{2.21}$$

It must be noted that $\zeta$ cannot be eliminated by any gauge transformation and thus it is physical and called (magnetic) flux.

As for OBC, it is almost trivial to extend the proof of the existence of the gauge transformation to higher dimensions. This can be achieved by drawing the lattice with a single stroke of the brush. For simplicity, we use the finite-size 2D honeycomb lattice with OBC. We begin from the following Hamiltonian.

$$H_{\text{2D}} = -\frac{t}{\sqrt{3}}\sum_{\langle ij\rangle}\psi_i^\dagger U_{ij}\psi_j + h.c. + \frac{U}{2}\sum_j \psi_j^\dagger\psi_j(\psi_j^\dagger\psi_j - 1), \tag{2.22}$$

where $U_{ij}$ is again an $N \times N$ unitary matrix defined for each bond, and $\psi_j$ is the $N$-component spinor on the $j$th site. Assuming each site is numbered in order for some nearest-neighbor site to have the subsequent number, we can do the same gauge transformation as the 1D OBC case. Again, this gauge transformation does not change the flux value for any loops, so there is a necessary condition to get an SU($N$)-symmetric model for each hexagonal plaquette (elementary loop) $p$.

$$\prod_{\langle ij\rangle\in p} U_{ij} = \zeta_p I_N \qquad (\text{for}\ ^\forall p). \tag{2.23}$$

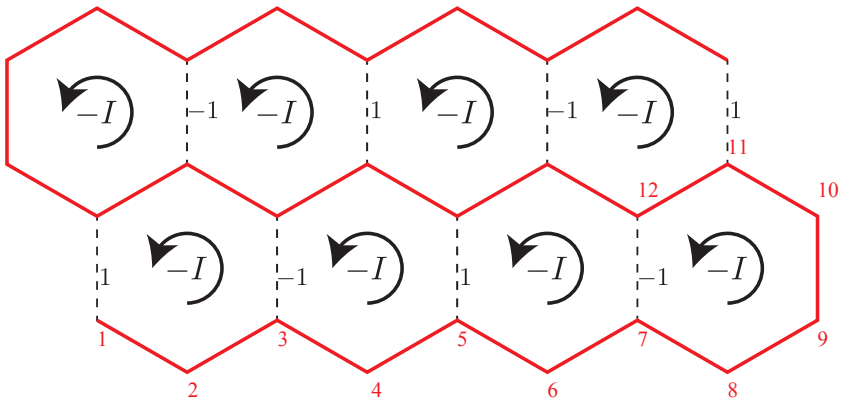


Figure 2.6: Flake of the honeycomb lattice to show how the gauge transformation works for OBC. Along the red solid line, we used 1D gauge transformation and the flux constraints automatically determines the transformed hopping matrices for the rest of the bonds shown in black dashed lines.

This condition is actually sufficient for OBC (assuming the existence of a single stroke path). We take a flake of the honeycomb lattice shown in Fig. 2.6. For simplicity, we use $\zeta_p = -1$ for $\alpha$-$ZrCl_3$, but $\zeta_p$ can generally depend on each plaquette $p$.

If we draw a single stroke path shown as the red solid line in Fig. 2.6, all the unitary matrices on the red bonds become identity by the gauge transformation for the 1D red line. Remaining are black dashed bonds, but their hopping matrices are fixed by the flux condition (Eq. (2.23)). In the case of Fig. 2.6, around the bottom plaquettes the hopping matrices are determined from right to left because five of the surrounding matrices are made identity one by one for each plaquette. By continuing this, all the unitary matrices are transformed into some $\eta_{ij}$ times identity with $|\eta_{ij}| = 1$, and thus the Hamiltonian becomes completely SU($N$)-symmetric. We call the following transformed gauge "theorists' gauge".

$$H_{\mathrm{2D}} = -\frac{t}{\sqrt{3}} \sum_{\langle ij \rangle} \eta_{ij} \psi_i'^{\dagger} \psi_j' + h.c. + \frac{U}{2} \sum_j \psi_j'^{\dagger} \psi_j' (\psi_j'^{\dagger} \psi_j' - 1), \tag{2.24}$$

where $\eta_{ij} = 1$ for red bonds, while the sign of $\eta_{ij} = \pm 1$ depends on each bond for black dashed bonds as indicated in Fig. 2.6 by the number near each black dashed bond. This is nothing but the model called a $\pi$-flux Hubbard model on the honeycomb lattice and the model can be constructed by changing the sign of the $c$-bonds alternately along the perpendicular direction. This gauge transformation effectively doubles the size of the unit cell.

Finally, we would like to discuss the 2D PBC case. In this case, we cannot find a gauge transformation, even if we assume the flux condition (Eq. (2.23)) for every hexagonal plaquette. The final obstructions to be considered are global (or topological) ones, which are two types of noncontractible loops on the 2D torus. The noncontractible loops in the same homotopy class are related by the flux conditions, so it is enough to consider only two noncontractible loops $C_1$ and $C_2$ along the 1- and 2-directions, respectively. Assuming the size of the torus to be $L_1 \times L_2$ original unit cells, the lengths of $C_1$ and $C_2$ become

multiples of $L_1$ and $L_2$, respectively. The necessary and sufficient conditions to find a gauge transformation in addition to Eq. (2.23) are two new flux conditions for $C_1$ and $C_2$,

$$\prod_{\langle ij\rangle\in C_1} U_{ij} = \zeta_{C_1} I_N, \qquad \prod_{\langle ij\rangle\in C_2} U_{ij} = \zeta_{C_2} I_N. \tag{2.25}$$

In general these fluxes cannot be Abelian for any sets of unitary matrices $U_{ij}$. Thus, we specifically consider the model of $\alpha$-$ZrCl_3$ discussed previously. In this model, all the hopping matrices are accidentally written by Pauli matrices, and their products only take some Pauli matrices times a complex number, which actually only takes $1, i, -1, -i$. In other words, their products are included in the Pauli group on 2 qubits. In this group, any element to the power of 4 becomes identity, so the flux inside the two noncontractible loops become trivial if both $L_1$ and $L_2$ are multiples of 4. This is a condition to find a gauge transformation to make the model explicitly SU($N$)-symmetric with a symmetric boundary condition, *i.e.* a boundary condition where both $C_1$ and $C_2$ have a zero flux. If we allow a more general boundary condition with a $\pi$ flux inside $C_1$ or $C_2$, then the conditions for $L_1$ or $L_2$ become milder.

Our effective model for the honeycomb $\alpha$-$ZrCl_3$ was derived based on the superexchange interactions between the $Zr^{3+}$ ions constructed from its geometry. However, similar superexchange interactions can also arise in the other structures listed in Fig. 2.3, or in face-shared systems. We note that $ZrCl_3$ has some polymorphs and a chain compound $\beta$-$ZrCl_3$ with face-shared Cl octahedra [116] can also host a 1D SU(4) Heisenberg model [18].

Since a nonlayered structure of $Na_2VO_3$ has already been reported [117], we can expect various 3D polymorphs of $ZrCl_3$ or $A_2M'O_3$ with $A$ = Na, Li and $M'$ = Nb, Ta, similarly to 3D $\beta$-$Li_2IrO_3$ [118] and $\gamma$-$Li_2IrO_3$ [119].

The generalization from the 2D case to the 3D case is straightforward. The difference is that in 3 dimensions not all the fluxes of the plaquettes (or elementary loops in Sec. 2.8) can be determined independently. This is called volume constraint and will be discussed in Sec. 2.8.

## 2.7 Hidden SO(4) symmetry in the Hund coupling

In reality, the multiorbital Hubbard model is not as simple as that with a Hubbard interaction which has been discussed in previous sections. The multiorbital Hubbard model usually includes four interaction terms $U$, $U'$, $J_H$, and $J'_H$. As discussed by Kanamori [120], $U$ and $U'$ have a similar magnitude, while $J_H$ and $J'_H (\sim J_H)$ are much smaller because they are from the exchange integral between different $d$-orbitals. Thus, it is natural to begin by assuming $U = U'$ and $J_H = J'_H = 0$ as the first approximation as was done so far, though we must consider $U' - U \sim 2J_H$ and Hund couplings to be perturbations of an order $J_H/U \sim \mathcal{O}(0.1)$. We assume $J_H/U \sim 0.1$ in $\alpha$-$ZrCl_3$. At least from the stability condition $J_H/U$ has to be smaller than $1/3$ in any case.

We here only consider an onsite Hund coupling $J_H = J'_H$, for simplicity. There are other possible perturbations like further-neighbor interactions, but we can expect that such effects are smaller than that of the Hund coupling similarly to $\alpha$-$RuCl_3$. Actually,

in Kitaev materials like $\alpha$-$RuCl_3$ the nearest-neighbor Kitaev interaction and the third-neighbor Heisenberg interaction are expected to be comparable [121], but this is probably due to fine tuning happening in the $J_{\text{eff}} = 1/2$ manifold and the Kiteav interaction has to be smaller than the naïve superexchange interaction expected in the whole $t_{2g}$ orbitals because of the destructive interference which cancels out the direct hopping between the $J_{\text{eff}} = 1/2$ manifold [14]. In our $J_{\text{eff}} = 3/2$ models realized *e.g.* in $\alpha$-$ZrCl_3$, such an accidental reduction of the highest-order contribution does not occur even in the nearest-neighbor interactions, so we expect the magnetic interaction in $\alpha$-$ZrCl_3$ is much larger than the dominant Kiteav interaction in $\alpha$-$RuCl_3$, and thus one- or two-order larger than the third-neighbor Heisenberg interactions in the case of $\alpha$-$ZrCl_3$.

Next, in order to evaluate the effect of the Hund coupling, we will change the ordering of the $J_{\text{eff}} = 3/2$ bases to compare the model with a so-called SO(5)-symmetric Hubbard model discussed in the literature on $S = 3/2$ cold atomic systems [81, 122, 123],

$$\psi = (\psi_{3/2}, \psi_{1/2}, \psi_{-1/2}, \psi_{-3/2})^t = (\psi_{\uparrow\uparrow}, \psi_{\downarrow\uparrow}, \psi_{\downarrow\downarrow}, \psi_{\uparrow\downarrow})^t. \tag{2.26}$$

In this basis it is easy to see a hidden SO(4) symmetry, which is a subgroup of $\mathrm{SO}(5) \simeq \mathrm{Sp}(4) \subset \mathrm{SU}(4)$ in the original model.

We will now show that the Hund coupling in $\alpha$-$ZrCl_3$ actually possesses the $\mathrm{SO}(5) \simeq \mathrm{Sp}(4)$ symmetry, although the hopping matrices break a part of this symmetry. If we add a Hund coupling for the hopping model inside the $t_{2g}$ orbitals [124], the Hamiltonian becomes

$$\begin{aligned} H =& -t \sum_{\sigma,\langle ij\rangle\in\alpha} (\beta^\dagger_{i\sigma}\gamma_{j\sigma} + \gamma^\dagger_{i\sigma}\beta_{j\sigma}) + h.c. \\ &+ \sum_j \left[ \frac{U - 3J_H}{2} N_j(N_j - 1) - 2J_H \boldsymbol{s}_j^2 - \frac{J_H}{2}\boldsymbol{L}_j^2 + \frac{5}{2}J_H N_j \right], \end{aligned} \tag{2.27}$$

where $\langle ij\rangle \in \alpha$ means that the bond $\langle ij\rangle$ is an $\alpha$-bond, $\langle \alpha, \beta, \gamma\rangle$ runs over every cyclic permutation of $\langle a, b, c\rangle$, $N_j$ is a number operator, $\boldsymbol{s}_j$ is a total spin, and $\boldsymbol{L}_j$ is a total effective angular momentum. In this form the stability condition $J_H/U < 1/3$ is apparent. Assuming a strong spin-orbit coupling limit $\lambda \gg |t|, J_H$, we project the Hilbert space onto the $J_{\text{eff}} = 3/2$ manifold. We note that we will ignore doublon/holon excitations with higher energies in the following discussions. In the original gauge before the gauge transformation, which we call "lab gauge", the projected Hamiltonian becomes

$$H = -\frac{t}{\sqrt{3}} \sum_{\langle ij\rangle} \psi_i^\dagger V_{ij} \psi_j + h.c. + \sum_j \left[ \frac{U - 3J_H}{2} \psi_j^\dagger \psi_j (\psi_j^\dagger \psi_j - 1) - \frac{4}{9} J_H \boldsymbol{J}_j^2 + \frac{5}{2} J_H \psi_j^\dagger \psi_j \right], \tag{2.28}$$

where $\boldsymbol{J}_j = \boldsymbol{s}_j + \boldsymbol{L}_j$ is a total effective angular momentum operator with a condition $J = 3/2$ after the projection, and

$$V_{ij} = \begin{cases} V^a = \tau^z \otimes \sigma^y = \Gamma^3 & (\langle ij\rangle \in a) \\ V^b = -\tau^z \otimes \sigma^x = -\Gamma^2 & (\langle ij\rangle \in b) \\ V^c = -\tau^y \otimes I_2 = \Gamma^1 & (\langle ij\rangle \in c) \end{cases}. \tag{2.29}$$

We used $\boldsymbol{s}_j = \boldsymbol{J}_j/3$ and $\boldsymbol{L}_j = 2\boldsymbol{J}_j/3$ inside the $J_{\rm eff} = 3/2$ manifold derived from the Wigner-Eckart theorem. Thus, ignoring the hopping terms, the Hubbard and Hund couplings possess a hidden SO(5) $\simeq$ Sp(4) symmetry in the same way as the $S = 3/2$ cold atomic systems with a spin-preserving interaction.

The hopping term partially breaks this SO(5) symmetry. To see this we use anticommuting Dirac gamma matrices in Ref. [81] defined as

$$(\Gamma^1, \Gamma^2, \Gamma^3, \Gamma^4, \Gamma^5) = (-\tau^y \otimes I_2, \tau^z \otimes \sigma^x, \tau^z \otimes \sigma^y, \tau^z \otimes \sigma^z, -\tau^x \otimes I_2). \tag{2.30}$$

Gamma matrices $\Gamma^p$ $(p = 1, \ldots, 5)$ are forming an SO(5) vector, which transforms as a vector in the same rotation for the hidden SO(5) symmetry of the Hund coupling. There is no way to eliminate the non-Abelian hopping just by the SO(5) $\simeq$ Sp(4) gauge transformation, but we can rotate SO(5) vectors locally to eliminate the bond dependence of the hopping.

For example, we can rotate all $V_{ij}$s to $\Gamma^5$ and then the Hamiltonian becomes almost uniform up to the same factors $\eta_{ij} = \pm 1$ as discussed in Sec. 2.6:

$$H = -\frac{t}{\sqrt{3}} \sum_{\langle ij \rangle} \eta_{ij} \psi_i'^{\dagger} \Gamma^5 \psi_j' + h.c. + \sum_j \left[ \frac{U - 3J_H}{2} \psi_j'^{\dagger} \psi_j' (\psi_j'^{\dagger} \psi_j' - 1) - \frac{4}{9} J_H \boldsymbol{J}_j'^2 + \frac{5}{2} J_H \psi_j'^{\dagger} \psi_j' \right]. \tag{2.31}$$

This model explicitly has a hidden SO(4) symmetry because $\Gamma^5$ is invariant under the SO(4) subgroup of the SO(5) rotation which keeps a vector $(0, 0, 0, 0, 1)$ invariant. The last term is constant in the large $(U - 3J_H)$ limit at quarter filling, so the first meaningful contribution of an order $J_H/U \sim \mathcal{O}(0.1)$ would be the SO(4)-invariant perturbation coming from the term $(4J_H/9)\boldsymbol{J}_j'^2$, which separates the degeneracy of the virtual state with two electrons per site into $J = 0$ and $J = 2$. However, this effect is again $\mathcal{O}(0.1)$ and, thus, we can expect this SU(4) breaking perturbation to be negligible.

We note that the SO(5) $\simeq$ Sp(4) gauge transformation is just a subgroup of the SU(4) gauge transformation, and it is not enough to go to "theorists' gauge" without any non-Abelian hopping matrices. In fact, Dirac gamma matrices are not included in the generator of the Sp(4) rotation for $\psi$ and the rotation is generated by $\Gamma^{pq} = -(i/2)[\Gamma^p, \Gamma^q] = -i\Gamma^p\Gamma^q$ $(1 \le p, q \le 5)$ [81]. Since the number of gamma matrices is conserved mod 2 by the SO(5) $\simeq$ Sp(4) rotation, the hopping matrices written by one gamma matrix cannot be rotated to an SO(5) scalar by the SO(5) gauge transformation, and this is why $\Gamma^5$ cannot be eliminated in Eq. (2.31).

In this analysis, we only considered the extreme limit $\lambda \gg J_H$ for simplicity to prove that the SU(4)-breaking term comes from the order of $\mathcal{O}(0.1)$ by employing the SO(5) gauge transformation intensively. While we no longer expect the existence of a hidden SO(4) symmetry in a general case, it is not difficult to show that in the second-order perturbation the contribution breaking the original SU(4) symmetry always involves an virtual state with an energy higher than the lowest order by $\lambda$ or $J_H$. Anyway, we can conclude that, as long as we ignore higher order contributions of $\mathcal{O}(0.1)$, the emergent SU(4) symmetry would be robust.

We note that recently it was argued that $\mathcal{O}(0.1)$ perturbation of $J_H$ and $U' - U$ would not destabilize the SU(4) spin liquid in the case of BCSO [125]. Although it is not clear this result is applicable to $\alpha$-$ZrCl_3$, we can expect that the stability region of a size $\mathcal{O}(0.1)$

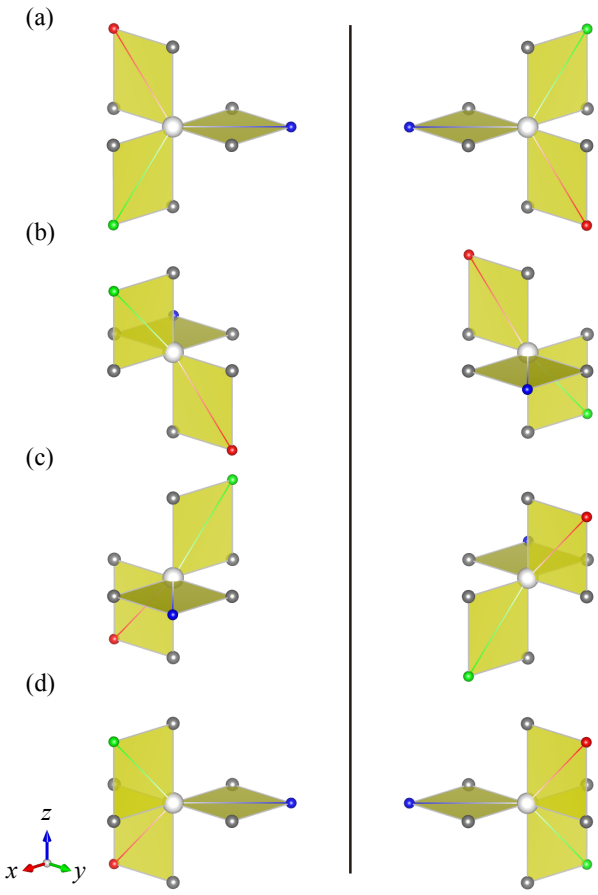


Figure 2.7: All possible ways to connect three bonds in the 3D tricoordinated lattices. (a) is the same one as that in the 2D honeycomb lattice, while (b), (c), and (d) are produced by rotating (a) by 180° around the $x$, $y$, and $z$-axes, respectively. The left-hand side and the right-hand side are related by the inversion for each figure.

will be reproduced for $\alpha$-$ZrCl_3$, too, by similar mean-field and variational calculations. While this is a preliminary discussion, further studies will disclose the effects of $J_H$ and $U' - U$ in the future.

## 2.8 Flux configurations for various tricoordinated lattices

The flux configurations for the tricoordinated lattices listed in Table 2.1 can be treated similarly to the Kitaev models on tricoordinated lattices [47, 100] except for the difference in the gauge group. Following Kitaev [47], we use terminology of the lattice gauge theory. The link variables $U_{ij}$ are Hermitian and unitary (in this case) $4 \times 4$ matrices defined for each bond (link) $\langle ij \rangle$ of the lattice. Each link variable depends on its type (color) of the

bond as

$$U_{ij} = \begin{cases} U^a = \tau^y \otimes I_2 & (\langle ij \rangle \in a) \\ U^b = -\tau^x \otimes \sigma^z & (\langle ij \rangle \in b) \\ U^c = -\tau^x \otimes \sigma^y & (\langle ij \rangle \in c) \end{cases}, \tag{2.32}$$

where $\boldsymbol{\tau}$ and $\boldsymbol{\sigma}$ are independent Pauli matrices, following the original gauge (basis) used in Sec. 2.2 (not the one used in the previous section). The bond type $abc$ is determined from which plane this bond belongs to in the same way as $\alpha$-$ZrCl_3$. We note that in the 3D case we actually have six types of bonds with additional $\pm 1$ factors, so $U_{ij} = \pm U^a$, $\pm U^b$, $\pm U^c$ depending on a detailed structure of the bond $\langle ij \rangle$. This comes from the spatial dependence of the sign of the wavefunctions of the $d$-orbitals.

These additional $\pm 1$ factors can simply be gauged out in the following way. In the 2D honeycomb lattice, there is no sign difference in the same bond type because all of them are related by the translation symmetry. In some 3D lattices, even if the two bonds belong to the same type, the hopping matrices can differ because they are related not by the translation symmetry, but by the screw or glide symmetry. Accompanied by the reflection or rotation, this symmetry can actually change the sign of the hopping matrix by $-1$ according to the shape of the $t_{2g}$-orbitals. When seen from the metal site, it is a 180° rotation around the $x$, $y$, or $z$-axis. If we consider the signs of the $t_{2g}$-orbitals, it is clear that 180° rotation changes the signs of some orbitals, while the inversion does not change the signs of the $d$-orbitals. As shown in Fig. 2.7, there are 8 types of metal sites, and all of them are related by some 180° rotation, which causes the sign difference, up to inversion. Fortunately, however, this additional sign can be eliminated by some gauge transformation, *i.e.* local rotations of the definition of the effective angular momentum $l = 1$ of the $t_{2g}$-orbitals. For example, if the metal site is rotated around the $x$-axis by 180°, the configuration of the surrounding ligands changes from Fig. 2.7(a) to Fig. 2.7(b). Then, according to the rotation, we rotate the definition of the angular momentum $l = 1$ around the $x$-axis by 180°, which can be done just by flipping the sign of the $yz$-orbital. Similarly, for the ones shown in Fig. 2.7(c), we just flip the sign of $zx$-orbital. Then, if we connect these two, Fig. 2.7(b) and (c), along the $xy$-plane, we obtain an additional $-1$ phase from this gauge transformation, and it completely cancels out the sign in question. If we do a similar local rotation in the fictitious orbital space for each metal site according to the physical 180° rotation, all the hopping matrices will be returned to the original ones in Eq. (2.32), and after all we do not have to care about the subtle difference among the same bond type. Thus, Eq. (2.32) is still valid after this "$\mathbb{Z}_2$" gauge transformation.

In order to find a gauge transformation to get an SU(4) Hubbard model, we have to check that every Wilson loop operator is Abelian. In an abuse of language, each Wilson loop will be called flux inside the loop. We regard a Wilson loop operator $I_4$ as a zero flux, and $-I_4$ as a $\pi$ flux. In order to get a desired gauge transformation, it is enough to show that the flux inside every elementary loop $C$ is Abelian:

$$\prod_{\langle ij \rangle \in C} U_{ij} = \zeta_C I_4, \tag{2.33}$$

with some phase factors $|\zeta_C| = 1$.

Since $U_{ij}^2 = I_4$, not all the fluxes are independent. In the case of a $\mathbb{Z}_2$ gauge field, the constraints between multiple fluxes are called volume constraints [100]. However, due to

the non-Abelian nature of the flux structure, it is subtle whether they apply. Fortunately, the above $U^\alpha$ ($\alpha = a$, $b$, $c$) obeys the following anticommutation relations.

$$\{U^\alpha, U^\beta\} = 2\delta^{\alpha\beta} I_4. \tag{2.34}$$

This algebraic relation proves the product of the fluxes of the loops surrounding some volume must vanish (volume constraints). Moreover, we can easily show that, if every bond color is used even times in each loop, which is a natural consequence for the lattices admitting materials realization, the flux inside should always be Abelian with $\zeta_C = \pm 1$. Actually, every lattice included in Table 2.2 obeys this condition, so we have already proven all of them have an Abelian flux value.

The remaining subtle problem is which flux these elementary loops have, a zero flux, or a $\pi$ flux. To check this, we need to investigate every loop one by one. To calculate every flux value systematically, we often use space group symmetries to relate two elementary loops, even though the system is in the strong spin-orbit coupling limit. We note that the threefold rotation symmetry of the $xyz$-axes of the Cartesian coordinate is not clear in the original gauge in Sec. 2.2. This symmetry is important for some 3D models, although the spin quantization axis along the (111) direction will make this symmetry explicit. We have checked all the elementary loops in the tricoordinated lattices listed here. In most cases, elementary loops of the same length have the same flux due to some symmetry. Only the flux value for the shortest elementary loops is shown in Table 2.2.

Table 2.2: Flux value of tricoordinated lattices. Only the flux value for the shortest elementary loops is shown here. Nonsymmorphic space group numbers are underlined. NS means that nonsymmorphic symmetries of the lattice are enough to protect a quantum spin-orbital liquid state. In addition to the contents of Table 2.1, we also include O'Keeffe's three-letter codes [126, 127].

| Wells' notation | Lattice name | O'Keeffe's code | Minimal loop length | Flux value | 120-degree bond | Number of sites | Space group symbol | Space group No. | LSMA constraints |
|---|---|---|---|---|---|---|---|---|---|
| (10,3)-$a$ | hyperoctagon | **srs** | 10 | 0-flux | ✓ | 4 | $I4_132$ | **<u>214</u>** | NS ✓ |
| (10,3)-$b$ | hyperhoneycomb | **ths** | 10 | 0-flux | ✓ | 4 | $Fddd$[6] | **<u>70</u>** | NS ✓ |
| (10,3)-$d$ | | **utp** | 10 | 0-flux | – | 8 | $Pnna$[7] | **<u>52</u>** | NS ✓ |
| nonuniform | $8^2$.10-$a$ | **lig** | 8 | $\pi$-flux | ✓ | 8 | $I4_1/amd$ | **<u>141</u>** | – |
| (8,3)-$b$ | hyperhexagon | **etb** | 8 | $\pi$-flux | ✓ | 6 | $R\bar{3}m$ | **166** | ✓ |
| nonuniform | stripyhoneycomb | **clh** | 6 | $\pi$-flux | ✓ | 8 | $Cccm$[8] | **<u>66</u>** | – |
| (6,3) | 2D honeycomb | **hcb** | 6 | $\pi$-flux | ✓ | 2 | | | ✓ |

[6]The most symmetric case should be $I4_1/amd$, including $Fddd$. Actually, $Fddd$ is enough for the filling constraint.
[7]There exists another phase with a $Pbcn$ symmetry. Both symmetries are enough for the filling constraint.
[8]There exists a more symmetric phase with a $P4_2/mmc$ symmetry, but it is not enough for the filling constraint.

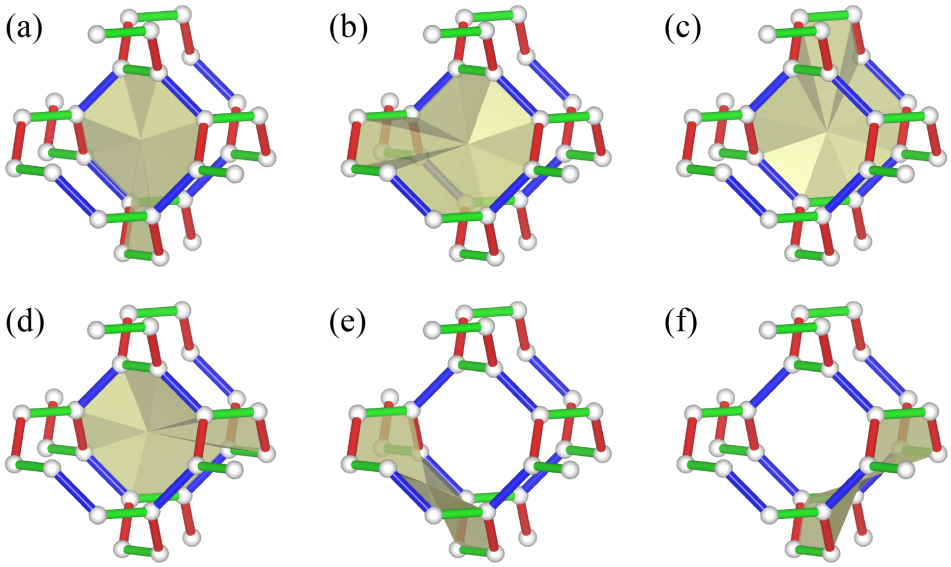


Figure 2.8: Part of (10,3)-$a$. All the six elementary loops [128] are highlighted by yellow surfaces. Loops (a)-(d) are related by the fourfold screw rotation, and loops (e) and (f) are again related by the same symmetry.

### 2.8.1 (10,3)-$a$

First of all, nonsymmorphic symmetries are useful to determine the flux value because nonsymmorphic transformations often do not change the bond coloring and effectively reduce the number of elementary loops. As a concrete example, we take the hyperoctagon lattice (10,3)-$a$ to show its usefulness. (10,3)-$a$ has six elementary loops of length 10 [128], and 4 of them are related by the fourfold screw rotation symmetry [see Fig. 2.8(a)-(d)]. This fourfold screw exchanges the $b$-bonds for the $c$-bonds, but this will not affect the flux value if the flux is Abelian because the choice of the $xyz$-axes and its chirality is arbitrary. The rest two elementary loops [see Fig. 2.8(e)-(f)] accidentally have the same coloring as they are related by the screw symmetry. Therefore, it is enough to check only two elementary loops, (a) and (e).

$$U^cU^aU^cU^aU^bU^aU^cU^aU^cU^b = (U^cU^a)^2U^b(U^aU^c)^2U^b = I_4, \tag{2.35}$$

$$U^bU^aU^bU^aU^cU^aU^bU^aU^bU^c = (U^bU^a)^2U^c(U^aU^b)^2U^c = I_4. \tag{2.36}$$

From the above symmetry arguments, or from volume constraints, we can conclude that all the six elementary loops (of length 10) in (10,3)-$a$ have a zero flux. This result agrees with the fact that this zero-flux configuration is the unique $Z_2$ flux configuration that obeys all the lattice symmetries of (10,3)-$a$ [100].

### 2.8.2 (10,3)-$b$

Among various point group symmetries, the inversion symmetry of the lattice is the most useful. As is the case in the honeycomb lattice, if an elementary loop has an inversion center, then the flux inside this loop becomes the square of some Pauli matrices times

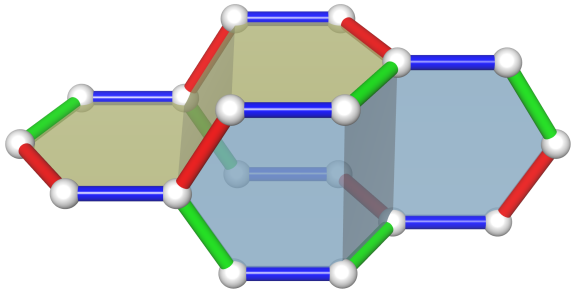

Figure 2.9: Part of (10,3)-$b$ including four loops forming a volume constraint. Two elementary loops with different coloring patterns are highlighted by yellow and cyan surfaces, respectively.

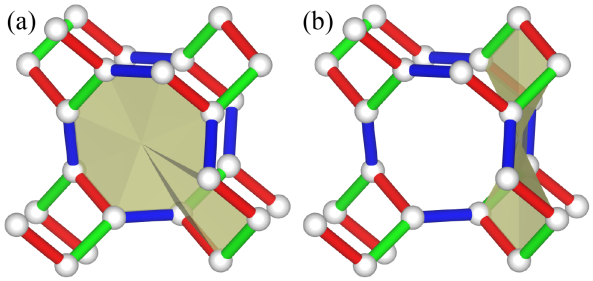


Figure 2.10: Part of (10,3)-$d$. (a) One of the type-A loops highlighted by the yellow surface. (b) One of the type-B loops highlighted by the yellow surface.

a complex number, which actually only takes $1, i, -1, -i$. Therefore, the existence of an inversion center automatically proves that the flux is Abelian and should be 0 or $\pi$. This is another proof that a non-Abelian flux vanishes on some lattices. This applies, for example, to the hyperhoneycomb lattice (10,3)-$b$. All the four elementary loops of length 10 (10-loops) have an inversion center, making the direct calculation easier. We can classify these four 10-loops into two pairs, where two loops are related by the glide mirror symmetry with the same coloring pattern for each pair. Therefore, it is enough to check two loops, shown in the yellow and cyan surfaces, respectively, in Fig. 2.9.

$$U^bU^cU^aU^cU^aU^bU^cU^aU^cU^a = [U^b(U^cU^a)^2]^2 = I_4. \tag{2.37}$$

$$U^aU^cU^bU^cU^bU^aU^cU^bU^cU^b = [U^a(U^cU^b)^2]^2 = I_4. \tag{2.38}$$

Therefore, all the four elementary loops in (10,3)-$b$ have a zero flux.

### 2.8.3 (10,3)-$d$

The structure of (10,3)-$d$ is related to (10,3)-$a$ because they share the same projection onto the (001) plane, the 2D squareoctagon lattice. Due to the difference in the chiralities of the square spirals, the unit cell is enlarged in (10,3)-$d$ and possess 8 elementary loops (of length 10) per unit cell.

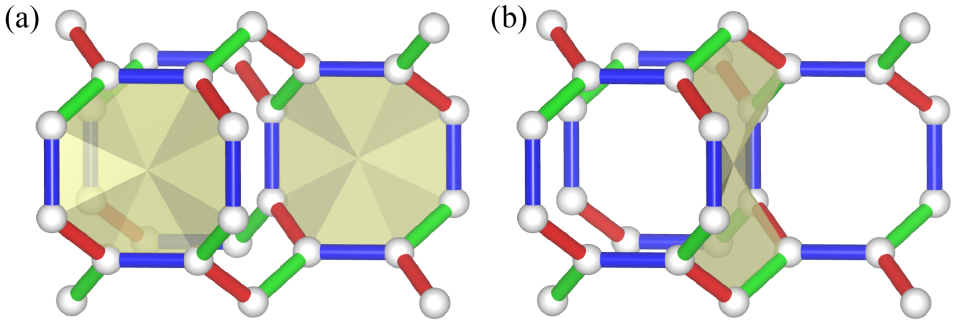


Figure 2.11: Part of $8^2.10$-$a$. (a) All the two 8-loops are shown by yellow surfaces. They are related by the fourfold screw rotation symmetry. (b) One of the four 10-loops is shown by the yellow surface. The rest are produced by applying the fourfold screw rotation around the square spiral.

Since this lattice does not allow any 120-degree configuration, we cannot simply decide the bond coloring. If we take the most symmetric bond coloring discussed in [2], then the calculation becomes simple. We can divide 8 elementary loops of length 10 into two types. Four type-A loops are spiraling up the octagon spiral and then spiraling down the square spiral [see Fig. 2.10(a)]. All the four type-A loops are related by the inversion symmetry or the twofold screw rotation symmetry (the combination of them is the glide mirror symmetry), and thus have the same flux. Four type-B loops are spiraling up the square spiral and then spiraling down the nearest-neighbor square spiral [see Fig. 2.10(b)]. Four type-B loops are related by the twofold screw rotation symmetry or by the glide mirror symmetry, and have the same flux. Thus, it is enough to check one for each type.

$$U^bU^cU^aU^cU^aU^bU^aU^cU^aU^c = U^b(U^cU^a)^2U^b(U^aU^c)^2 = I_4. \tag{2.39}$$

$$U^bU^aU^bU^aU^cU^bU^aU^bU^aU^c = [(U^bU^a)^2U^c]^2 = I_4. \tag{2.40}$$

The direct calculation tells us that the hopping model is in a zero-flux configuration.

### 2.8.4 $8^2.10$-$a$

$8^2.10$-$a$ is nonuniform, but Archimedean. Therefore, each site is included in the two types of elementary loops, some of length 8 and others of length 10. The unit cell includes two elementary loops of length 8 (8-loops) [see Fig. 2.11(a)] and four elementary loops of length 10 (10-loops) [see Fig. 2.11(b)]. It is enough to check one of the 8-loops and one of the 10-loops because all the elementary loops of the same length are related by the fourfold screw rotation symmetry.

$$U^aU^cU^bU^cU^aU^cU^bU^c = [U^aU^cU^bU^c]^2 = -I_4. \tag{2.41}$$

$$U^cU^aU^bU^aU^bU^cU^aU^bU^aU^b = [U^c(U^aU^b)^2]^2 = I_4. \tag{2.42}$$

Therefore, all the 8-loops have a $\pi$ flux and all the 10-loops have a zero flux. We note that the hopping model in this $\pi$-flux configuration does not break the original translation symmetry [2].

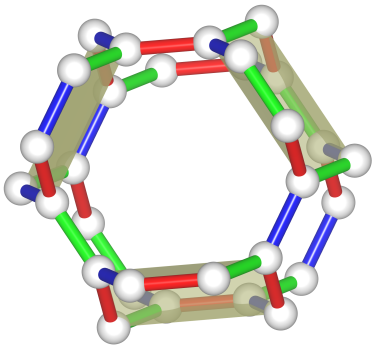

Figure 2.12: Part of (8,3)-$b$. All the three elementary loops of length 8 are highlighted by yellow surfaces. They are related by the threefold rotation symmetry.

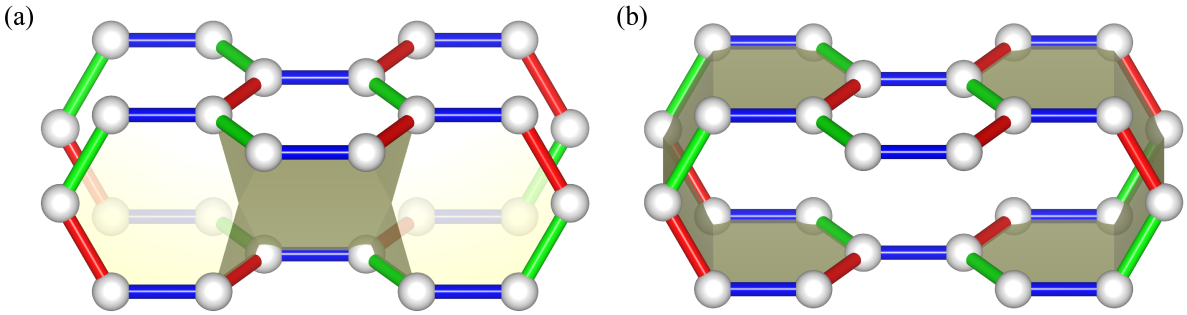


Figure 2.13: Part of the stripyhoneycomb lattice. (a) A loop of length 14 is highlighted. (b) A pair of loops of length 12 are highlighted. They are related by the inversion symmetry (or the volume constraint) and thus have the same flux.

### 2.8.5 (8,3)-$b$

The hyperhexagon lattice (8,3)-$b$ has three elementary loops of length 8, and they are related by the threefold rotation symmetry changing the $xyz$-axes, as shown in Fig. 2.12. Therefore, it is enough to check only one of them. The direct calculation tells us that it has a $\pi$ flux.

$$U^a U^c U^b U^c U^a U^c U^b U^c = [U^a U^c U^b U^c]^2 = -I_4. \tag{2.43}$$

Therefore, (8,3)-$b$ is in the $\pi$-flux configuration. We note that there is another elementary loop of length 12, but the flux value is immediately determined to be zero due to the accidental fourfold symmetry of the coloring. It is worth mentioning the hopping model in this $\pi$-flux configuration does not break the original translation symmetry, and thus the LSMA theorem applies as it is to the $\pi$-flux SU(4) Hubbard model, as well as the SU(4) Heisenberg model.

### 2.8.6 Stripyhoneycomb lattice

The stripyhoneycomb lattice is nonuniform, so the length of the shortest elementary loops differs in space. Every elementary loop of length 6 is the same as the honeycomb, and thus has a $\pi$ flux. The structure includes two types of the $\pi$-flux hexagons aligning in different planes [129]. In addition, there exist a long loop of length 14 (14-loop) and a twisted loop of length 12 (12-loop) [see Fig. 2.13]. These four types of elementary loops are enough to determine the flux values.

One 14-loop shown in Fig. 2.13(a) has a zero flux because

$$U^aU^cU^aU^bU^cU^bU^cU^aU^cU^aU^bU^cU^bU^c = [U^aU^cU^a(U^bU^c)^2]^2 = I_4. \tag{2.44}$$

One 12-loop shown on the right-hand side of Fig. 2.13(b) also has a zero flux because

$$U^aU^bU^cU^aU^bU^cU^bU^aU^cU^bU^aU^c = (U^aU^bU^c)^2(U^bU^aU^c)^2 = I_4. \tag{2.45}$$

There are many other tricoordinated lattices not discussed in this thesis, so it is future work to determine the flux values for all the possible tricoordinated lattices.

# Chapter 3

# Summary and Discussions

## 3.1 Summary

As discussed in the Introduction, the SU($N$) magnetism has a distinct feature with additional degrees of freedom to realize new QSLs beyond geometric/exchange frustration. Especially, a stable Dirac spin liquid is expected in the SU(4) Heisenberg model on the honeycomb lattice, but no material candidates were found for this exotic model, and even the realization in cold atoms has not been achieved.

In summary, we newly found that, as a consequence of the combination of the octahedral ligand field and SOC, an SU(4) symmetry *emerges* in $\alpha$-$ZrCl_3$. This is contrary to the ordinary expectation that SOC reduces the symmetry of spins. The derivation is similar to Ref. 14, but we employed the language of a lattice gauge theory to simplify the discussions. This would pave a new way to realize the SU(4) magnetism in real materials, not restricted to cold atomic systems.

In addition to the $\alpha$-$ZrCl_3$ (or $A_2M'O_3$) family we have discussed, Zr- or Hf-based MOFs could also realize SU(4) Heisenberg models on various tricoordinated lattices. Especially, 3D (10,3)-$a$ [130], (10,3)-$b$ [131], and $8^2$.10-$a$ [2, 132] lattices, as well as the 2D honeycomb lattice [133], were already realized in some MOFs with an oxalate ligand. Thus we can expect that microscopic models defined by Eq. (2.4) on various tricoordinated lattices will apply in the same way as the honeycomb $\alpha$-$ZrCl_3$ if we replace the metal ions of these MOFs with $Zr^{3+}$, $Hf^{3+}$, $Nb^{4+}$, or $Ta^{4+}$ [1].

Such orbital physics can be sought in other systems like $f$-electron systems. For example, $ErCl_3$ may have twofold orbital degeneracy at low temperature [134, 135]. In most cases, orbitals have twofold degeneracy, so the highest achievable symmetry of QSOLs in spin-orbital materials is SU(4). Whether it is possible to realize SU(6) spin systems in spin-orbital systems is an interesting open question. So far a cold atomic system is the only candidate for SU(6).

The JT term which couples the orbital to the lattice has been ignored so far. Usually, this term breaks a symmetry of the lattice, resulting a JT transition to the low-symmetry phase [85]. In order for the symmetric phase to survive, the itinerant quantum fluctuation which can tunnel between classical ground states may be necessary. Thus, the competition between QSOLs and JT phases (orbital order) can be understood by the spinon/orbitalon band width $W \sim J = 8t^2/(3U)$ [84]. If $J$ is large enough to stabilize the (orbital)

symmetric state, then the kinetic energy gain of orbitalons may destabilize the JT order. Thus, such energy gain may be maximized around the Mott transition, and thus the $4d$- or $5d$-materials with a smaller $U$ may be beneficial. In the Dirac spin-orbital liquid phase, the Dirac dispersion of mobile spinons and orbitalons result in characteristic specific heat and thermal conductivity. The specific heat $C$ behaves as $C \propto T^2$ as the temperature $T$ goes to 0, and with a magnetic field it should behave $C \propto T$ in Dirac spin liquids within the mean-field approximation [136]. In reality, the gauge field also contributes to $C$. The correction from the gauge field is a future problem, but there is a possibility that a characteristic correction exists in the gauge sector if the low-energy gauge theory is SU(4) QCD.

Experimentally, muon spin resonance or nuclear magnetic resonance (NMR) experiments can rule out the existence of long-range magnetic ordering or spin freezing in the spin sector. In the orbital sector, a possible experimental signature to observe the absence of orbital ordering or freezing should be ESR [89] or EXAFS [12], similarly to BCSO. Especially, (finite-frequency) ESR can observe the dynamical JT effect [137, 138], where the $g$-factor isotropy directly signals the quantum fluctuation between different orbitals [89, 139, 140]. For example, in the case of BCSO [89], the orbital ordering of the $d_{x^2-y^2}$ and $d_{z^2}$ orbitals directly couples to the tetragonal distortion of the octahedron. Thus, the strained direction of the anisotropic $g$-tensor signals the direction of the orbital "polarization" between the two $e_g$ orbitals. This is also applicable to our $t_{2g}$ case because of the shape difference in the $J_{\text{eff}} = 3/2$ orbitals [22], and the static JT distortion will result in the anisotropy in the in-plane $g$-factors [141]. Here we note that the trigonal distortion existing *a priori* in real materials only splits the degeneracy between the out-of-plane and in-plane $g$-factors, and the splitting of the two in-plane modes clearly indicates some (*e.g.* tetragonal) distortion. The emergent SU(4) symmetry would result in changing the universality class of critical phenomena, or in an accidental coincidence between the time scales of two different excitations for spins and orbitals observed by NMR and ESR, respectively.

On the other hand, the direct detection of orbitalons may be challenging. (Charged) orbitalons carry an orbital angular momentum as well as heat. Magnetically an orbital angular momentum is indistinguishable and mixed with a spin by SOC. However, since the orbital fluctuation is coupled to the lattice, an electric field, light, or x-rays can directly affect the orbital sector [85]. Especially, a light beam with an orbital angular momentum has been investigated recently [142], and may be useful for the detection of orbitalons. It is future work to discover the connection between such technology and fractionalized orbital excitations.

## 3.2 Discussion and comparison with twisted bilayer graphene

Finally, we would like to mention another candidate material for SU(4) models. Specifically, twisted bilayer graphene (TBG) attracted attention after the discovery of a correlated insulating state and accompanied superconductivity [143, 144]. Graphene is a honeycomb lattice sheet of carbon [145]. Bilayer graphene is a van der Waals structure

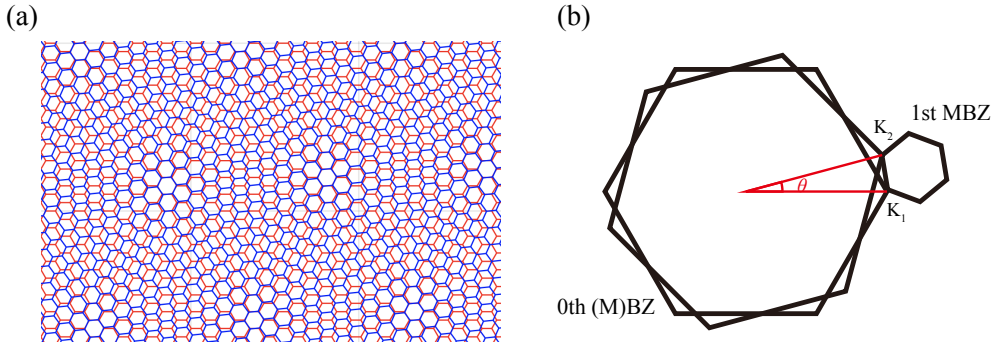


Figure 3.1: (a) Typical moiré pattern of TBG. The first and second layers are shown in red and blue, respectively. (b) Moiré Brillouin zone (MBZ). The original (first) Brillouin zone is shown by two large hexagons, each of which represents a Brillouin zone for each layer. Since the two layers are twisted by a (magic) angle $\theta$, Brillouin zones are also twisted by this angle. The first MBZ is shown as a smaller hexagon, which connects the two K points of the original Brillouin zones differed by the angle $\theta$. When $\theta \sim 1.1^\circ$ (a magic angle), flat bands are expected in the effective model. When $\theta = 0$, we can regard the original Brillouin zones as the "zeroth" MBZ and due to the degeneracy of two layers and spins the effective model of TBG has an effective SU(4) symmetry within the zeroth-order approximation.

made of two graphene layers. When two graphene layers are twisted by an angle $\theta$, the so-called moiré pattern appears in the real space [see Fig. 3.1(a)]. At some specific $\theta$ called magic angle, the bandwidth approaches zero [146], leading to strong correlation due to a large $U/t$ in the effective Hubbard model. Though the correct low-energy theory of TBG is complicated and requires a so-called moiré Brillouin zone [see Fig. 3.1(b)], the SU(4) Hubbard model is still a good approximation in the "zeroth" order for this system consisting of spin and valley degrees of freedom with a strong correlation [147]. However, the zeroth-order case $\theta = 0$ is weakly correlated and in the strongly correlated insulating phase ($\theta \sim 1.1^\circ$) requires different maximally localized Wannier functions, and the low-energy model has no SU(4) symmetry in the first moiré Brillouin zone [148, 149]. Thus, $\alpha$-$ZrCl_3$ still has superiority because it has an exact SU(4) symmetry even in the strongly correlated region $U \to \infty$ with a strong SOC $\lambda \to \infty$.

After the discovery of TBG, similar 2D heterostructures were also investigated. Twisted bilayer TMDC is one of them [150, 151]. Those spin-valley systems are also important candidates for SU(4) magnetism and seeking an ideal SU(4) system among them would be important future work. There is an important DMRG result for the 0-flux SU(4) Hubbard model on the honeycomb lattice at quarter filling [152], though the results are not directly applicable to $\alpha$-$ZrCl_3$ due to the existence of a $\pi$ flux inside a plaquette.

# Appendix A

# Implications from the Lieb-Schultz-Mattis-Affleck theorem

The SU($N$) Heisenberg model on the two-dimensional (2D) honeycomb lattice admits the application of the Lieb-Schultz-Mattis-Affleck (LSMA) theorem [29, 67, 69, 70] for $N > 2$. However, the original paper by Affleck and Lieb [70] only discussed one-dimensional (1D) systems, so we would like to extend the claim to higher dimensions and systems with a space group symmetry. Let us first consider a periodic 2D lattice with the primitive lattice vectors $\boldsymbol{a}_{1,2}$, as defined in Fig. 2.1 in the main text. We define the lattice translation operators $\mathcal{T}_\mu$ along $\boldsymbol{a}_\mu$ for $\mu = 1, 2$.

Here we consider the case with a fundamental representation on each site of the honeycomb lattice, which includes the SU(4) Heisenberg model discussed in the main text. We call each basis of the SU($N$) fundamental representation "flavor". The Hamiltonian of the SU($N$) Heisenberg model on the honeycomb lattice in general can be written as

$$H_{\mathrm{SU}(N)} = \frac{J_a}{N} \sum_{\langle ij \rangle \in a} P_{ij} + \frac{J_b}{N} \sum_{\langle ij \rangle \in b} P_{ij} + \frac{J_c}{N} \sum_{\langle ij \rangle \in c} P_{ij}, \tag{A.1}$$

up to constant terms, where $J_\gamma$s are the bond-dependent coupling constants for the $\gamma$-bonds, as defined in the main text, and $P_{ij}$ is the permutation operator of the flavors between the $i$th and $j$th sites. The translation symmetries, $\mathcal{T}_1$ and $\mathcal{T}_2$, exist independently of the values of $J_\gamma$s, so the following discussions apply to any positive $J_\gamma$s. Since the spin-1/2 Heisenberg antiferromagnetic interaction for the SU(2) spin can also be written as Eq. (A.1) with $N = 2$ dimensional Hilbert space at each site.

Now we discuss the generalization of the LSMA theorem to SU($N$) spin systems [28, 70, 95] in 2 dimensions following the logic of Ref. 67. One of the generators $I^0$ of the SU($N$) in the fundamental representation is given by the traceless $N \times N$ diagonal matrix:

$$I^0 = \frac{1}{N} \begin{pmatrix} 1 & 0 & \cdots & 0 & 0 \\ 0 & 1 & & 0 & 0 \\ \vdots & & \ddots & & \vdots \\ 0 & 0 & & 1 & 0 \\ 0 & 0 & \cdots & 0 & -(N-1) \end{pmatrix}. \tag{A.2}$$

We introduce an Abelian gauge field $\boldsymbol{\mathcal{A}}(\boldsymbol{r})$, which couples to the charge $I^0$, where $\boldsymbol{r}$ is the coordinate.

We assume that the (possibly degenerate) ground states are separated from the continuum of the excited states by a nonvanishing gap, and that the gap does not collapse during the flux insertion process discussed below. We consider the system consisting of $L_1 \times L_2$ unit cells on a torus, namely with periodic boundary conditions $\boldsymbol{r} \sim \boldsymbol{r} + L_1\boldsymbol{a}_1 \sim \boldsymbol{r} + L_2\boldsymbol{a}_2$. A ground state, which is SU($N$)-symmetric and has a definite crystal momentum (*i.e.* eigenstate of $\mathcal{T}_\mu$ with $\mu = 1, 2$), is chosen as the initial state. We adiabatically increase the gauge field from $\boldsymbol{\mathcal{A}} = 0$ to $\boldsymbol{\mathcal{A}} = \boldsymbol{k}_1/L_1$, so that the "magnetic flux" contained in the "hole" of the torus increases. When "magnetic flux" reaches the unit flux quantum $2\pi$, the Hamiltonian of the system becomes equivalent to the initial one. This happens precisely when the Hamiltonian is obtained from the original Hamiltonian with a large gauge transformation. The minimal large gauge transformation with respect to the charge $I^0$ is given by

$$\mathcal{U}_1 = \exp\left[\frac{i}{L_1}\sum_{\boldsymbol{r}} \boldsymbol{k}_1 \cdot \boldsymbol{r} I^0(\boldsymbol{r})\right], \tag{A.3}$$

where $\boldsymbol{k}_\mu$s are primitive reciprocal lattice vectors satisfying

$$\boldsymbol{k}_\mu \cdot \boldsymbol{a}_\nu = 2\pi\delta_{\mu\nu}. \tag{A.4}$$

The large gauge transformation satisfies the commutation relation,

$$\mathcal{U}_1\mathcal{T}_1 = \mathcal{T}_1\mathcal{U}_1 \exp\left[\frac{2\pi i}{L_1}\Big(I_T^0 - \sum_{\boldsymbol{r}\cdot\boldsymbol{k}_1 = 2\pi(L_1-1)} L_1 I^0(\boldsymbol{r})\Big)\right]. \tag{A.5}$$

Here $I_T^0 = \sum_{\boldsymbol{r}} I^0(\boldsymbol{r})$. Since the ground state is assumed to be an SU($N$)-singlet when the number of sites is a multiple of $N$, it belongs to the eigenstate with $I_T^0 = 0$. Furthermore, because eigenvalues of $I^0(\boldsymbol{r})$ are equivalent to $1/N \mod 1$, we find,

$$\mathcal{T}_1^{-1}\mathcal{U}_1\mathcal{T}_1 \sim \mathcal{U}_1 e^{-(2\pi i n L_2/N)}, \tag{A.6}$$

where $n$ is the number of sites in the unit cell.

Since the uniform increase in the vector potential does not change the crystal momentum, this phase factor due to the large gauge transformation alone gives the change of the crystal momentum in the flux insertion process. Choosing $L_2$ to be coprime with $N$, we find a nontrivial phase factor when $n/N$ is not an integer. This implies that, if $n$ is not an integer multiple of $N$, the system must be gapless or has degenerate ground states.

For the honeycomb lattice, $n = 2$, and there is no LSMA constraint for SU(2) spin systems. In contrast, for the SU(4) spin system we discussed in the main text, the ground-state degeneracy (or gapless excitations) is required even on the honeycomb lattice. Thus, the resulting quantum spin-orbital liquid (QSOL) [8] cannot be a "trivial" featureless Mott insulator when the symmetry is not broken spontaneously.

As explained in the above proof, the existence of a nontrivial generator $I^0$ is important for this theorem. In the case of $\alpha$-$ZrCl_3$ discussed in the main text, this element is not included in the generators of the original SU(2) × SU(2) symmetry of the spin-orbital

space, but included in the emergent SU(4) symmetry in the strong spin-orbit coupling limit. Thus, we can say that the SU(4) symmetry actually protects the nontrivial ground state of the SU(4) Heisenberg model on the honeycomb lattice.

This proof of the LSMA theorem is not restricted to bosonic systems, and applies to both bosonic and fermionic systems. Thus, the generalization to the (zero-flux) SU($N$)-symmetric Hubbard models is straightforward. With $N$-flavor fermionic degrees of freedom in the SU($N$) fundamental representation at each site, the necessary condition for the existence of a featureless insulator is that there exists a multiple of $N$ fundamental representations per unit cell, which can form an SU($N$) singlet. We note that the LSMA theorem for SU($N$) spin systems can be derived from the $U \to \infty$ limit of the SU($N$) Hubbard model at $1/N$ filling. One can also extend the LSMA theorem to the systems with general representations on each site, starting from a Hubbard model. That is, we include an appropriate onsite "Hund" coupling $J_H$ in the Hubbard model so that the desired representation have the lowest energy, and then take the $J_H \to \infty$ limit afterwards.

The generalization to the three-dimensional (3D) case with three translation operators, $\mathcal{T}_1$, $\mathcal{T}_2$, and $\mathcal{T}_3$, is again straightforward and we will omit the proof here, but it is useful to extend the LSMA theorem to the case with a space group symmetry. Recently, tighter constraints are obtained for nonsymmorphic space group symmetries [103,104] than what is implied by the LSMA theorem based on the translation symmetries only. This is because a nonsymmorphic symmetry behaves as a "half" translation, which would reduce the size of the effective unit cell.

As a demonstration, here we only discuss the constraint given by one nonsymmorphic (glide mirror or screw rotation) operation $\mathcal{G}$, by generalizing the flux insertion argument as in Ref. 104. We note that a tighter condition can be derived by dividing the torus into the largest flat manifold, which is called Bieberbach manifold, for some of the nonsymmorphic space groups [103].

Among the 157 nonsymmorphic space groups, the 155 except for $I2_12_12_1$ (No. **24**) and $I2_13$ (No. **199**) include an unremovable (essential) glide mirror or screw rotation symmetry $\mathcal{G}$ [153], so we will concentrate on these 155 to show how $\mathcal{G}$ works to impose a stronger constraint on filling. The nonsymmorphic operation $\mathcal{G}$ consists of a point-group operation $G$ followed by a fractional (nonlattice) translation with a vector $\boldsymbol{\alpha}$ in a direction left invariant by $G$, *i.e.* $\mathcal{G} : \boldsymbol{r} \mapsto G\boldsymbol{r} + \boldsymbol{\alpha}$ with $G\boldsymbol{\alpha} = \boldsymbol{\alpha}$. We again assume that the (possibly degenerate) ground states are separated from the continuum of the excited states by a nonvanishing gap, and that the gap does not collapse during the flux insertion process discussed below. A ground state $|\psi\rangle$, which is SU($N$)-symmetric and has a definite eigenvalue of all the crystalline symmetries including $\mathcal{G}$ (*i.e.* eigenstate of $\mathcal{G}$), is chosen as the initial state.

We note that, for every nonsymmorphic space group except for $I2_12_12_1$ (No. **24**) and its key nonsymmorphic operation $\mathcal{G}$, we can take an appropriate choice of primitive lattice vectors $\boldsymbol{a}_1$, $\boldsymbol{a}_2$, $\boldsymbol{a}_3$ with the following properties [103]: (i) The associated translation $\boldsymbol{\alpha}$ is along the direction of $\boldsymbol{a}_1$, and (ii) The plane spanned by $\boldsymbol{a}_2$ and $\boldsymbol{a}_3$ is invariant under $G$. Assuming this condition, we can show the tightest condition derived from only one nonsymmorphic operation $\mathcal{G}$. For simplicity, we consider the system consisting of $L_1 \times L_2 \times L_3$ unit cells on a 3D torus (*i.e.* impose the periodic boundary conditions $\boldsymbol{r} \sim \boldsymbol{r} + L_\mu \boldsymbol{a}_\mu$ for $\mu = 1, 2, 3$).

We take the smallest reciprocal lattice vector $\tilde{\boldsymbol{k}}_1$ left invariant by $G$, *i.e.* $G\tilde{\boldsymbol{k}}_1 = \tilde{\boldsymbol{k}}_1$ and $\tilde{\boldsymbol{k}}_1$ generates the invariant sublattice of the reciprocal lattice along $\tilde{\boldsymbol{k}}_1$. We insert a flux on a torus by introducing a vector potential $\boldsymbol{\mathcal{A}} = \tilde{\boldsymbol{k}}_1/L_1$. Since the "magnetic flux" reaches a multiple of $2\pi$ after this process because $\tilde{\boldsymbol{k}}_1$ is a reciprocal lattice vector, the Hamiltonian of the system becomes equivalent to the initial one. This happens precisely when the Hamiltonian is obtained from the original Hamiltonian with a large gauge transformation. The large gauge transformation to remove the inserted flux is

$$\mathcal{U}_{\tilde{\boldsymbol{k}}_1} = \exp\left[\frac{i}{L_1}\sum_{\boldsymbol{r}} \tilde{\boldsymbol{k}}_1 \cdot \boldsymbol{r} I^0(\boldsymbol{r})\right]. \tag{A.7}$$

Since $\boldsymbol{\mathcal{A}}$ is left invariant under $\mathcal{G}$, the inserted flux does not change the eigenvalues of $\mathcal{G}$. Thus, this phase factor due to the large gauge transformation alone gives the change of the eigenvalue of $\mathcal{G}$ for $|\psi\rangle$ in the flux insertion process. On the other hand,

$$\mathcal{G}^{-1}\mathcal{U}_{\tilde{\boldsymbol{k}}_1}\mathcal{G} \sim \mathcal{U}_{\tilde{\boldsymbol{k}}_1} e^{-(2\pi i \Phi_G(\tilde{\boldsymbol{k}}_1) n L_2 L_3/N)}, \tag{A.8}$$

where $\Phi_G(\tilde{\boldsymbol{k}}_1) = \boldsymbol{\alpha}\cdot\tilde{\boldsymbol{k}}_1/(2\pi)$. For an unremovable glide or screw symmetry, this phase factor has to be fractional.[1] Thus, if we write $\Phi_G(\tilde{\boldsymbol{k}}_1) = p/\mathcal{S}_G$ with $p, \mathcal{S}_G$ relatively coprime, we can show a tighter bound for the filling constraint to get a featureless Mott insulator without ground state degeneracy because $\mathcal{S}_G > 1$. In fact, to get a featureless Mott insulator $pnL_2L_3/(N\mathcal{S}_G)$ must at least be integer. However, if we choose $L_2$ and $L_3$ relatively prime to $N\mathcal{S}_G$, $n$ has to be a multiple of $N\mathcal{S}_G$.

If $n$ is not a multiple of $N\mathcal{S}_G$ for some nonsymmorphic operation $\mathcal{G}$, this means the existence of degenerate ground states with a different eigenvalue of $\mathcal{G}$, *i.e.* implies the existence of gapless excitations or a gapped topological order if the symmetry $\mathcal{G}$ is not broken. For example, in the case of the SU(4) Heisenberg model on the hyperhoneycomb lattice, $n = 4$, and the system can be trivial with respect to the translation symmetry. However, the space group of the hyperhoneycomb lattice includes some nonsymmorphic operations, such as one glide mirror with $\mathcal{S}_G = 2$. If we assume that nonsymmorphic symmetries are unbroken, the resulting QSOL (a possible symmetric ground state) cannot be a trivial featureless Mott insulator. Thus, we can say this QSOL is protected by the nonsymmorphic space group symmetry of the lattice and it can be called crystalline spin-orbital liquid (XSOL).

We note that as for the lattice (10,3)-$d$, it is not enough to consider only one symmetry operation and one has to consider the interplay of multiple nonsymmorphic operations [104]. The derivation of the tightest bound for all the 157 nonsymmorphic space groups with an SU($N$) symmetry is outside of the scope of this thesis. As we will discuss *e.g.* in Appendix B, a nonsymmorphic symmetry sometimes exchanges the bond label, and then it only exists when $J_\gamma$ obeys some condition. In this limited case, the generalized LSMA theorem only applies in some parameter region defined by this condition.

[1] We can show that if $\Phi_G(\tilde{\boldsymbol{k}}_1)$ is an integer, then this nonsymmorphic operation is removable, *i.e.* can be reduced to a point-group operation times a lattice translation by change of origin [153].

# Appendix B

# Basic theory for crystalline spin liquids in Kitaev spin liquids

Since in the main text we have treated the notion of crystalline spin (or spin-orbital) liquids in an abstract way, we would like to review how it is materialized in real models. We only give one typical example of crystalline spin liquids, a Kitaev model on the $8^2.10$-$a$ lattice. In this case a nonsymmorphic symmetry of the lattice space group protects the existence of fourfold degeneracy[1] and the emergence of a 3D Dirac cone in the Majorana spectrum, which is impossible in the original classification of 3D Kitaev models based on time-reversal and inversion symmetries [100]. The difference between topological crystalline insulators and crystalline spin liquids (XSLs) lies in how the space group symmetry acts on quasiparticle excitations. Projective representations are allowed in spin liquids. In some sense, it can be regarded as a gapless version of symmetry-enriched topological (SET) phases. The discussion here follows Ref. 2. The notation is slightly different from the original one in the main text. We use the standard $xyz$-notation instead of the $abc$-notation. We note that we only solve pure Kitaev models and ignore any kinds of interactions, although it has to be discussed if we wish to claim the phase to be stable.

## B.1 Kitaev's solution to the Kitaev model

The construction of the Kitaev (honeycomb) model is based on exchange frustration. It has a bond-dependent anisotropic interactions between spin-1/2 degrees of freedom. The Kitaev model can host both a gapless spin liquid phase and a gapped $Z_2$ spin liquid phase, which is related to the toric code [57]. This section follows Ref. 53.

The Kitaev model on the honeycomb lattice is defined as follows.

$$\begin{aligned} H_{\text{Kitaev}} &= K_x \sum_{\langle jk\rangle\in x} S_j^x S_k^x + K_y \sum_{\langle jk\rangle\in y} S_j^y S_k^y + K_z \sum_{\langle jk\rangle\in z} S_j^z S_k^z \\ &= -J_x \sum_{\langle jk\rangle\in x} \sigma_j^x \sigma_k^x - J_y \sum_{\langle jk\rangle\in y} \sigma_j^y \sigma_k^y - J_z \sum_{\langle jk\rangle\in z} \sigma_j^z \sigma_k^z, \end{aligned} \tag{B.1}$$

[1] In a correct sense there is twofold redundancy coming from the Majorana property. From now on, we ignore this subtlety and regard it as fourfold degeneracy.

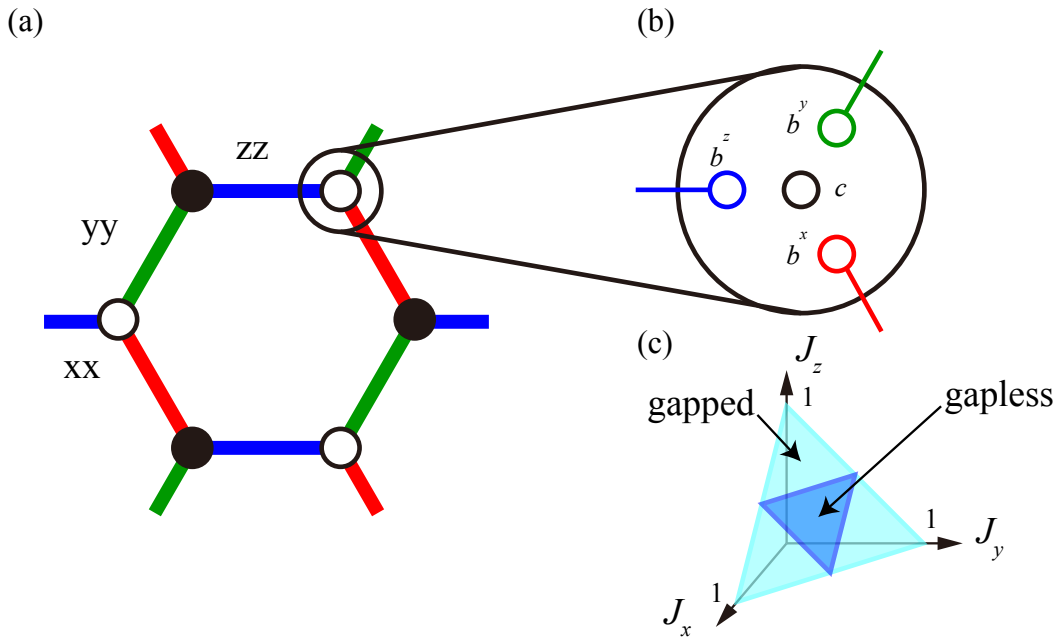


Figure B.1: Kitaev model on the honeycomb lattice. (a) Coloring of the honeycomb lattice and the bond-dependent anisotropic interactions. Red, green, and blue bonds show $x$-, $y$-, and $z$-directional anisotropy, respectively. (b) Majorana representation of spin-1/2 degrees of freedom. (c) Phase diagram of the Kitaev model on the honeycomb lattice.

where $\langle jk \rangle \in \alpha$ means that a nearest neighbor bond $\langle jk \rangle$ belongs to the $\alpha$-directional bond with the same color as shown in Fig. B.1(a), $K_x$, $K_y$, $K_z$ are real parameters, and $J_\alpha = |K_\alpha|/4$ for each $\alpha = x, y, z$. This model is known to have the properties of quantum spin liquids with any nonzero parameters $K_x$, $K_y$, $K_z$, but we here concentrate on the ferromagnetic case where $K_x < 0$, $K_y < 0$, and $K_z < 0$, for simplicity.[2] In this case, the exchange frustration is clear because the red (resp. green and blue) bonds want to align spin in the $x$- (resp. $y$- and $z$-) direction, and these conditions cannot be met simultaneously for the classical spin.

The ground state is exactly solved by introducing a so-called Majorana representation of the spin operators and mapping the problem to finding a correct flux sector. For each site $j$, we introduce four anticommuting real Majorana fermions $b_j^x$, $b_j^y$, $b_j^z$, and $c_j$, as shown in Fig. B.1(b). From the anticommutation relations like $\{b_j^\alpha, b_k^\beta\} = 2\delta_{jk}\delta^{\alpha\beta}$, it is easy to show that the spin-1/2 Pauli matrices can be represented as $\sigma_j^\alpha = ib_j^\alpha c_j$. Even in the minimal representations for these Majorana operators, the Hilbert space is expanded from the original spin-1/2 space (with 2 dimensions per site). Therefore, the Hilbert space must be projected out from the Fock space $\tilde{\mathcal{L}}$ (with 4 dimensions per site because two Majorana fermions become one complex fermion) to the physical subspace $\mathcal{L}$ to go back to the original spin representation. The physical subspace $\mathcal{L}$ is defined by the condition $|\xi\rangle \in \mathcal{L}$ iff $D_j |\xi\rangle = |\xi\rangle$ for all $j$, where $D_j = ib_j^x b_j^y b_j^z c_j$. It is really physical because every algebra of Pauli matrices like $\sigma_j^x \sigma_j^y \sigma_j^z = i$ is reproduced in this subspace.

[2] This is because the sign change can always be compensated by the gauge transformation.

If we define a $Z_2$ gauge flux $\hat{u}_{jk}$ by $\hat{u}_{jk} = ib_j^{\alpha_{jk}} b_k^{\alpha_{jk}}$, where $\alpha_{jk}$ is the bond direction between $j$ and $k$, then the Hamiltonian in $\tilde{\mathcal{L}}$ becomes $\tilde{H} = \frac{i}{2}\sum_{\langle jk\rangle} J_{\alpha_{jk}} \hat{u}_{jk} c_j c_k$, where each bond $\langle jk\rangle$ is counted twice with $\hat{u}_{kj} = -\hat{u}_{jk}$. This is nothing but a $Z_2$ lattice gauge theory for Majorana fermions $c_j$ with an external magnetic field with a $Z_2$ gauge field defined by $\hat{u}_{jk}$. Because $\hat{u}_{jk}$s all commute with $\tilde{H}$, after defining the eigenstates of $\hat{u}_{jk}$s and replacing them by $c$-variables $u_{jk}$, we can diagonalize the quadratic Hamiltonian $\frac{i}{2}\sum_{\langle jk\rangle} J_{\alpha_{jk}} u_{jk} c_j c_k$ for itinerant $c_j$ fermions to get the ground state for each flux sector by applying projection operators $(1+D_j)/2$ to $\mathcal{L}$. Given a magnetic flux $w_p$ for each hexagonal plaquette $p$, this uniquely determines the ground state spectrum by diagonalizing a one-particle Hamiltonian for $c_j$ fermions. The ground state of this free model $|\tilde{\Psi}\rangle \in \tilde{\mathcal{L}}$ can be projected onto the physical subspace $\mathcal{L}$ by

$$|\Psi\rangle = \prod_j \frac{1+D_j}{2} |\tilde{\Psi}\rangle \in \mathcal{L}. \tag{B.2}$$

Therefore, the only thing left is to determine the correct flux sector including the exact ground state of the original Hamiltonian. From Lieb's beautiful theorem on the flux sector with the lowest energy [66], we can rigorously conclude that the answer is the flux sector with zero magnetic flux. Therefore, we can replace $u_{jk}$ by 1 and the ground state spectrum completely becomes a Majorana version of the nearest-neighbor honeycomb tight-binding model. In the case $J_x = J_y = J_z$, this is the same model as that for graphene and it is a well-known fact that there are Dirac cones at K and K′ points in the Brillouin zone [see also Fig. B.2(b)], and we can conclude that the ground state is a gapless spin liquid. From triangular inequalities, we can determine the region where the Majorana spectrum is gapless, *i.e.* the one-particle Hamiltonian has a zero eigenstate as $J_\alpha \le J_\beta + J_\gamma$, where $\alpha$, $\beta$, $\gamma$ is a permutation of $x$, $y$, $z$. The phase diagram (gapless or gapped) on the plane $J_x + J_y + J_z = 1$ is shown in Fig. B.1(c). Dirac cones in the gapless region are protected by the time-reversal symmetry and the topological nature of the vector bundle of the wavefunction, which will be discussed in the next section again.

## B.2 Lieb's theorem and ground state flux sectors

In the case of the honeycomb lattice, Lieb's theorem [66] is applicable to the flux problem when $J_x = J_y$, but it requires a specific reflection (mirror) symmetry on the lattice and it will not apply to most of the generalized 3D Kitaev models. Let us quickly review the claim of Lieb's theorem without giving a proof. Assuming the existence of a translation symmetry and a reflection symmetry whose mirror plane cuts bonds, not sites [see Fig. B.2(a) for comparison], we can prove the following theorem.

**Theorem 2.** *For any periodic bipartite lattices, the flux problem for the half-filled tight-binding (Hubbard) model is solved for each plaquette of length $l$ containing a cutting mirror plane as follows.*

1. *A plaquette $C$ will carry zero flux, i.e. $\prod_{\langle jk\rangle\in C} u_{jk} = 1$, when $l \equiv 2 \mod 4$.*
2. *A plaquette $C$ will carry $\pi$ flux, i.e. $\prod_{\langle jk\rangle\in C} u_{jk} = -1$, when $l \equiv 0 \mod 4$.*

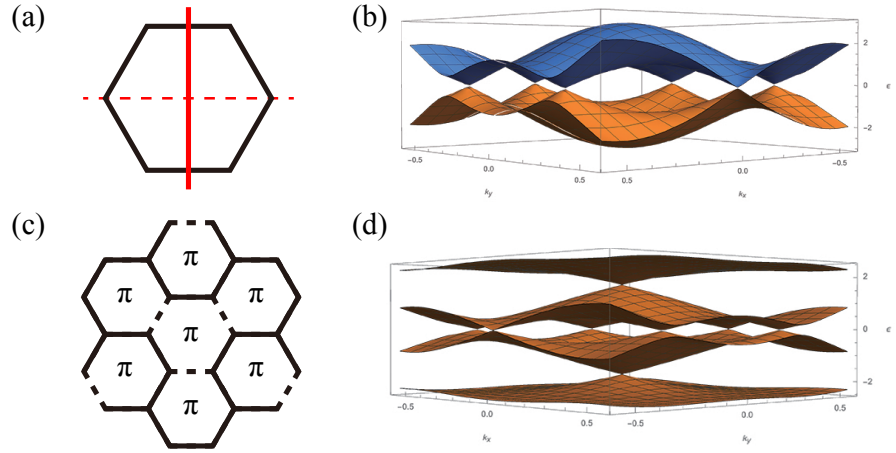


Figure B.2: (a) Mirror planes of the honeycomb lattice. A solid red line shows a mirror plane used in Lieb's theorem, and a dashed red line shows an irrelevant one. (b) Band structure for the 0-flux state. At half filling, there are six Dirac cones shown in the figure. Only two of them are independent, located at K and K′ points. (c) "Benzene" gauge for the $\pi$-flux state. $-1$ bonds are shown by dashed lines. (d) Band structure for the $\pi$-flux state. At quarter filling it looks like there is only one Dirac cone at $\Gamma$ point, but it is actually doubly degenerate because the enlarged unit cell of the benzene gauge has redundancy, being twice larger than that of the minimal one. At half filling, the spectrum is similar to (b).

We note that this theorem is generic not only for the free model, but also for interacting models. In Ref. 66 many types of reflection-positive interactions are considered and Lieb's theorem applies to many interacting fermion models. Since this theorem is very generic, only involving a periodic array of mirror planes, it is applicable to any dimensions and, if we could solve a flux problem for every elementary loop, we can decide the correct ground state for the underlying Kitaev model. Otherwise, a numerical simulation is always necessary to determine the ground state flux sector.

If this theorem is applied to the square lattice, as originally proposed by Lieb [66], a $\pi$ flux for each square plaquette should be optimal in accordance with Affleck-Marston's theory [44]. In the case of the honeycomb lattice, it becomes 0-flux instead.[3] In this 0-flux case, the ground state Majorana spectrum of the Kitaev model is the same as that of graphene. We quickly review a one-body band structure of graphene to solve the nearest-neighbor tight-binding model for the Kitaev honeycomb model.

For simplicity, we focus on the gapless phase of the 0-flux Kitaev model, and assume $J_x = J_y = J_z \equiv J$. Then, the ground state can be constructed from the half-filled Fermi sea of the tight-binding model. As already explained, it has two Dirac cones at K and K′ points. The spectrum is conical and is effectively described by a relativistic theory. Because of the Nielsen-Ninomiya-type theorem [154], the spectrum cannot be gapped unless two Dirac cones collide by a nonperturbative threefold rotation symmetry

[3] We note that in the honeycomb lattice only the mirror planes cutting bonds work and such planes exist only when $J_x = J_y$, $J_y = J_z$, or $J_z = J_x$.

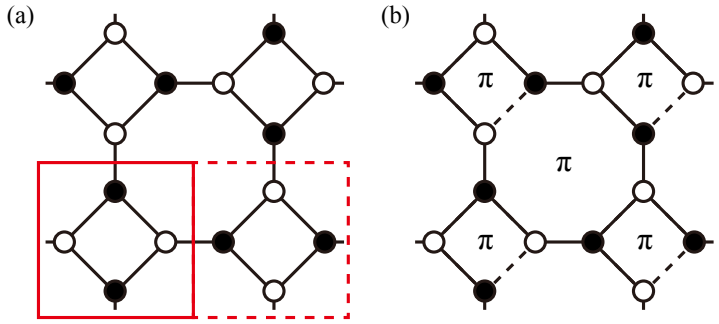


Figure B.3: Kitaev model on the squareoctagon lattice. (a) The squareoctagon lattice and its sublattice labels (white and black circles). The unit cell is shown by a red solid line and the neighboring one is shown by a red dashed line. (b) One translation-symmetric gauge for the $\pi$-flux state. $-1$ bonds are shown by dashed lines.

breaking term. The overview of the spectrum in the hexagonal Brillouin zone is shown in Fig. B.2(b).

Just for a comparison, we also review the spectrum of the $\pi$-flux honeycomb lattice. The most symmetric view for the band structure of the $\pi$-flux model can be achieved by taking a "benzene" gauge, where only double bonds of benzene are set to have $-1$, as shown in Fig. B.2(c). We again assume $J_x = J_y = J_z \equiv J$. The spectrum has Dirac cones not only at half filling but also at 1/4 and 3/4 fillings [see Fig. B.2(d)].[4] According to Kitaev [47], the energy difference between the 0-flux and $\pi$-flux sectors is $0.067J$ per hexagon at half filling. We note that an isolated vison (flux) excitation from the 0-flux ground state has an energy $\Delta E \sim 0.27J$.

## B.3 Classification of Kitaev models by internal symmetries

The general discussion for the classification of 3D Kitaev models is complicated, so we just give known results on the classification, and present one 2D example, which is more intuitive for most readers than 3D systems, in order to show how internal symmetries are implemented projectively in Kitaev models. This section follows Ref. 100 and thus include the inversion symmetry in the set of "internal" symmetries for simplicity.[5]

The classification of the Kitaev model is not as straightforward as the free-fermion topological periodic table [155]. In order to see this we first take up the Kitaev model on the 2D squareoctagon lattice [156–158]. The squareoctagon lattice is shown in Fig. B.3(a). This lattice is related to the 3D hyperoctagon lattice, but has a better property because Lieb's theorem is applicable.[6] They share the same property that the projective implementation of the time-reversal symmetry plays an important role.

[4] This is why this $\pi$-flux state is important not in half-filled Majorana models, but in SU(4) models discussed in the main text.

[5] In a correct sense, the inversion symmetry is also a lattice (spatial) symmetry.

[6] The 3D hyperhexagon lattice has a nice property, too, but not suitable for our purpose here.

In the same way as Affleck-Marston's ansatz [44] discussed in the main text, the ground state of the squareoctagon lattice is described by a $\pi$-flux state. Both square and octagon plaquettes are likely to bind a $\pi$ flux in accordance with Lieb's theorem [66]. The translation is implemented trivially in contrast to Affleck-Marston's ansatz [44], but other lattice symmetries are implemented projectively in a way similar to Affleck-Marston's [see Fig. B.3(b)]. Due to the property of the Kiteav model (or the Majorana representation), there is an additional feature nonexistent in other complex fermion models. Especially, the implementation of the time-reversal symmetry is the most exotic one specific to the Kitaev model, so we only review its projective property in this appendix.

The time-reversal symmetry is different not only because it is antiunitary, but also because it involves the sublattice symmetry of the lattice. As already discussed by Kitaev [47], if the lattice is not bipartite (*i.e.* has a loop of an odd length), the time-reversal symmetry is spontaneously broken leading to degenerate chiral spin liquid (CSL) states at the ground state, as is the case with the Kitaev models *e.g.* on the (9,3) lattices. Fortunately, the squareoctagon lattice is bipartite, so the time-reversal symmetry is preserved. However, as shown in Fig. B.3(a), the sublattice symmetry is not compatible with translation, so the time-reversal symmetry, too, becomes projective.

In the squareoctagon lattice, the translation along the $x$- or $y$-axis changes the sublattice parity, so the projective symmetry group (PSG) of the time-reversal operation $T$ always involves a gauge transformation extended across the unit cell to repair the sublattice. Naïvely, the action of $T$ is $Tc_jT^{-1} = c_j$ and $Tb_j^\alpha T^{-1} = b_j^\alpha$. Thus, $T\hat{u}_{jk}T^{-1} = -\hat{u}_{jk}$. However, since Kitaev's Majorana Hamiltonian itself is defined from the sublattice index for bipartite lattices, the gauge transformation is determined very easily. If we define a sublattice parity as $(-1)^j$ for the $j$th site, then the time-reversal operation supplemented by a gauge transformation $\tilde{T}$ can only act like $\tilde{T}c_j\tilde{T}^{-1} = (-1)^j c_j$ and $\tilde{T}b_j^\alpha\tilde{T}^{-1} = (-1)^j b_j^\alpha$. Thus, because this gauge transformation is possible only in the extended unit cell (both solid and dashed red unit cells are necessary in Fig. B.3(a)) the action of $\tilde{T}$ requires a supplemental translation in the $k$-space. In particular, in the case of the square/squareoctagon lattice $\boldsymbol{k}_0 = (\pi/2, \pi/2)^t$ is necessary to maintain the gauge transformation [100]. Since $T$ (or $\tilde{T}$) is antiunitary, the final form of the implementation of the time-reversal symmetry becomes

$$\hat{h}(\boldsymbol{k}) = U_T \hat{h}^*(-\boldsymbol{k} + \boldsymbol{k}_0) U_T^{-1}, \tag{B.3}$$

$$\varepsilon(\boldsymbol{k}) = \varepsilon(-\boldsymbol{k} + \boldsymbol{k}_0), \tag{B.4}$$

where $\hat{h}(\boldsymbol{k})$ is a (one-body) Bloch Hamiltonian for itinerant Majorana fermions, and $\varepsilon(\boldsymbol{k})$ is its spectrum. $U_T$ is a unitary matrix defined from the action of $\tilde{T}$.

As for 2D lattices, the classification is almost completed: when $\boldsymbol{k}_0 = 0$, a stable object is a Dirac cone at the Fermi level if gapless, and when $\boldsymbol{k}_0 \neq 0$, a stable object is a Fermi surface if gapless, where each Fermi surface may be related by the reciprocal lattice vector $\boldsymbol{k}_0$. In the 3D case, it is more complicated because the (projective) inversion symmetry may require a different $k$-space translation $\boldsymbol{k}_0'$ depending on its flux sector, even if gapless. If $\boldsymbol{k}_0 = 0$, a stable gapless object is a nodal line, which is a natural generalization of a Dirac cone. If $\boldsymbol{k}_0 \neq 0$, the inversion symmetry becomes important in the 3D case. If $\boldsymbol{k}_0 \neq 0$ and $\boldsymbol{k}_0' = 0$, the inversion symmetry is implemented trivially and a stable object becomes a Weyl node. Otherwise, $\hat{h}(\boldsymbol{k})$ has no trivially-implemented internal symmetry,

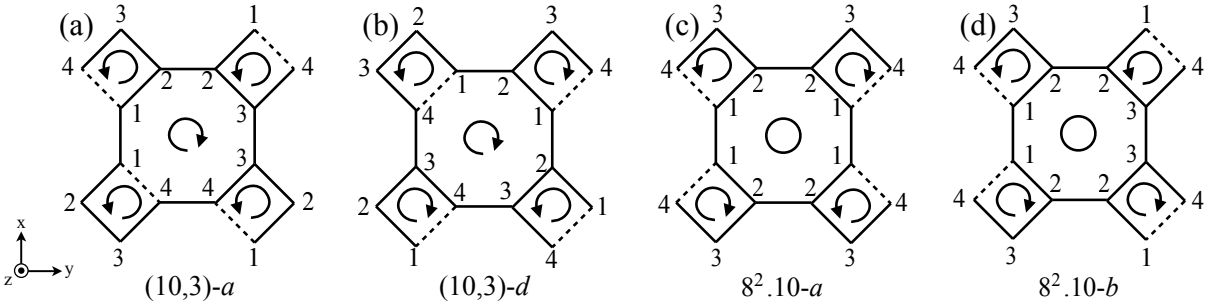


Figure B.4: 3D lattices constructed from the squareoctagon lattice. Every lattice is constructed by extending the squareoctagon lattice along the $z$-direction. (a) (10,3)-$a$. (b) (10,3)-$d$. (c) $8^2$.10-$a$. (d) $8^2$.10-$b$. Reprinted figure with permission from [M. G. Yamada, V. Dwivedi, and M. Hermanns, Phys. Rev. B, **96**, 155107 (2017).] Copyright 2017 by the American Physical Society.

and the only remaining gapless object is a Fermi surface.[7] The classification becomes rich if we break one of these symmetries explicitly/spontaneously [98], but this already completed the classification based on the internal symmetries [100].[8] One interesting thing in this classification is that a Weyl semimetal of Majorana fermions is possible even with time-reversal and inversion symmetries due to their projective nature.

While from the symmetry analysis the spectrum of the squareoctagon lattice has a Fermi surface if gapless, the $\pi$-flux state is actually gapped. However, the 0-flux sector is known to have Fermi surfaces (or more accurately Fermi circles), and would be stabilized by an additional flux stabilization term [157]. In this 0-flux sector, the phase diagram is similar to the honeycomb case [see Fig. B.1(c)], and in the gapless regime Fermi surfaces are always stable. Anyway, the Kitaev model on the squareoctagon lattice shows a rich variety of phases depending on its flux sector, while it is not a main topic of this appendix. Even though in both 0-flux and $\pi$-flux sectors translation is implemented trivially, the time-reversal symmetry still plays an important role in the Kitaev model. A take-home message here is that the projective implementation (PSG) of the time-reversal/inversion symmetry topologically determines the spectrum in gapless phases in most 2D cases, and the same is true for the 3D hyperoctagon lattice, hyperhexagon lattice, etc.

## B.4 Lieb's flux sector and Majorana spectrum

The general classification discussed above for the 3D Kiteav model does not apply to the $8^2$.10-$a$ lattice, and thus it is meaningful to solve this model explicitly. Fortunately, Lieb's theorem is applicable to $8^2$.10-$a$ when $J_x = J_y$. Thus, we mostly concentrate on the case $J_x = J_y$, but we assume the same flux configuration even for other parameters. From the statement of Lieb's theorem 8-loops have to have a $\pi$ flux and 10-loops have to have a zero

[7] This type of Fermi surfaces is usually unstable with interaction [99].

[8] It seems that a possibility that the time-reversal and inversion symmetries share the same $\boldsymbol{k_0}$ is ignored, but this never happens in the examples discussed in Ref. 100.

flux in the ground state. This completely determines the flux configuration of $8^2.10\text{-}a$.[9]

In $8^2.10\text{-}a$, the time-reversal symmetry is implemented trivially, and thus the stable object should be a nodal line. However, it is not the case for $J_x = J_y$. When $J_x = J_y$, the nodal lines get degenerate, reduced to two gapless points with fourfold degenerate 3D Dirac cones. This is beyond the classification based on the internal symmetries.

The lattice structure of $8^2.10\text{-}a$ is schematically shown in Fig. B.4(c), but the number labelled in the figure is just to show the height along the $z$-axis in 2D. The real site numbering used in the following discussion is included in Ref. 2, instead. The coloring of bonds and the flux sector are accidentally the same as those discussed for the SU(4) model [see Subsec. 2.8.4].[10] Thus, we omit a detailed description of the lattice structure and directly move on to the construction of a Hamiltonian. Using the crystallographic axes, $\boldsymbol{a}_1$, $\boldsymbol{a}_2$, and $\boldsymbol{a}_3$ are defined as lattice vectors, and $\boldsymbol{R}$ spans every lattice point, *i.e.* $\boldsymbol{R} \in \mathbb{Z}\boldsymbol{a}_1 + \mathbb{Z}\boldsymbol{a}_2 + \mathbb{Z}\boldsymbol{a}_3$.

$$\begin{aligned} H_{\mathrm{XSL}} = -\sum_{\boldsymbol{R}} \{ & J_x \left[\sigma_1^x(\boldsymbol{R})\sigma_2^x(\boldsymbol{R}) + \sigma_3^x(\boldsymbol{R})\sigma_4^x(\boldsymbol{R})\right. \\ & \left. +\sigma_5^x(\boldsymbol{R})\sigma_8^x(\boldsymbol{R}+\boldsymbol{a}_3) + \sigma_6^x(\boldsymbol{R})\sigma_7^x(\boldsymbol{R})\right] \\ & + J_y \left[\sigma_1^y(\boldsymbol{R})\sigma_4^y(\boldsymbol{R}-\boldsymbol{a}_3) + \sigma_2^y(\boldsymbol{R})\sigma_3^y(\boldsymbol{R})\right. \\ & \left. +\sigma_5^y(\boldsymbol{R})\sigma_6^y(\boldsymbol{R}) + \sigma_7^y(\boldsymbol{R})\sigma_8^y(\boldsymbol{R})\right] \\ & + J_z \left[\sigma_1^z(\boldsymbol{R})\sigma_6^z(\boldsymbol{R}+\boldsymbol{a}_2-\boldsymbol{a}_3)\right. \\ & +\sigma_2^z(\boldsymbol{R})\sigma_7^z(\boldsymbol{R}-\boldsymbol{a}_1+\boldsymbol{a}_2) \\ & \left. +\sigma_3^z(\boldsymbol{R})\sigma_8^z(\boldsymbol{R}-\boldsymbol{a}_1+\boldsymbol{a}_3) + \sigma_4^z(\boldsymbol{R})\sigma_5^z(\boldsymbol{R})\right]\} \end{aligned} \tag{B.5}$$

This can be solved simply by introducing Majorana fermions. The desired flux configuration can be realized by setting the bond operators $u_{jk} = +1$ (resp. $-1$) if $j$ is odd (resp. even), except for the 1-6 bond where $u_{16} = -1$. The resulting one-body Majorana Hamiltonian $\hat{h}(\boldsymbol{k})$ after a Fourier transformation looks like

$$\hat{h}(\boldsymbol{k}) = \begin{pmatrix} 0 & A(\boldsymbol{k}) \\ A^\dagger(\boldsymbol{k}) & 0 \end{pmatrix}. \tag{B.6}$$

As before the spectrum of $\hat{h}(\boldsymbol{k})$ is $\varepsilon(\boldsymbol{k})$. $A(\boldsymbol{k})$ is defined by

$$A(\boldsymbol{k}) = i \begin{pmatrix} 0 & -J_z e^{2\pi i k_{23}} & J_x & J_y e^{-2\pi i k_3} \\ J_z e^{2\pi i k_{31}} & 0 & J_y & J_x \\ J_x e^{2\pi i k_3} & J_y & 0 & J_z \\ J_y & J_x & J_z e^{2\pi i k_{12}} & 0 \end{pmatrix}, \tag{B.7}$$

where $\boldsymbol{k}$ is a reciprocal vector normalized by $k_i \in [0, 1)$, and $k_{mn} = k_m - k_n$. We note that the matrix index is reordered to make it symmetric. Just by diagonalizing this Hamiltonian, we can see that in a gapless region with $J_x = J_y$ the spectrum of Majorana

[9] The naming of $8^2.10\text{-}a$ itself comes from the fact that it is constructed from elementary 8-loops and 10-loops [101].

[10] As for the SU(4) model, the flux sector here means the embedded flux configuration.

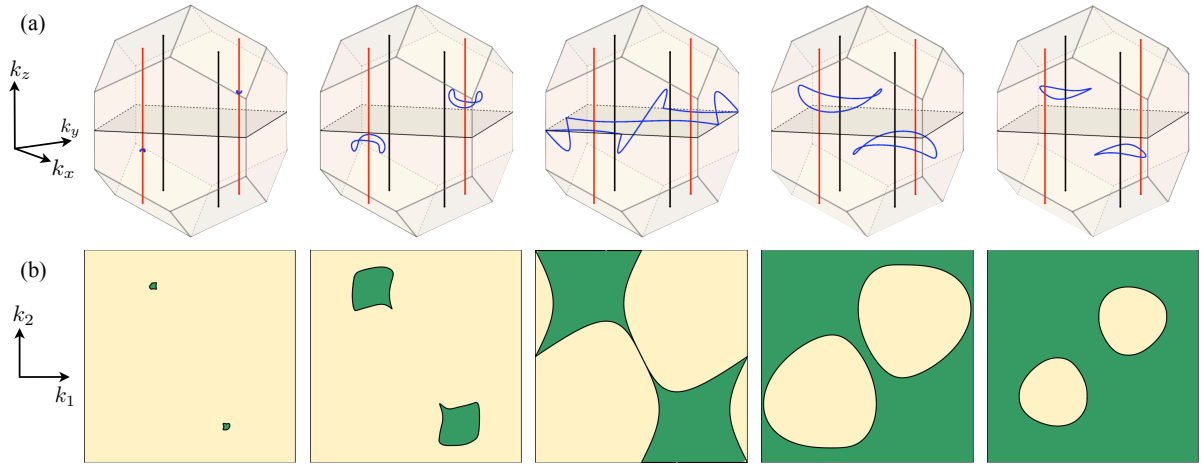


Figure B.5: (a) Zero-energy locus (blue) in the Brillouin zone (yellow) for the $8^2.10$-$a$ lattice for parameters $J_x = \frac{1}{3} + \Delta J, J_y = J_z = \frac{1}{3} - \frac{1}{2}\Delta J$, with $\Delta J = 0.01, 0.05, 0.0808, 0.10, 0.12$ (from left to right). Red solid lines are invariant under only the fourfold screw symmetry, while black solid lines are invariant under the twofold and fourfold screw symmetries. (b) Chiral invariant $\theta$ computed for the loops along the $k_3$ axis as a function of $(k_1, k_2)$ for a corresponding parameter, where the values 0, and $-1$ are represented by yellow and green, respectively. The black solid line depicts the projection of the bulk nodal line along $k_3$. Reprinted figure with permission from [2] Copyright 2017 by the American Physical Society.

fermions is described by 3D Dirac cones with fourfold degeneracy at some points in the Brillouin zone. These Dirac points actually lie on the invariant line of the fourfold screw symmetry. Fig. B.5 clearly shows how the zero-energy object evolves from Dirac cones to nodal lines by changing the parameters from $J_x = J_y$ to $J_x \neq J_y$. Detailed description is included in Ref. 2.

A chiral invariant $\theta$ in Fig. B.5(b) is defined by $A(\boldsymbol{k})$ as

$$\theta = \frac{1}{4\pi i} \oint_{\mathcal{C}} \mathrm{tr} \left\{ A^{-1} dA - \left(A^\dagger\right)^{-1} dA^\dagger \right\}, \tag{B.8}$$

for a contour $\mathcal{C}$ in the $k$-space.

## B.5 Physics of crystalline spin liquids

We claim it to be a crystalline phase because the fourfold degeneracy can only be protected under the space group symmetry in Majorana systems, while 2D Dirac cones are protected in the Kitaev model on the honeycomb lattice just by the time-reversal symmetry, and breaking the lattice symmetry just moves the location of the Dirac cones in the Brillouin zone. In order to see this we will check PSG of the screw symmetry of this lattice.

As easily seen from the spiral lattice structure [see Fig. B.4], there is a fourfold screw rotation symmetry, and we name it $S_4$ and its subgroup twofold screw rotation $S_2$. Of

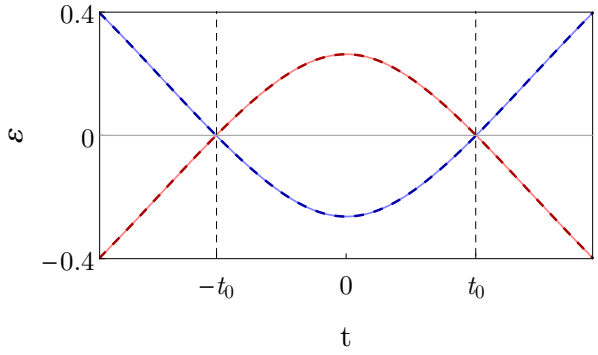


Figure B.6: Spectrum of the four bulk bands that are closest to $\varepsilon(t) = 0$ and that form the Dirac nodes, plotted along the screw symmetric line Eq. (B.11). The parameters are given by $J_x = J_y = 0.37$, $J_z = 0.26$, with the Dirac nodes corresponding to $t_0 \sim \pm 0.21$, solutions of $\varepsilon(t) = 0$. The bands are labeled by their screw eigenvalues $\rho_n e^{-3\,i\pi t}$ with $\rho_n = e^{i(2n+1)\pi/4}$. The bands with eigenvalues $\rho_0, \rho_1$ are denoted by red solid and dashed lines, and those with eigenvalues $\rho_2, \rho_3$ by blue solid and dashed lines, respectively. Reprinted figure with permission from [2] Copyright 2017 by the American Physical Society.

course, four $S_4$ and two $S_2$ operations are reduced to translation along the $z$-direction.[11] The importance of this symmetry is clearly shown in Fig. B.5(a) because the screw-invariant lines are always surrounded by the zero-energy objects and at the center of the spectrum. We note that all invariant lines do not pass through the origin because the symmetry is implemented projectively and the screw rotation involves the reciprocal lattice translation in the $k$-space. In Fig. B.5(a), those lines look like separated, but the ones in the same color are actually a single line connected on the boundary.

When $J_x = J_y$, the action of the fourfold screw symmetry is as follows.

$$\hat{h}(S_4\boldsymbol{k}) = \mathcal{U}_{S4}(\boldsymbol{k})\hat{h}(\boldsymbol{k})\mathcal{U}_{S4}^{\dagger}(\boldsymbol{k}), \tag{B.9}$$

where

$$S_4\,(k_1, k_2, k_3) = \left(k_3 - k_2, k_1 + \frac{1}{2}, k_3\right), \tag{B.10}$$

and the unitary matrix $\mathcal{U}_{S4}(\boldsymbol{k})$ depends on the rotation axis. Though we will not show an explicit form of the matrix representation, an important fact is that there is an invariant line where a Majorana Hamiltonian has some commuting unitary matrix. The invariant line can be parametrized as

$$\boldsymbol{\gamma}_t = t\,\boldsymbol{q}_1 + \left(t + \frac{1}{2}\right)\boldsymbol{q}_2 + \left(2t + \frac{1}{2}\right)\boldsymbol{q}_3, \tag{B.11}$$

where $\boldsymbol{q}_i$ are reciprocal lattice vectors obeying $\boldsymbol{q}_i \cdot \boldsymbol{a}_j = 2\pi\delta_{ij}$, and is periodic under $t \mapsto t + 1$. This line is shown in red in Fig. B.5(a). Explicitly, we note that for any momentum $\boldsymbol{\gamma}_t$,

$$[\mathcal{U}_{S4}(\boldsymbol{\gamma}_t), \hat{h}(\boldsymbol{\gamma}_t)] = 0, \tag{B.12}$$

[11] This Cartesian $xyz$-axis is different from the one used to derive the Jackeli-Khaliullin mechanism.

and $[\mathcal{U}_{S4}(\boldsymbol{\gamma}_t)]^4 = -e^{-12\,i\pi t} I_8$. Thus, the eigenstates $|\varphi_t\rangle$ of $\hat{h}(\boldsymbol{\gamma}_t)$ satisfy

$$\mathcal{U}_{S4}(\boldsymbol{\gamma}_t)\,|\varphi_t\rangle = \rho_n e^{-3\,i\pi t}\,|\varphi_t\rangle\,, \tag{B.13}$$

with $\rho_n = \exp\left(i\frac{2n+1}{4}\pi\right)$; $n = 0, 1, 2$, or 3, and to each bulk band we associate a screw eigenvalue corresponding to $\rho_n$.

Finally, we can plot the value of $\rho_n$ for each band on the line defined by $\boldsymbol{\gamma}_t$. This is shown around $\varepsilon(t) = 0$ in Fig. B.6,[12] and all the four bands consisting of Dirac cones have a different quantum number. Thus, we have proven that the fourfold degeneracy is indeed protected by the screw symmetry in a projective form, and breaking the fourfold screw or time-reversal symmetry will result in a gap opening of the Dirac cones. All of these phenomena are beyond the previous study, and in this sense we can regard it as a new crystalline phase. We note that the double degeneracy of bulk bands shown in Fig. B.6 is protected by anticommutivity of screw and glide symmetries [2].

In summary, the role of symmetry in spin liquids is still not fully understood, and there should be a rich variety of new exotic phases. Especially, the classification of crystalline phases is completely beyond the classification in free-fermion systems, and almost nothing is known for this huge iceberg, except for a small number of exactly solvable models. This is because we still do not have a systematic theory which can treat the projective implementation of the lattice symmetry beyond the mean-field approximation. Interacting systems, especially in the gapless case, are difficult in many senses. For example, it is difficult to include a gauge fluctuation correctly, and we have ignored it even in this thesis in most spin liquids. We believe that this analysis is complementary to Appendix F of Ref. 47 because we discussed the importance of symmetry fractionalization, which was mostly discussed in gapped systems so far, in gapless Kitaev spin liquids.

[12] $\varepsilon(t)$ is defined as eigenvalues of $\hat{h}(\boldsymbol{\gamma}_t)$.

# Bibliography


[1] M. G. Yamada, H. Fujita and M. Oshikawa. "Designing Kitaev Spin Liquids in Metal-Organic Frameworks". *Phys. Rev. Lett.* **119**, 057202 (2017).

[2] M. G. Yamada, V. Dwivedi and M. Hermanns. "Crystalline Kitaev spin liquids". *Phys. Rev. B* **96**, 155107 (2017).

[3] M. G. Yamada, M. Oshikawa and G. Jackeli. "Emergent SU(4) Symmetry in $\alpha$-$ZrCl_3$ and Crystalline Spin-Orbital Liquids". *Phys. Rev. Lett.* **121**, 097201 (2018).

[4] L. Balents. "Spin liquids in frustrated magnets". *Nature* **464**, 199–208 (2010).

[5] L. Savary and L. Balents. "Quantum spin liquids: a review". *Rep. Prog. Phys.* **80**, 016502 (2017).

[6] Y. Q. Li, M. Ma, D. N. Shi and F. C. Zhang. "SU(4) Theory for Spin Systems with Orbital Degeneracy". *Phys. Rev. Lett.* **81**, 3527–3530 (1998).

[7] M. Hermele and V. Gurarie. "Topological liquids and valence cluster states in two-dimensional SU($N$) magnets". *Phys. Rev. B* **84**, 174441 (2011).

[8] P. Corboz, M. Lajkó, A. M. Läuchli, K. Penc and F. Mila. "Spin-Orbital Quantum Liquid on the Honeycomb Lattice". *Phys. Rev. X* **2**, 041013 (2012).

[9] M. Lajkó and K. Penc. "Tetramerization in a SU(4) Heisenberg model on the honeycomb lattice". *Phys. Rev. B* **87**, 224428 (2013).

[10] M. A. Cazalilla and A. M. Rey. "Ultracold Fermi gases with emergent SU(N) symmetry". *Rep. Prog. Phys.* **77**, 124401 (2014).

[11] H. D. Zhou, E. S. Choi, G. Li, L. Balicas, C. R. Wiebe, Y. Qiu, J. R. D. Copley and J. S. Gardner. "Spin Liquid State in the $S = 1/2$ Triangular Lattice $Ba_3CuSb_2O_9$". *Phys. Rev. Lett.* **106**, 147204 (2011).

[12] S. Nakatsuji, K. Kuga, K. Kimura, R. Satake, N. Katayama, E. Nishibori, H. Sawa, R. Ishii, M. Hagiwara, F. Bridges, T. U. Ito, W. Higemoto, Y. Karaki, M. Halim, A. A. Nugroho, J. A. Rodriguez-Rivera, M. A. Green and C. Broholm. "Spin-Orbital Short-Range Order on a Honeycomb-Based Lattice". *Science* **336**, 559–563 (2012).

[13] A. Smerald and F. Mila. "Exploring the spin-orbital ground state of $Ba_3CuSb_2O_9$". *Phys. Rev. B* **90**, 094422 (2014).

[14] G. Jackeli and G. Khaliullin. "Mott Insulators in the Strong Spin-Orbit Coupling Limit: From Heisenberg to a Quantum Compass and Kitaev Models". *Phys. Rev. Lett.* **102**, 017205 (2009).

[15] F. J. Ohkawa. "Ordered States in Periodic Anderson Hamiltonian with Orbital Degeneracy and with Large Coulomb Correlation". *J. Phys. Soc. Jpn.* **52**, 3897–3906 (1983).

[16] R. Shiina, H. Shiba and P. Thalmeier. "Magnetic-Field Effects on Quadrupolar Ordering in a $\Gamma_8$-Quartet System $CeB_6$". *J. Phys. Soc. Jpn.* **66**, 1741–1755 (1997).

[17] F. Wang and A. Vishwanath. "$Z_2$ spin-orbital liquid state in the square lattice Kugel-Khomskii model". *Phys. Rev. B* **80**, 064413 (2009).

[18] K. I. Kugel, D. I. Khomskii, A. O. Sboychakov and S. V. Streltsov. "Spin-orbital interaction for face-sharing octahedra: Realization of a highly symmetric SU(4) model". *Phys. Rev. B* **91**, 155125 (2015).

[19] B. Swaroop and S. N. Flengas. "THE SYNTHESIS OF ANHYDROUS ZIRCONIUM TRICHLORIDE". *Can. J. Chem.* **42**, 1495–1498 (1964).

[20] B. Swaroop and S. N. Flengas. "CRYSTAL STRUCTURE OF ZIRCONIUM TRICHLORIDE". *Can. J. Phys.* **42**, 1886–1889 (1964).

[21] G. Brauer. *Handbuch der Präparativen Anorganischen Chemie, Bd. II.* Ferdinand Enke Verlag, Stuttgart (1978).

[22] J. Romhányi, L. Balents and G. Jackeli. "Spin-Orbit Dimers and Noncollinear Phases in $d^1$ Cubic Double Perovskites". *Phys. Rev. Lett.* **118**, 217202 (2017).

[23] K. I. Kugel and D. I. Khomskii. "The Jahn-Teller effect and magnetism: transition metal compounds". *Sov. Phys. Usp.* **25**, 231 (1982).

[24] J. D. Reger, J. A. Riera and A. P. Young. "Monte Carlo simulations of the spin-1/2 Heisenberg antiferromagnet in two dimensions". *J. Phys. Condens. Matter.* **1**, 1855 (1989).

[25] J. Fouet, P. Sindzingre and C. Lhuillier. "An investigation of the quantum $J_1$-$J_2$-$J_3$ model on the honeycomb lattice". *Eur. Phys. J. B* **20**, 241–254 (2001).

[26] M. Hermele, V. Gurarie and A. M. Rey. "Mott Insulators of Ultracold Fermionic Alkaline Earth Atoms: Underconstrained Magnetism and Chiral Spin Liquid". *Phys. Rev. Lett.* **103**, 135301 (2009).

[27] A. V. Gorshkov, M. Hermele, V. Gurarie, C. Xu, P. S. Julienne, J. Ye, P. Zoller, E. Demler, M. D. Lukin and A. M. Rey. "Two-orbital $SU(N)$ magnetism with ultracold alkaline-earth atoms". *Nat. Phys.* **6**, 289–295 (2010).

[28] M. Lajkó, K. Wamer, F. Mila and I. Affleck. "Generalization of the Haldane conjecture to SU(3) chains". *Nucl. Phys. B* **924**, 508 – 577 (2017).

[29] E. Lieb, T. Schultz and D. Mattis. "Two soluble models of an antiferromagnetic chain". *Ann. Phys.* **16**, 407–466 (1961).

[30] P. W. Anderson. "Resonating valence bonds: A new kind of insulator?" *Mater. Res. Bull.* **8**, 153 – 160 (1973).

[31] P. W. Anderson. "The Resonating Valence Bond State in $La_2CuO_4$ and Superconductivity". *Science* **235**, 1196–1198 (1987).

[32] G. Baskaran, Z. Zou and P. W. Anderson. "The resonating valence bond state and high-Tc superconductivity – A mean field theory". *Solid State Commun.* **63**, 973 – 976 (1987).

[33] R. R. P. Singh and D. A. Huse. "Three-sublattice order in triangular- and Kagomé-lattice spin-half antiferromagnets". *Phys. Rev. Lett.* **68**, 1766–1769 (1992).

[34] N. Elstner, R. R. P. Singh and A. P. Young. "Finite temperature properties of the spin-1/2 Heisenberg antiferromagnet on the triangular lattice". *Phys. Rev. Lett.* **71**, 1629–1632 (1993).

[35] Y. Shimizu, K. Miyagawa, K. Kanoda, M. Maesato and G. Saito. "Spin Liquid State in an Organic Mott Insulator with a Triangular Lattice". *Phys. Rev. Lett.* **91**, 107001 (2003).

[36] Y. Li, H. Liao, Z. Zhang, S. Li, F. Jin, L. Ling, L. Zhang, Y. Zou, L. Pi, Z. Yang, J. Wang, Z. Wu and Q. Zhang. "Gapless quantum spin liquid ground state in the two-dimensional spin-1/2 triangular antiferromagnet $YbMgGaO_4$". *Sci. Rep.* **5**, 16419 (2015).

[37] L. Balents and A. Paramekanti. "XY ring-exchange model on the triangular lattice". *Phys. Rev. B* **67**, 134427 (2003).

[38] C. K. Majumdar and D. K. Ghosh. "On Next-Nearest-Neighbor Interaction in Linear Chain. I". *J. Math. Phys.* **10**, 1388–1398 (1969).

[39] F. D. M. Haldane. "Continuum dynamics of the 1-D Heisenberg antiferromagnet: Identification with the O(3) nonlinear sigma model". *Phys. Lett. A* **93**, 464–468 (1983).

[40] F. D. M. Haldane. "Nonlinear Field Theory of Large-Spin Heisenberg Antiferromagnets: Semiclassically Quantized Solitons of the One-Dimensional Easy-Axis Néel State". *Phys. Rev. Lett.* **50**, 1153–1156 (1983).

[41] I. Affleck, T. Kennedy, E. H. Lieb and H. Tasaki. "Rigorous results on valence-bond ground states in antiferromagnets". *Phys. Rev. Lett.* **59**, 799–802 (1987).

[42] D. S. Rokhsar and S. A. Kivelson. "Superconductivity and the Quantum Hard-Core Dimer Gas". *Phys. Rev. Lett.* **61**, 2376–2379 (1988).

[43] G. Misguich. *Quantum Spin Liquids and Fractionalization*, 407–435. Springer, Berlin, Heidelberg (2011).

[44] I. Affleck and J. B. Marston. "Large-$n$ limit of the Heisenberg-Hubbard model: Implications for high-$T_c$ superconductors". *Phys. Rev. B* **37**, 3774–3777 (1988).

[45] J. B. Marston and I. Affleck. "Large-$n$ limit of the Hubbard-Heisenberg model". *Phys. Rev. B* **39**, 11538–11558 (1989).

[46] X.-G. Wen. "Quantum orders and symmetric spin liquids". *Phys. Rev. B* **65**, 165113 (2002).

[47] A. Kitaev. "Anyons in an exactly solved model and beyond". *Ann. Phys.* **321**, 2–111 (2006). January Special Issue.

[48] S. Yan, D. A. Huse and S. R. White. "Spin-Liquid Ground State of the S=1/2 Kagome Heisenberg Antiferromagnet". *Science* **332**, 1173–1176 (2011).

[49] P. W. Leung and V. Elser. "Numerical studies of a 36-site kagomé antiferromagnet". *Phys. Rev. B* **47**, 5459–5462 (1993).

[50] W. Zhu, X. Chen, Y.-C. He and W. Witczak-Krempa. "Entanglement signatures of emergent Dirac fermions: Kagome spin liquid and quantum criticality". *Sci. Adv.* **4** (2018).

[51] K. A. Ross, L. Savary, B. D. Gaulin and L. Balents. "Quantum Excitations in Quantum Spin Ice". *Phys. Rev. X* **1**, 021002 (2011).

[52] N. Shannon, O. Sikora, F. Pollmann, K. Penc and P. Fulde. "Quantum Ice: A Quantum Monte Carlo Study". *Phys. Rev. Lett.* **108**, 067204 (2012).

[53] M. G. Yamada. "Designing various quantum spin liquids in metal-organic frameworks" (2017). Master's thesis, the Department of Physics, the University of Tokyo.

[54] A. Shitade, H. Katsura, J. Kuneš, X.-L. Qi, S.-C. Zhang and N. Nagaosa. "Quantum Spin Hall Effect in a Transition Metal Oxide $Na_2IrO_3$". *Phys. Rev. Lett.* **102**, 256403 (2009).

[55] J. Chaloupka, G. Jackeli and G. Khaliullin. "Kitaev-Heisenberg Model on a Honeycomb Lattice: Possible Exotic Phases in Iridium Oxides $A_2IrO_3$". *Phys. Rev. Lett.* **105**, 027204 (2010).

[56] J. Chaloupka, G. Jackeli and G. Khaliullin. "Zigzag Magnetic Order in the Iridium Oxide $Na_2IrO_3$". *Phys. Rev. Lett.* **110**, 097204 (2013).

[57] A. Y. Kitaev. "Fault-tolerant quantum computation by anyons". *Ann. Phys.* **303**, 2–30 (2003).

[58] J. Nasu, M. Udagawa and Y. Motome. "Vaporization of Kitaev Spin Liquids". *Phys. Rev. Lett.* **113**, 197205 (2014).

[59] B. Sutherland. "Model for a multicomponent quantum system". *Phys. Rev. B* **12**, 3795–3805 (1975).

[60] I. Affleck. "Exact critical exponents for quantum spin chains, non-linear $\sigma$-models at $\theta = \pi$ and the quantum hall effect". *Nucl. Phys. B* **265**, 409–447 (1986).

[61] F. Bloch. "Bremsvermögen von Atomen mit mehreren Elektronen". *Z. Phys.* **81**, 363–376 (1933).

[62] S.-i. Tomonaga. "Remarks on Bloch's Method of Sound Waves applied to Many-Fermion Problems". *Progress of Theoretical Physics* **5**, 544–569 (1950).

[63] J. M. Luttinger. "An Exactly Soluble Model of a Many- Fermion System". *J. Math. Phys.* **4**, 1154–1162 (1963).

[64] I. Affleck. "Field Theory Methods and Quantum Critical Phenomena". *Les Houches 1988, Proceedings, Fields, strings and critical phenomena* 563 (1988).

[65] B. Frischmuth, F. Mila and M. Troyer. "Thermodynamics of the One-Dimensional SU(4) Symmetric Spin-Orbital Model". *Phys. Rev. Lett.* **82**, 835–838 (1999).

[66] E. H. Lieb. "Flux Phase of the Half-Filled Band". *Phys. Rev. Lett.* **73**, 2158–2161 (1994).

[67] M. Oshikawa. "Commensurability, Excitation Gap, and Topology in Quantum Many-Particle Systems on a Periodic Lattice". *Phys. Rev. Lett.* **84**, 1535–1538 (2000).

[68] M. Oshikawa. "Insulator, Conductor, and Commensurability: A Topological Approach". *Phys. Rev. Lett.* **90**, 236401 (2003).

[69] M. B. Hastings. "Sufficient conditions for topological order in insulators". *Europhys. Lett.* **70**, 824 (2005).

[70] I. Affleck and E. H. Lieb. "A proof of part of Haldane's conjecture on spin chains". *Lett. Math. Phys.* **12**, 57–69 (1986).

[71] B. Nachtergaele and R. Sims. "A Multi-Dimensional Lieb-Schultz-Mattis Theorem". *Commun. Math. Phys.* **276**, 437–472 (2007).

[72] M. P. Zaletel and A. Vishwanath. "Constraints on Topological Order in Mott Insulators". *Phys. Rev. Lett.* **114**, 077201 (2015).

[73] I. Kimchi, S. A. Parameswaran, A. M. Turner, F. Wang and A. Vishwanath. "Featureless and nonfractionalized Mott insulators on the honeycomb lattice at 1/2 site filling". *Proc. Natl. Acad. Sci. USA* **110**, 16378–16383 (2013).

[74] Y.-C. He, M. P. Zaletel, M. Oshikawa and F. Pollmann. "Signatures of Dirac Cones in a DMRG Study of the Kagome Heisenberg Model". *Phys. Rev. X* **7**, 031020 (2017).

[75] J. Gubernatis, N. Kawashima and P. Werner. *Quantum Monte Carlo Methods: Algorithms for Lattice Models*. Cambridge University Press, Cambridge (2016).

[76] P. Corboz, A. M. Läuchli, K. Penc, M. Troyer and F. Mila. "Simultaneous Dimerization and SU(4) Symmetry Breaking of 4-Color Fermions on the Square Lattice". *Phys. Rev. Lett.* **107**, 215301 (2011).

[77] P. Corboz, K. Penc, F. Mila and A. M. Läuchli. "Simplex solids in SU($N$) Heisenberg models on the kagome and checkerboard lattices". *Phys. Rev. B* **86**, 041106 (2012).

[78] W. M. H. Natori, E. C. Andrade and R. G. Pereira. "SU(4)-symmetric spin-orbital liquids on the hyperhoneycomb lattice". *Phys. Rev. B* **98**, 195113 (2018).

[79] M. A. Cazalilla, A. F. Ho and M. Ueda. "Ultracold gases of ytterbium: ferromagnetism and Mott states in an SU(6) Fermi system". *New J. Phys.* **11**, 103033 (2009).

[80] S. Giorgini, L. P. Pitaevskii and S. Stringari. "Theory of ultracold atomic Fermi gases". *Rev. Mod. Phys.* **80**, 1215–1274 (2008).

[81] C. Wu, J.-P. Hu and S.-C. Zhang. "Exact SO(5) Symmetry in the Spin-3/2 Fermionic System". *Phys. Rev. Lett.* **91**, 186402 (2003).

[82] R. K. Kaul, R. G. Melko and A. W. Sandvik. "Bridging Lattice-Scale Physics and Continuum Field Theory with Quantum Monte Carlo Simulations". *Annu. Rev. Condens. Matter Phys.* **4**, 179–215 (2013).

[83] B. Keimer, D. Casa, A. Ivanov, J. W. Lynn, M. v. Zimmermann, J. P. Hill, D. Gibbs, Y. Taguchi and Y. Tokura. "Spin Dynamics and Orbital State in $LaTiO_3$". *Phys. Rev. Lett.* **85**, 3946–3949 (2000).

[84] G. Khaliullin and S. Maekawa. "Orbital Liquid in Three-Dimensional Mott Insulator: $LaTiO_3$". *Phys. Rev. Lett.* **85**, 3950–3953 (2000).

[85] Y. Tokura and N. Nagaosa. "Orbital Physics in Transition-Metal Oxides". *Science* **288**, 462–468 (2000).

[86] L. F. Feiner, A. M. Oleś and J. Zaanen. "Quantum Melting of Magnetic Order due to Orbital Fluctuations". *Phys. Rev. Lett.* **78**, 2799–2802 (1997).

[87] N. Katayama, K. Kimura, Y. Han, J. Nasu, N. Drichko, Y. Nakanishi, M. Halim, Y. Ishiguro, R. Satake, E. Nishibori, M. Yoshizawa, T. Nakano, Y. Nozue, Y. Wakabayashi, S. Ishihara, M. Hagiwara, H. Sawa and S. Nakatsuji. "Absence of Jahn-Teller transition in the hexagonal $Ba_3CuSb_2O_9$ single crystal". *Proc. Natl. Acad. Sci. USA* (2015).

[88] A. Smerald and F. Mila. "Disorder-Driven Spin-Orbital Liquid Behavior in the $Ba_3XSb_2O_9$ Materials". *Phys. Rev. Lett.* **115**, 147202 (2015).

[89] Y. Han, M. Hagiwara, T. Nakano, Y. Nozue, K. Kimura, M. Halim and S. Nakatsuji. "Observation of the orbital quantum dynamics in the spin-$\frac{1}{2}$ hexagonal antiferromagnet $Ba_3CuSb_2O_9$". *Phys. Rev. B* **92**, 180410 (2015).

[90] K. W. Plumb, J. P. Clancy, L. J. Sandilands, V. V. Shankar, Y. F. Hu, K. S. Burch, H.-Y. Kee and Y.-J. Kim. "$\alpha$-$RuCl_3$: A spin-orbit assisted Mott insulator on a honeycomb lattice". *Phys. Rev. B* **90**, 041112 (2014).

[91] S. Ogawa. "Magnetic Transition in $TiCl_3$". *J. Phys. Soc. Jpn.* **15**, 1901–1901 (1960).

[92] G. Jackeli and D. A. Ivanov. "Dimer phases in quantum antiferromagnets with orbital degeneracy". *Phys. Rev. B* **76**, 132407 (2007).

[93] Y. Yao, C.-T. Hsieh and M. Oshikawa. "Anomaly Matching and Symmetry-Protected Critical Phases in SU($N$) Spin Systems in $1 + 1$ Dimensions". *Phys. Rev. Lett.* **123**, 180201 (2019).

[94] I. Affleck. "Spin gap and symmetry breaking in $CuO_2$ layers and other antiferromagnets". *Phys. Rev. B* **37**, 5186–5192 (1988).

[95] K. Totsuka. "Lieb-Schultz-Mattis approach to SU($N$)-symmetric Mott insulators," JPS 72nd Annual Meeting (2017).

[96] C.-M. Jian and M. Zaletel. "Existence of featureless paramagnets on the square and the honeycomb lattices in 2+1 dimensions". *Phys. Rev. B* **93**, 035114 (2016).

[97] A. Catuneanu, J. G. Rau, H.-S. Kim and H.-Y. Kee. "Magnetic orders proximal to the Kitaev limit in frustrated triangular systems: Application to $Ba_3IrTi_2O_9$". *Phys. Rev. B* **92**, 165108 (2015).

[98] M. Hermanns, K. O'Brien and S. Trebst. "Weyl Spin Liquids". *Phys. Rev. Lett.* **114**, 157202 (2015).

[99] M. Hermanns, S. Trebst and A. Rosch. "Spin-Peierls Instability of Three-Dimensional Spin Liquids with Majorana Fermi Surfaces". *Phys. Rev. Lett.* **115**, 177205 (2015).

[100] K. O'Brien, M. Hermanns and S. Trebst. "Classification of gapless $\mathbb{Z}_2$ spin liquids in three-dimensional Kitaev models". *Phys. Rev. B* **93**, 085101 (2016).

[101] A. F. Wells. *Three-dimensional Nets and Polyhedra*. Wiley, New York (1977).

[102] Y.-M. Lu, Y. Ran and M. Oshikawa. "Filling-enforced constraint on the quantized Hall conductivity on a periodic lattice". *Ann. Phys.* 168060 (2020).

[103] H. Watanabe, H. C. Po, A. Vishwanath and M. Zaletel. "Filling constraints for spin-orbit coupled insulators in symmorphic and nonsymmorphic crystals". *Proc. Natl. Acad. Sci. USA* **112**, 14551–14556 (2015).

[104] S. A. Parameswaran, A. M. Turner, D. P. Arovas and A. Vishwanath. "Topological order and absence of band insulators at integer filling in non-symmorphic crystals". *Nat. Phys.* **9**, 299–303 (2013).

[105] H. C. Po, H. Watanabe, C.-M. Jian and M. P. Zaletel. "Lattice Homotopy Constraints on Phases of Quantum Magnets". *Phys. Rev. Lett.* **119**, 127202 (2017).

[106] C. Schrade and L. Fu. "Spin-valley density wave in moiré materials". *Phys. Rev. B* **100**, 035413 (2019).

[107] K. T. Law and P. A. Lee. "1T-$TaS_2$ as a quantum spin liquid". *Proc. Natl. Acad. Sci. USA* **114**, 6996–7000 (2017).

[108] Y. J. Yu, Y. Xu, L. P. He, M. Kratochvilova, Y. Y. Huang, J. M. Ni, L. Wang, S.-W. Cheong, J.-G. Park and S. Y. Li. "Heat transport study of the spin liquid candidate $1T-TaS_2$". *Phys. Rev. B* **96**, 081111 (2017).

[109] H. Murayama, Y. Sato, T. Taniguchi, R. Kurihara, X. Z. Xing, W. Huang, S. Kasahara, Y. Kasahara, I. Kimchi, M. Yoshida, Y. Iwasa, Y. Mizukami, T. Shibauchi, M. Konczykowski and Y. Matsuda. "Effect of quenched disorder on the quantum spin liquid state of the triangular-lattice antiferromagnet $1T - TaS_2$". *Phys. Rev. Research* **2**, 013099 (2020).

[110] M. H. N. Assadi and Y. Shigeta. "The effect of octahedral distortions on the electronic properties and magnetic interactions in O3 $NaTMO_2$ compounds (TM = Ti–Ni & Zr–Pd)". *RSC Adv.* **8**, 13842–13849 (2018).

[111] S. P. Singh, M. Tomar, Y. Ishikawa, S. B. Majumder and R. S. Katiyar. "Density-Functional Theoretical Study on the Intercalation Properties of Layered $LiMO_2$ (M = Zr, Nb, Rh, Mo, and Ru)". *MRS Proc.* **835**, K6.3 (2004).

[112] D. P. Arovas and A. Auerbach. "Tetrahis(dimethylamino)ethylene-$C_{60}$: Multicomponent superexchange and Mott ferromagnetism". *Phys. Rev. B* **52**, 10114–10121 (1995).

[113] S. K. Pati, R. R. P. Singh and D. I. Khomskii. "Alternating Spin and Orbital Dimerization and Spin-Gap Formation in Coupled Spin-Orbital Systems". *Phys. Rev. Lett.* **81**, 5406–5409 (1998).

[114] C. Itoi, S. Qin and I. Affleck. "Phase diagram of a one-dimensional spin-orbital model". *Phys. Rev. B* **61**, 6747–6756 (2000).

[115] X. Chen, Z.-C. Gu and X.-G. Wen. "Classification of gapped symmetric phases in one-dimensional spin systems". *Phys. Rev. B* **83**, 035107 (2011).

[116] J. A. Watts. "The Structure of $\beta$-Zirconium Trichloride". *Inorg. Chem.* **5**, 281–283 (1966).

[117] W. Rüdorff, G. Walter and H. Becker. "Über einige Oxoverbindungen und Doppeloxyde des vierwertigen Vanadins". *Z. Anorg. Allg. Chem.* **285**, 287–296 (1956).

[118] T. Takayama, A. Kato, R. Dinnebier, J. Nuss, H. Kono, L. S. I. Veiga, G. Fabbris, D. Haskel and H. Takagi. "Hyperhoneycomb Iridate $\beta-Li_2IrO_3$ as a Platform for Kitaev Magnetism". *Phys. Rev. Lett.* **114**, 077202 (2015).

[119] K. A. Modic, T. E. Smidt, I. Kimchi, N. P. Breznay, A. Biffin, S. Choi, R. D. Johnson, R. Coldea, P. Watkins-Curry, G. T. McCandless, J. Y. Chan, F. Gandara, Z. Islam, A. Vishwanath, A. Shekhter, R. D. McDonald and J. G. Analytis. "Realization of a three-dimensional spin–anisotropic harmonic honeycomb iridate". *Nat. Commun.* **5**, 4203 (2014).

[120] J. Kanamori. "Electron Correlation and Ferromagnetism of Transition Metals". *Prog. Theor. Phys.* **30**, 275–289 (1963).

[121] S. M. Winter, Y. Li, H. O. Jeschke and R. Valentí. "Challenges in design of Kitaev materials: Magnetic interactions from competing energy scales". *Phys. Rev. B* **93**, 214431 (2016).

[122] C. Wu. "Competing Orders in One-Dimensional Spin-3/2 Fermionic Systems". *Phys. Rev. Lett.* **95**, 266404 (2005).

[123] C. Wu. "HIDDEN SYMMETRY AND QUANTUM PHASES IN SPIN-3/2 COLD ATOMIC SYSTEMS". *Mod. Phys. Lett. B* **20**, 1707–1738 (2006).

[124] A. Georges, L. de' Medici and J. Mravlje. "Strong Correlations from Hund's Coupling". *Annu. Rev. Condens. Matter Phys.* **4**, 137–178 (2013).

[125] W. M. H. Natori, R. Nutakki, R. G. Pereira and E. C. Andrade. "SU(4) Heisenberg model on the honeycomb lattice with exchange-frustrated perturbations: Implications for twistronics and Mott insulators". *Phys. Rev. B* **100**, 205131 (2019).

[126] O. Delgado Friedrichs, M. O'Keeffe and O. M. Yaghi. "Three-periodic nets and tilings: regular and quasiregular nets". *Acta Crystallogr. Sect. A* **59**, 22–27 (2003).

[127] O. Delgado Friedrichs, M. O'Keeffe and O. M. Yaghi. "Three-periodic nets and tilings: semiregular nets". *Acta Crystallogr. Sect. A* **59**, 515–525 (2003).

[128] M. Hermanns and S. Trebst. "Quantum spin liquid with a Majorana Fermi surface on the three-dimensional hyperoctagon lattice". *Phys. Rev. B* **89**, 235102 (2014).

[129] I. Kimchi, J. G. Analytis and A. Vishwanath. "Three-dimensional quantum spin liquids in models of harmonic-honeycomb iridates and phase diagram in an infinite-$D$ approximation". *Phys. Rev. B* **90**, 205126 (2014).

[130] E. Coronado, J. R. Galán-Mascarós, C. J. Gómez-García and J. M. Martínez-Agudo. "Molecule-Based Magnets Formed by Bimetallic Three-Dimensional Oxalate Networks and Chiral Tris(bipyridyl) Complex Cations. The Series $[Z^{II}(bpy)_3][ClO_4][M^{II}Cr^{III}(ox)_3]$ ($Z^{II}$ = Ru, Fe, Co, and Ni; $M^{II}$ = Mn, Fe, Co, Ni, Cu, and Zn; ox = Oxalate Dianion)". *Inorg. Chem.* **40**, 113–120 (2001).

[131] B. Zhang, Y. Zhang and D. Zhu. "$[(C_2H_5)_3NH]_2Cu_2(C_2O_4)_3$: a three-dimensional metal-oxalato framework showing structurally related dielectric and magnetic transitions at around 165 K". *Dalton Trans.* **41**, 8509–8511 (2012).

[132] M. Clemente-León, E. Coronado and M. López-Jordà. "2D and 3D bimetallic oxalate-based ferromagnets prepared by insertion of $Mn^{III}$-salen type complexes". *Dalton Trans.* **42**, 5100–5110 (2013).

[133] B. Zhang, Y. Zhang, Z. Wang, D. Wang, P. J. Baker, F. L. Pratt and D. Zhu. "Candidate Quantum Spin Liquid due to Dimensional Reduction of a Two-Dimensional Honeycomb Lattice". *Sci. Rep.* **4**, 6451 (2014).

[134] K. W. Krämer, H. U. Güdel, B. Roessli, P. Fischer, A. Dönni, N. Wada, F. Fauth, M. T. Fernandez-Diaz and T. Hauss. "Noncollinear two- and three-dimensional magnetic ordering in the honeycomb lattices of Er$X_3$ ($X$=Cl,Br,I)". *Phys. Rev. B* **60**, R3724 (1999).

[135] K. W. Krämer, H. U. Güdel, P. Fischer, F. Fauth, M. T. Fernandez-Diaz and T. Hauß. "Triangular antiferromagnetic order in the honeycomb layer lattice of $ErCl_3$". *Eur. Phys. J. B* **18**, 39–47 (2000).

[136] Y. Ran, M. Hermele, P. A. Lee and X.-G. Wen. "Projected-Wave-Function Study of the Spin-1/2 Heisenberg Model on the Kagomé Lattice". *Phys. Rev. Lett.* **98**, 117205 (2007).

[137] J. Nasu and S. Ishihara. "Dynamical Jahn-Teller effect in a spin-orbital coupled system". *Phys. Rev. B* **88**, 094408 (2013).

[138] J. Nasu and S. Ishihara. "Resonating valence-bond state in an orbitally degenerate quantum magnet with dynamical Jahn-Teller effect". *Phys. Rev. B* **91**, 045117 (2015).

[139] I. Bersuker. "The jahn-teller effect in crystal chemistry and spectroscopy". *Coord. Chem. Rev.* **14**, 357 – 412 (1975).

[140] A. Abragam and B. Bleaney. *Electron Paramagnetic Resonance of Transition Ions.* Clarendon Press, Oxford (1970).

[141] N. Iwahara, V. Vieru, L. Ungur and L. F. Chibotaru. "Zeeman interaction and Jahn-Teller effect in the $\Gamma_8$ multiplet". *Phys. Rev. B* **96**, 064416 (2017).

[142] L. Marrucci, C. Manzo and D. Paparo. "Optical Spin-to-Orbital Angular Momentum Conversion in Inhomogeneous Anisotropic Media". *Phys. Rev. Lett.* **96**, 163905 (2006).

[143] Y. Cao, V. Fatemi, S. Fang, K. Watanabe, T. Taniguchi, K. Efthimios and P. Jarillo-Herrero. "Unconventional superconductivity in magic-angle graphene superlattices". *Nature* **556**, 43–50 (2018).

[144] Y. Cao, V. Fatemi, A. Demir, S. Fang, S. L. Tomarken, J. Y. Luo, J. D. Sanchez-Yamagishi, K. Watanabe, T. Taniguchi, E. Kaxiras, R. C. Ashoori and P. Jarillo-Herrero. "Correlated insulator behaviour at half-filling in magic-angle graphene superlattices". *Nature* **556**, 80–84 (2018).

[145] K. S. Novoselov, A. K. Geim, S. V. Morozov, D. Jiang, Y. Zhang, S. V. Dubonos, I. V. Grigorieva and A. A. Firsov. "Electric Field Effect in Atomically Thin Carbon Films". *Science* **306**, 666–669 (2004).

[146] R. Bistritzer and A. H. MacDonald. "Moiré bands in twisted double-layer graphene". *Proc. Natl. Acad. Sci. USA* **108**, 12233–12237 (2011).

[147] C. Xu and L. Balents. "Topological Superconductivity in Twisted Multilayer Graphene". *Phys. Rev. Lett.* **121**, 087001 (2018).

[148] N. N. T. Nam and M. Koshino. "Lattice relaxation and energy band modulation in twisted bilayer graphene". *Phys. Rev. B* **96**, 075311 (2017).

[149] N. F. Q. Yuan and L. Fu. "Model for the metal-insulator transition in graphene superlattices and beyond". *Phys. Rev. B* **98**, 045103 (2018).

[150] M. H. Naik and M. Jain. "Ultraflatbands and Shear Solitons in Moiré Patterns of Twisted Bilayer Transition Metal Dichalcogenides". *Phys. Rev. Lett.* **121**, 266401 (2018).

[151] F. Wu, T. Lovorn, E. Tutuc, I. Martin and A. H. MacDonald. "Topological Insulators in Twisted Transition Metal Dichalcogenide Homobilayers". *Phys. Rev. Lett.* **122**, 086402 (2019).

[152] Z. Zhu, D. N. Sheng and L. Fu. "Spin-Orbital Density Wave and a Mott Insulator in a Two-Orbital Hubbard Model on a Honeycomb Lattice". *Phys. Rev. Lett.* **123**, 087602 (2019).

[153] A. König and N. D. Mermin. "Screw rotations and glide mirrors: Crystallography in Fourier space". *Proc. Natl. Acad. Sci. USA* **96**, 3502–3506 (1999).

[154] Y. Hatsugai. "Topological aspect of graphene physics". *J. Phys. Conf. Ser.* **334**, 012004 (2011).

[155] A. Kitaev. "Periodic table for topological insulators and superconductors". *AIP Conf. Proc.* **1134**, 22–30 (2009).

[156] S. Yang, D. L. Zhou and C. P. Sun. "Mosaic spin models with topological order". *Phys. Rev. B* **76**, 180404 (2007).

[157] G. Baskaran, G. Santhosh and R. Shankar. "Exact quantum spin liquids with Fermi surfaces in spin-half models". *arXiv* 0908.1614.

[158] G. Kells, J. Kailasvuori, J. K. Slingerland and J. Vala. "Kaleidoscope of topological phases with multiple Majorana species". *New J. Phys.* **13**, 095014 (2011).

[159] K. Persson. “Materials Data on $ZrCl_3$ (SG:162) by Materials Project” (2016). An optional note.

# Acknowledgement

We thank Arash Banisafar, Kelsey Collins, Kedar Damle, Eugene Demler, Vatsal Dwivedi, Shu Ebihara, Tim Eschmann, Danna E. Freedman, Liang Fu, Yohei Fuji, Hiroyuki Fujita, Bertrand I. Halperin, Maria Hermanns, Hosho Katsura, Giniyat Khaliullin, Daniel I. Khomskii, Ryohei Kobayashi, Miklós Lajkó, Linhao Li, Frédéric Mila, Yuki Nagai, Yuji Nakagawa, Judit Romhányi, Ryoya Sano, Constantin Schrade, Kirill Shtengel, Andrew Smerald, Tomohiro Soejima, Yasuhiro Tada, Hidenori Takagi, Tomohiro Takayama, T. Senthil, Ryo Takahashi, Simon Trebst, Shinji Tsuneyuki, and especially Itamar Kimchi for helpful comments. M.G.Y. thanks George Jackeli, Masaki Oshikawa, and personally Atsuko Tsuji for effortless help to write a thesis, and is also grateful to Nami Ishiyama for her help. The crystal data included in this work have been taken from Materials Project [159]. M.G.Y. is supported by the Materials Education program for the future leaders in Research, Industry, and Technology (MERIT), and by JSPS. This work was supported by JSPS KAKENHI Grant Numbers JP15H02113, JP17J05736, and JP18H03686, and by JSPS Strategic International Networks Program No. R2604 "TopoNet". M.G.Y. acknowledges the support of the Max-Planck-UBC-UTokyo Centre for Quantum Materials. M.G.Y. also acknowledges the Quantum Materials Department at MPI-FKF, Stuttgart for kind hospitality during his visits, and the Department of Physics, MIT. This research was supported in part by the National Science Foundation under Grant No. NSF PHY-1748958.